

DETERMINATION OF DYNAMIC STABILITY DERIVATIVES FOR A
GENERIC COMBAT AIRCRAFT UNDER FORCED OSCILLATIONS

A THESIS SUBMITTED TO
THE GRADUATE SCHOOL OF NATURAL AND APPLIED SCIENCES
OF
THE MIDDLE EAST TECHNICAL UNIVERSITY

BY

114970

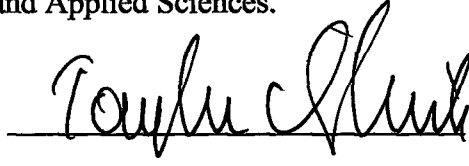
İBRAHİM İYİĞÜN

IN PARTIAL FULFILLMENT OF THE REQUIREMENTS FOR THE DEGREE OF
MASTER OF SCIENCE
IN
THE DEPARTMENT OF AERONAUTICAL ENGINEERING

MARCH 2001

TC YÜKSEK ÖĞRETİM BAKANLIĞI
DOKÜMAN YAYINLARI

Approval of the Graduate School of Natural and Applied Sciences.



Prof. Dr. Tayfur ÖZTÜRK

Director

I certify that this thesis satisfies all the requirements as a thesis for the degree of Master of Science.



Prof. Dr. Nafiz ALEMDAROĞLU

Head of Department

This is to certify that we have read this thesis and that in our opinion it is fully adequate, in scope and quality, as a thesis for the degree of Master of Science.

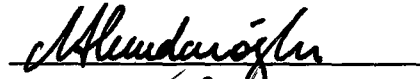


Prof. Dr. Nafiz ALEMDAROĞLU

Supervisor

Examining Committee Members

Prof. Dr. Nafiz ALEMDAROĞLU



Assoc. Prof. Dr. Kahraman ALBAYRAK



Assoc. Prof. Dr. Mehmet AKGÜN



Assoc. Prof. Dr. Mehmet Şerif KAVSAOĞLU



Assoc. Prof. Dr. Yusuf ÖZYÖRÜK



ABSTRACT

DETERMINATION OF DYNAMIC STABILITY DERIVATIVES FOR A GENERIC COMBAT AIRCRAFT UNDER FORCED OSCILLATIONS

İYİGÜN, İbrahim

M. S., Department of Aeronautical Engineering

Supervisor: Prof. Dr. Nafiz ALEMDAROĞLU

March 2001, 133 pages

The purpose of this thesis is to measure the dynamic stability derivatives of an oscillating generic combat aircraft model in the Ankara Wind Tunnel using forced oscillation technique. In forced oscillation technique the model is set to oscillate around a mean angle of attack about its center of gravity with small amplitude and low frequency. The aerodynamic forces and moments are measured with a five-component internal strain gauge balance placed inside the oscillating model. The data is collected and analyzed by using a data acquisition system operating under the Labview programming language. The thesis gives a brief description of the experimental set-up, and details of the forced oscillation technique used. The software written for the analysis of static and dynamic test data is presented. The thesis presents the results obtained for the dynamic stiffness and damping coefficients for the pitch and the roll moments as well as for the normal force coefficient. Comparison of the present results with those already obtained in other test facilities is also given.

Keywords: Forced oscillation, Dynamic Stability Derivatives, Standard Dynamic Model, Low Speed Wind Tunnel

ÖZ

SALINIMA ZORLANMIŞ JENERİK BİR SAVAŞ UÇAĞININ DİNAMİK KARARLILIK TÜREVLERİNİN ÖLÇÜLMESİ

İYİĞÜN, İbrahim

Yüksek Lisans, Havacılık Mühendisliği Bölümü

Tez Yöneticisi: Prof. Dr. Nafiz ALEMDAROĞLU

Mart 2001, 133 sayfa

Bu tezin amacı, “Forced Oscillation” tekniği kullanılarak, salınım hareketi yapan bir generic savaş uçağı modelinin dinamik kararlılık türevlerinin Ankara Rüzgar Tünelinde ölçülmesidir. “Forced Oscillation” tekniğinde, model belli bir hücum açısına getirilerek ağırlık merkezi etrafında küçük salınımlarda ve küçük frekanslarda salınım yaptırılır. Aerodinamik kuvvet ve momentler salınım yapan modelin içine yerleştirilen beş bileşenli “strain gage”li iç balans ile ölçülür. Datalar “Labview” programlama dili altında çalışan bir data toplama sistemi tarafından toplanır ve analiz edilir. Tezde, deney düzeneğinin kısa bir tanıtımı ve kullanılan “Forced Oscillation” tekniği detaylı olarak verilmiştir. Statik ve dinamik test datalarının analizleri için yazılan program sunulmuştur. Tezde, yunuslama ve yuvarlanma momentine ek olarak normal kuvvet için elde edilen statik ve dinamik katsayıların sonuçları sunulmuştur. Sunulan sonuçlar ile diğer ülkelerin halihazırda elde ettikleri sonuçların karşılaştırmaları da verilmiştir.

Anahtar Sözcükler: “Forced Oscillation”, Dinamik Kararlılık Türevleri, Standart Dinamik Model, Ses Altı Rüzgar Tüneli

ACKNOWLEDGMENTS

In the course of the manufacturing and installing of the experimental set-up and the measurement of dynamic stability derivatives, many people helped us.

I wish to express my gratitude and appreciation to my advisor Prof. Dr. Nafiz ALEMDAROĞLU, for his guidance and encouragement during the course of this project. The completion of this thesis would not have been possible without his assistance and encouragement.

I want to express my sincere thanks to the Aeronautical Engineering Department of Politecnico di Torino of Italy. I offer my special thanks to Prof. Dr. Fulvia Quagliotti and Assoc. Prof. Dr. Giorgio Guglieri for their technical guidance during the realization of this thesis.

I want to express my appreciation for the support of Turkish Air Force, especially, Colonel İsmail PAKEL, 1st Lt. Çağlayan PINAR, Noncommissioned-officer Mehmet ÇELİK and all staff of Education Department of Turkish Air Force Headquarter.

I would like to thank 1st Lt. Mehmet ALTUN; we made everything together and thanks to Utku DİNÇER for his technical assistance.

I express my appreciation to 2nd Air Supply and Maintenance Center for the manufacturing of the experimental set-up. I also offer special thanks to Major İbrahim ÇIVİCİ, Captain Şükrü PAZAR, 1st Lt. İbrahim GEÇİT, Technician Cemal KAYA, Osman IŞIK and to all of the staff of 2nd Air Supply and Maintenance Center.

I want to express my thanks to TÜBİTAK for the financial support they provided through the support project MISAG-131. The completion of this project would not be possible without this support.

I would like to express my special thanks to Tübitak-Sage for permitting the use of the Ankara Wind Tunnel for this project. I offer my special thanks to Alper ÜNVER and to all technical staff of Tübitak-Sage.

Last but not the least, I would like to express my deepest thanks to my wife for her patience and continuous support throughout this study. Without her encouragement I would not be able to finish this thesis.

TABLE OF CONTENTS

ABSTRACT	iii
ÖZ.....	iv
ACKNOWLEDGEMENTS	v
TABLE OF CONTENTS	vii
LIST OF TABLES	ix
LIST OF FIGURES.....	x
LIST OF SYMBOLS.....	xv
CHAPTER	
1. INTRODUCTION	1
2. BACKGROUND ON DYNAMIC TESTING.....	5
2.1 Description of Experiment Types and Techniques	5
2.1.1 Large Amplitude Oscillations Technique.	6
2.1.2 Rotary Techniques	6
2.1.3 Control Surface Oscillation Techniques	9
2.1.4 Other Techniques	9
2.2 Examples of Facilities.....	13
2.2.1 Aermacchi (AEM), Italy	13
2.2.2 Defence Research Agency (DRA), United Kingdom	14
2.2.3 Deutsche Forschungsanstalt Für Luft und Raumfahrt (DLR), GERMANY..	15
2.2.4 Eidetics International / NASA Ames (EI), USA.....	18
2.2.5 Institute for Aerospace Research (IAR), Canada.....	19
2.2.6 ONERA-IMFL, France	21
2.2.7 Politecnico di Torino (TPI), Italy.....	23

2.2.8 Aeronautical Research Institute of Sweden (FFA)	24
2.2.9 NASA Langley/Bihrlle Applied Research/DRA	24
3. EXPERIMENTAL SET UP.....	27
3.1 Description of the Apparatus.....	27
3.2 The Standard Dynamic Model (SDM).....	30
3.3 Data Acquisition System (DAQ)	32
3.3.1 Components of DAQ.....	32
3.3.2 Description and Properties of Components of DAQ System	33
3.4 The Layout of Hardware and Wiring Connectors.....	38
3.5 Interface of the Elements of the Experimental Set-up	38
4. DYNAMIC DERIVATIVES	40
4.1 Equations of Motion.....	42
4.2 Forced Oscillation Technique	47
5. STATIC AND DYNAMIC TEST RESULTS	59
5.1 Static Test Results and Comparison with Other Facilities.....	61
5.2 Dynamic Test Results and Comparison with Other Facilities	70
6. CONCLUSION AND DISCUSSION.....	92
REFERENCES.....	97
APPENDIX A SEQUENCE OF STATIC TESTS AND LABVIEW PROGRAMMING.....	100
APPENDIX B SEQUENCE OF DYNAMIC TESTS AND LABVIEW PROGRAMMING.....	112

LIST OF TABLES

TABLE

3.1 Parts List of the Experimental Set-up Given in Figure 3.1	28
3.2 Main Dimensions of the SDM	32
4.1 Dynamic Moment Derivatives	41
5.1 The Test Matrix for Static Tests.....	59
5.2 Test Matrix for Oscillatory Tests-pitch mode	60

LIST OF FIGURES

FIGURES

1.1	Road Map for the Progress of the Project.....	3
2.1	Large Amplitude Free Oscillation Pitch Apparatus at AEDC-VKF.....	6
2.2	Rolling Technique at British Aerospace.....	8
2.3	Ames Research Center's Large-Scale Rotary Balance (Coning Rig).....	8
2.4	Orbital Fixed-Plane Motion.....	9
2.5	Control-Surface Oscillation at NAE.....	10
2.6	Model Free Technique.....	12
2.7	Free-Oscillation Pitch Apparatus at NAE.....	12
2.8	Sketch of the Curved-Flow Test Section of the Stability Tunnel.....	13
2.9	AEM Rotary Balance Stings.....	16
2.10	DRA Inexorable Drive Rig.....	16
2.11	DRA Rotary Balance.....	17
2.12	DLR Rotary Balance.....	17
2.13	General Arrangements of NASA Ames/Eidetics Rotary Balance.....	18
2.14	IAR Asymmetric Support System for Oscillatory Tests.....	20
2.15	ONERA-IMFL Rig.....	22
2.16	The TPI Oscillatory Balance.....	25
2.17	FFA Rotary Balance.....	26
3.1	Parts of the AWT Test Rig (Perspective View).....	29
3.2	The Geometry of the Standard Dynamic Model Used in the Tests.....	30
3.3	Components of a Data Acquisition System.....	33
3.4	Technical Drawing of the Internal Balance.....	35
3.5	The Layout of Hardware and Wiring Connectors.....	37
4.1	Characteristic Motions in the Aerodynamic Axis System.....	43

4.2	Characteristic Motions in the Body Axis System	43
4.3	Reference Frame: Body Axis.....	44
4.4	The Body Axes Reference System	48
4.5	Second Order Oscillator Equivalent System for the Response of the Aircraft Model Under Small Oscillations	52
4.6	In-phase and Out-of-phase Components of $M(t)$	54
5.1	The Static Values for Roll Moment Coefficient C_l for $V=20$ m/s (Data Repeatability)	61
5.2	The Static Values for Roll Moment Coefficient C_l for $V=30$ m/s (Data Repeatability)	62
5.3	The Static Values for Roll Moment Coefficient C_l for $V=40$ m/s (Data Repeatability)	62
5.4	The Static Values for Normal Force Coefficient C_z for $V=20$ m/s (Data Repeatability)	63
5.5	The Static Values for Normal Force Coefficient C_z for $V=30$ m/s (Data Repeatability)	64
5.6	The Static Values for Normal Force Coefficient C_z for $V=40$ m/s (Data Repeatability)	64
5.7	The Static Values for Pitching Moment Coefficient C_m for $V=20$ m/s (Data Repeatability)	65
5.8	The Static Values for Pitching Moment Coefficient C_m for $V=30$ m/s (Data Repeatability)	65
5.9	The Static Values for Pitching Moment Coefficient C_m for $V=40$ m/s (Data Repeatability).....	66
5.10	The Effect of Velocity on C_l	67
5.11	The Effect of Velocity on C_z	67
5.12	The Effect of Velocity on C_m	68
5.13	The Facility Comparison for the Static Coefficient C_l Variation with Angle of Attack	68
5.14	The Facility Comparison for the Static Coefficient C_z Variation with Angle of Attack	69

5.15 The Facility Comparison for the Static Coefficient C_m Variation with Angle of Attack	69
5.16 The Stiffness Derivative $C_{l\alpha}$ for $V = 30 \text{ m/s}$, $f = 1 \text{ Hz}$, $\theta = \pm 1^\circ$ (Data Repeatability)	70
5.17 The Stiffness Derivative $C_{l\alpha}$ for $V = 30 \text{ m/s}$, $f = 1 \text{ Hz}$, $\theta = \pm 2^\circ$ (Data Repeatability)	71
5.18 The Stiffness Derivative $C_{l\alpha}$ for $V = 30 \text{ m/s}$, $f = 2 \text{ Hz}$, $\theta = \pm 1^\circ$ (Data Repeatability)	71
5.19 The Damping Derivative $C_{lq} + C_{l\dot{\alpha}}$ for $V = 30 \text{ m/s}$, $f = 1 \text{ Hz}$, $\theta = \pm 1^\circ$ (Data Repeatability)	72
5.20 The Damping Derivative $C_{lq} + C_{l\dot{\alpha}}$ for $V = 30 \text{ m/s}$, $f = 1 \text{ Hz}$, $\theta = \pm 2^\circ$ (Data Repeatability)	72
5.21 The Damping Derivative $C_{lq} + C_{l\dot{\alpha}}$ for $V = 30 \text{ m/s}$, $f = 2 \text{ Hz}$, $\theta = \pm 1^\circ$ (Data Repeatability)	73
5.22 The Stiffness Derivative $C_{z\alpha}$ for $V = 30 \text{ m/s}$, $f = 1 \text{ Hz}$, $\theta = \pm 1^\circ$ (Data Repeatability)	74
5.23 The Stiffness Derivative $C_{z\alpha}$ for $V = 30 \text{ m/s}$, $f = 1 \text{ Hz}$, $\theta = \pm 2^\circ$ (Data Repeatability)	74
5.24 The Stiffness Derivative $C_{z\alpha}$ for $V = 30 \text{ m/s}$, $f = 2 \text{ Hz}$, $\theta = \pm 1^\circ$ (Data Repeatability)	75
5.25 The Damping Derivative $C_{zq} + C_{z\dot{\alpha}}$ for $V = 30 \text{ m/s}$, $f = 1 \text{ Hz}$, $\theta = \pm 1^\circ$ (Data Repeatability)	75
5.26 The Damping Derivative $C_{zq} + C_{z\dot{\alpha}}$ for $V = 30 \text{ m/s}$, $f = 1 \text{ Hz}$, $\theta = \pm 2^\circ$ (Data Repeatability)	76
5.27 The Damping Derivative $C_{zq} + C_{z\dot{\alpha}}$ for $V = 30 \text{ m/s}$, $f = 2 \text{ Hz}$, $\theta = \pm 1^\circ$ (Data Repeatability)	76
5.28 The Stiffness Derivative $C_{m\alpha}$ for $V = 30 \text{ m/s}$, $f = 1 \text{ Hz}$, $\theta = \pm 1^\circ$ (Data Repeatability)	77

5.29 The Stiffness Derivative $C_{m\alpha}$ for $V = 30 \text{ m/s}$, $f = 1 \text{ Hz}$, $\theta = \pm 2^\circ$ (Data Repeatability)	78
5.30 The Stiffness Derivative $C_{m\alpha}$ for $V = 30 \text{ m/s}$, $f = 2 \text{ Hz}$, $\theta = \pm 1^\circ$ (Data Repeatability)	78
5.31 The Damping Derivative $C_{mq} + C_{m\dot{\alpha}}$ for $V = 30 \text{ m/s}$, $f = 1 \text{ Hz}$, $\theta = \pm 1^\circ$ (Data Repeatability)	79
5.32 The Damping Derivative $C_{mq} + C_{m\dot{\alpha}}$ for $V = 30 \text{ m/s}$, $f = 1 \text{ Hz}$, $\theta = \pm 2^\circ$ (Data Repeatability)	79
5.33 The Damping Derivative $C_{mq} + C_{m\dot{\alpha}}$ for $V = 30 \text{ m/s}$, $f = 2 \text{ Hz}$, $\theta = \pm 1^\circ$ (Data Repeatability)	80
5.34 The Effect of Amplitude on $C_{l\alpha}$ for $V=30 \text{ m/s}$, $f=1 \text{ Hz}$	81
5.35 The Effect of Amplitude on $C_{lq} + C_{l\dot{\alpha}}$ for $V=30 \text{ m/s}$, $f=1 \text{ Hz}$	81
5.36 The Effect of Amplitude on $C_{z\alpha}$ for $V=30 \text{ m/s}$, $f=1 \text{ Hz}$	82
5.37 The Effect of Amplitude on $C_{zq} + C_{z\dot{\alpha}}$ for $V=30 \text{ m/s}$, $f=1 \text{ Hz}$	82
5.38 The Effect of Amplitude on $C_{m\alpha}$ for $V=30 \text{ m/s}$, $f=1 \text{ Hz}$	83
5.39 The Effect of Amplitude on $C_{mq} + C_{m\dot{\alpha}}$ for $V=30 \text{ m/s}$, $f=1 \text{ Hz}$	83
5.40 The Effect of Frequency on $C_{l\alpha}$ for $V=30 \text{ m/s}$, $\theta = \pm 1^\circ$	84
5.41 The Effect of Frequency on $C_{lq} + C_{l\dot{\alpha}}$ for $V=30 \text{ m/s}$, $\theta = \pm 1^\circ$	85
5.42 The Effect of Frequency on $C_{z\alpha}$ for $V=30 \text{ m/s}$, $\theta = \pm 1^\circ$	85
5.43 The Effect of Frequency on $C_{zq} + C_{z\dot{\alpha}}$ for $V=30 \text{ m/s}$, $\theta = \pm 1^\circ$	86
5.44 The Effect of Frequency on $C_{m\alpha}$ for $V=30 \text{ m/s}$, $\theta = \pm 1^\circ$	86
5.45 The Effect of Frequency on $C_{mq} + C_{m\dot{\alpha}}$ for $V=30 \text{ m/s}$, $\theta = \pm 1^\circ$	87
5.46 Comparisons of $C_{l\alpha}$ Coefficient Measurements with Results Obtained in Other Test Facilities	88
5.47 Comparisons of $C_{lq} + C_{l\dot{\alpha}}$ Coefficient Measurements with Results Obtained in Other Test Facilities	89

5.48 Comparisons of $C_{z\alpha}$ Coefficient Measurements with Results Obtained in Other Test Facilities	89
5.49 Comparisons of $C_{zq} + C_{z\dot{\alpha}}$ Coefficient Measurements with Results Obtained in Other Test Facilities	90
5.50 Comparisons of $C_{m\alpha}$ Coefficient Measurements with Results Obtained in Other Test Facilities	90
5.51 Comparisons of $C_{mq} + C_{m\dot{\alpha}}$ Coefficient Measurements with Results Obtained in Other Test Facilities	91
A.1 Static Test Flowchart	102
A.2 Diagram of "data top.vi"	108
A.3 Diagram of "balanssinyal.vi"	109
A.4 Diagram of "akis parametreleri.vi"	110
A.5 Diagram of "force.vi"	111
B.1 Dynamic Test Flowchart.....	115
B.2 Diagram of "final.vi"	123
B.3 Diagram of "akis.vi"	124
B.4 Diagram of "windoff load.vi"	125
B.5 Diagram of "tbalansvolt.vi"	126
B.6 Diagram of "trefvoltfreq.vi"	127
B.7 Diagram of "trefvolttest1.vi"	128
B.8 Diagram of "trefvolttest2.vi"	129
B.9 Diagram of "tphase.volt.vi"	130
B.10 Diagram of "tvoltaj hesaplamaları.vi"	131
B.11 Diagram of "tload component.vi"	132
B.12 Diagram of "windon load.vi"	133

LIST OF SYMBOLS

a_{Mj}	: Balance calibration matrix
b	: Wing span (m)
\bar{c}	: Model mean aerodynamic chord (m)
c_s	: Damping constant
k_s	: Mechanical stiffness
K	: Reduced oscillation frequency ($\omega l/2V_\infty$)
l	: Reference length (m)
L	: Rolling moment
M	: Pitching moment
N	: Yawing moment
S	: Model wing surface
S_{WT}	: Wind tunnel cross section
Y	: Side force
Z	: Normal force
C_l	: Rolling moment coefficient ($=L/qSb$)
C_z	: Normal force coefficient ($=F_z/qS$)
C_m	: Pitching moment coefficient ($=M/qSc$)
C_n	: Yawing moment coefficient ($=N/qSb$)
C_x	: Axial force coefficient ($=F_x/qS$)
C_y	: Side force coefficient ($=F_y/qS$)
$C_{l\alpha}$: Rolling moment stiffness coefficient
$C_{l\beta} \sin \alpha$: Rolling moment stiffness coefficient
$C_{l\dot{\beta}} + C_{l\dot{\alpha}} \sin \alpha$: Rolling moment damping coefficient

$C_{lq} + C_{l\dot{\alpha}}$: Rolling moment damping coefficient
$C_{z\alpha}$: Normal force stiffness coefficient
$C_{zq} + C_{z\dot{\alpha}}$: Normal force damping coefficient
$C_{m\alpha}$: Pitching moment stiffness coefficient
$C_{m\beta} \sin \alpha$: Pitching moment stiffness coefficient
$C_{mq} + C_{m\dot{\alpha}}$: Pitching moment damping coefficient
$C_{n\beta} \sin \alpha$: Yawing moment stiffness coefficient
$C_{n\beta} \cos \alpha$: Yawing moment stiffness coefficient
$C_{np} + C_{n\dot{\beta}} \sin \alpha$: Yawing moment damping coefficient
$C_{nr} - C_{n\dot{\beta}} \cos \alpha$: Yawing moment damping coefficient
$C_{Y\beta} \sin \alpha$: Side force stiffness coefficient
$C_{Yp} + C_{Y\dot{\beta}} \sin \alpha$: Side force damping coefficient
$E(t)$: Balance output voltage
$E_{IN}(t)$: In-phase voltage component
\bar{E}_{IN}	: Amplitude of the in-phase voltage component
$E_{OUT}(t)$: Out-of-phase voltage component
\bar{E}_{OUT}	: Amplitude of the out-of-phase voltage component
$\bar{M}(t)$: Driving torque
$M_{aer}(t)$: Aerodynamic pitching moment wrt body axes
M_{α}	: Static pitching moment derivative
$M_{\dot{\alpha}}$: Dynamic pitching moment derivative
M_q	: Dynamic pitching moment derivative
F	: Force
f	: Oscillation frequency (Hz)
g	: Acceleration of gravity

I	: Moment or product of inertia
m	: Mass (kg)
Ma	: Mach number
N	: Newton (Kg m/s ²)
p, q, r	: Body axes angular velocities around the corresponding x, y, z axes
u, v, w	: Velocity components in x, y, z body axes directions, respectively
q	: Dynamic pressure
Re	: Reynolds number
T	: Thrust
t	: Time
x,y,z	: Body-fixed axes (origin at mass center)
α	: Angle of attack (rad or deg)
$\dot{\alpha}$: Time rate of change of angle of attack
α_{mean}	: Mean angle of attack (rad or deg)
β	: Angle of sideslip (rad or deg)
σ	: Measurement uncertainty (percentage)
$\Delta\alpha$: Primary oscillation in pitch
θ	: Oscillation amplitude in pitch experiments (deg)
ω	: Oscillation frequency ($2\pi f$, rad/sec.)
ρ	: Air density (Kg/m ³)
V_{∞}	: Airspeed (m/s)
ϕ	: Roll angle (rad or deg)
V_0	: Voltage supply (Volt)
V_{rms}	: Volts, root mean square
A	: Amperes
A/D	: Analog to digital converter
AGARD	: Advisory Group for Aerospace Research and Development
AR	: Aspect ratio
AWT	: Ankara Wind Tunnel
B	: Body

BW	: Body-Wing
BWL	: Body-Wing-LEX
BWLHV	: Body-Wing-LEX-Horizontal/Vertical Tails
BWLHVST	: Body-Wing-LEX-Horizontal/Vertical Tails-Forebody Strakes (S)- Cross-flow Transition fixing (T)
CG	: Center of gravity
DAQ	: Data Acquisition
D/A	: Digital-to-analog
DRA	: Defence Research Agency, United Kingdom
EI	: Eidetics International
FDP	: Fluid Dynamics Panel
FFA	: Aeronautical Research Institute
Hz	: Hertz
IAR	: Institute for Aerospace Research, Canada
IMFL	: Institut de Mecanique des Fluides de Lille, France
LEX	: Leading edge root extension
MDF	: Multi Degree-of-freedom
NAE	: National Aeronautical Establishment
NRC	: National Research Council
OC	: Oscillation center of the model
RTD	: Resistance temperature detector
RTO	: Research and Technology Organization
SDF	: Single degree-of-freedom
SCXI	: Signal Conditioning eXtensions for Instrumentation (bus)
SDM	: Standard dynamic model
T/H	: Track and hold
TPI	: Politecnico di Torino
VI	: Virtual Instruments
WG	: Working Group

Subscripts

IN : In-phase voltage component

OUT : Out-of-phase voltage component

j : Balance output index

O : Refers to value at time zero

T : Refers to trimmed flight condition

$\alpha, \beta, \dot{\alpha}, \dot{\beta}, p, q, r$: Denote derivative (of a moment) with respect to α, β , etc.

Superscripts

T : Wind-off mode of wind tunnel

W : Wind-on mode of wind tunnel

.

: Time derivative

CHAPTER 1

INTRODUCTION

The purpose of the present thesis is to measure the dynamic stability derivatives of a generic combat aircraft model in the Ankara Wind Tunnel (AWT) using the forced oscillation technique. Forced oscillation technique is one of the methods used to measure the dynamic stability derivatives where as one other technique is the rotary technique. In forced oscillation technique the model is set to oscillate about a mean angle of attack by small amplitude and at very low frequency.

The generic combat aircraft model is used for the tests is the AGARD Standard Dynamic Model (SDM), which is provided by the Politecnico di Torino (TPI) under a research programme supported by the NATO, Research and Technology Organization, RTO. Hence, in this respect, this thesis is a continuation of a series of research initiated in 1999, producing two theses preceding this one, [1], [2].

Today, highly agile fighter aircraft takes more attention than ever before for their capability of flying at high angles of attack and performing rapid, large-amplitude maneuvers under adverse conditions. These maneuvers result in highly non-linear, asymmetric and unsteady flows, which contain several systems of vortices. In order to predict the flight performance of aircraft undergoing such high angle-of-attack maneuvers precisely and efficiently, the structure of these very complex flows must be properly understood and the resulting aerodynamic loads must be accurately determined. Currently, the best way to accomplish this goal is to perform these tests in wind-tunnels using aircraft models at high angles-of-attack undergoing rotary or oscillatory motions.

Rotary and oscillatory experiments are performed in wind-tunnels since the beginning of the century. These tests opened up a new era in the history of wind-tunnel testing setting-up new performance requirements and expanding the range of test conditions, for highly agile aircraft.

Recognizing the need and the requirements for wind-tunnel dynamic tests, the Fluid Dynamics Panel of AGARD (FDP) has set up a Working Group (WG-16), to assess the reliability of various dynamic testing methodology in this expanded range of test conditions and to provide a data base for dynamic experiments which would illustrate the effects of systematic variation of some of the many geometric and fluid dynamics parameters involved.

In order to accomplish this mission, 7 countries from Europe and North America jointly set up an experimental programme, which involved 10 wind-tunnel facilities. Most of the experiments were carried out using three conformal models of a schematic fighter configuration denoted as WG16A, WG16CA and WG16B. In addition to the above programme, a smaller experimental programme was carried out using two generic forebody models [3].

Following these activities undertaken by AGARD, a similar program has been initiated in the Ankara Wind Tunnel as an AGARD support project. Fig.1.1 shows the road map for the progress of the current project. So far, total of three consequent theses including the current one have been prepared. The first project was the preliminary design of the experimental set-up and determining the specifications of motion control unit [1]. The second thesis was on the manufacturing, assembly and the commissioning of the experimental set-up and the integration of the data acquisition system. Some preliminary tests were already presented in this thesis to demonstrate the functionality and the reliability of the system realized [2]. Present thesis elaborates further the static and the dynamic measurements and demonstrates their validity.

This thesis consists of six chapters. In the first chapter, an introduction to the project is made.

In the second chapter, a brief literature survey with a description of the available experimental facilities and the types of experiments performed and the techniques used are given.

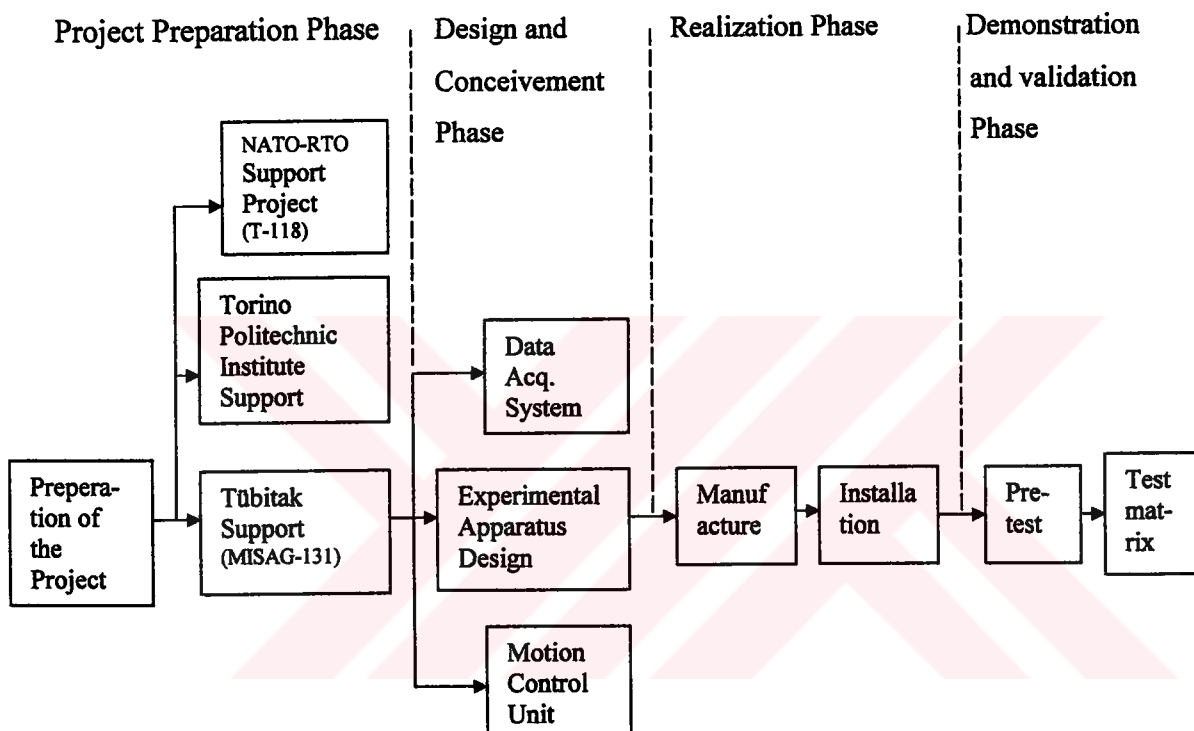


Figure 1.1 Road map for the progress of the project

In the third chapter, a brief description of the experimental set up is given. A detailed explanation of the experimental facility can be found in Mehmet Altun's thesis [2].

In the fourth chapter, the equations of motion and the dynamic derivatives involved in flight mechanics are explained. The technique of forced oscillation to measure the dynamic derivatives is discussed. The sequence of tests performed is mentioned by

using the flowchart for static and dynamic tests as well as the software written to perform these tests is explained in detail in Appendices.

The results of the static and dynamic tests are presented in chapter 5. The results of these tests, their discussion and future modifications of the experimental set-up are suggested in chapter 6.



CHAPTER 2

BACKGROUND ON DYNAMIC TESTING

In this chapter, various techniques and wind tunnel experiment types used to determine the dynamic stability derivatives will be discussed with reference to the test rigs used in the experiments.

2.1 Description of Experiment Types and Techniques

Dynamic experiments can be performed as rotary or oscillatory types. Wind tunnel dynamic experimental techniques can be classified as:

- 1) Forced oscillation techniques for single degree-of-freedom (SDF) and multi degree-of-freedom (MDF),
- 2) Large amplitude oscillations technique,
- 3) Rotary techniques,
- 4) Control surface oscillation techniques
- 5) Other techniques.

In what follows below, all these techniques will be elaborated except the forced oscillation technique, which is the technique used in this thesis and will be discussed in detail in chapter 4.

2.1.1 Large Amplitude Oscillations Technique

This wind tunnel technique is based on large amplitude, high frequency forced angular motions of the model where the restrictions of local linearity required for the small amplitude oscillatory methods are removed (Figure 2.1).

Large power outputs are necessary to generate the forcing torque on the model. The mechanical suspension system may become massive to limit both the vibrations induced by the driving unit and the deflections of the sting during wind on runs. The results of these types of tests are provided as functions of amplitude and rate (reaction surfaces instead of conventional aerodynamic derivatives) [4].

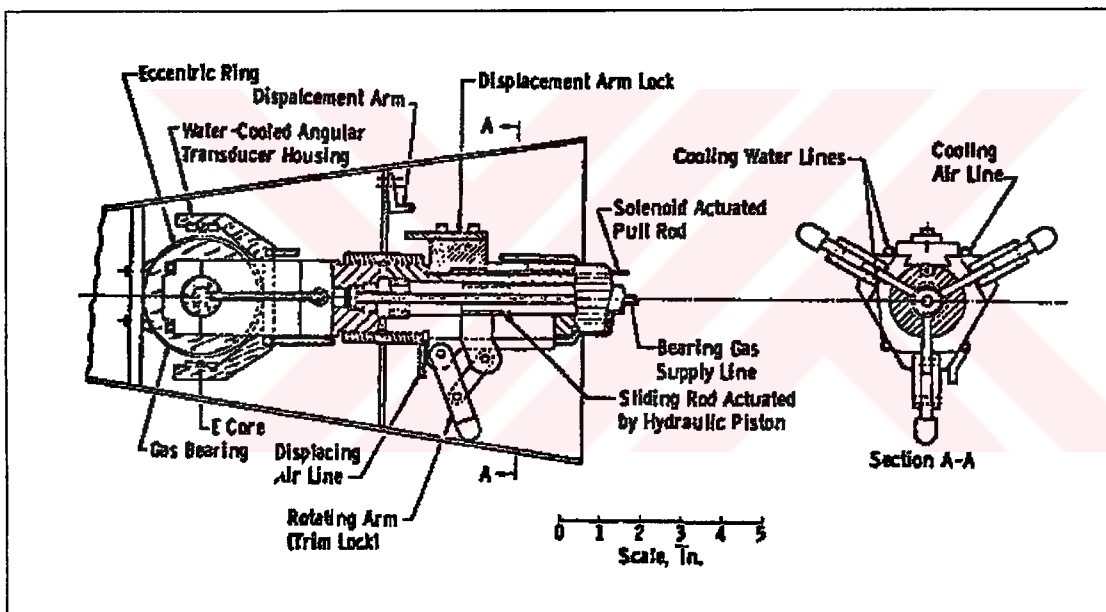


Figure 2.1 Large Amplitude Free Oscillation Pitch Apparatus at AEDC-VKF

2.1.2 Rotary Techniques

There are a number of wind tunnel techniques where the model is performing a continuous rotary motion, rather than an oscillatory motion. Some confusion exists at the present time when attempting to identify and label the individual techniques. After this explanation, the rotary experimental techniques can be classified as [5]:

- **Rolling Technique**

A rotary motion of the model around the body axis or around the wind axis, at zero to moderate angles of attack, zero sideslip and low to moderate rotation rates. The main purpose of the rolling experiments is to determine stability derivatives due to rolling (Figure 2.2).

- **Spinning Technique (as applied to missiles and projectiles)**

A rotary motion of the model around the body axis, at arbitrary angles of attack, zero sideslip and high rotation rates. The main purpose of the spinning experiments is to determine the Magnus effects.

- **Coning Technique**

A rotary motion of the model around the body axis, at arbitrary non-zero angles of attack, usually non-zero angles of sideslip and low to moderate rotation rates. The motion is sometimes referred to as the lunar motion and the apparatus employed for such experiments are often called rotary balances (Figure 2.3). The main purpose of the coning experiment is to obtain the aerodynamic reactions as functions of the coning rate.

- **Spinning Technique (as applied to aircraft)**

A coning motion where the center of gravity of the model is located off the axis of rotation and describes a circular motion with a radius called spin radius.

- **Oscillatory Coning Technique**

A coning motion around an axis that is slightly inclined to the wind axis, permitting (in principle) the determination of oscillatory stability derivatives.

- **Orbital fixed plane motion Technique**

An orbital motion of the model such that the transverse axis of the model remains in a plane which maintains a fixed orientation in the inertial frame of reference. It can be used to obtain various rotary or acceleration derivatives individually or in combinations (Figure 2.4).

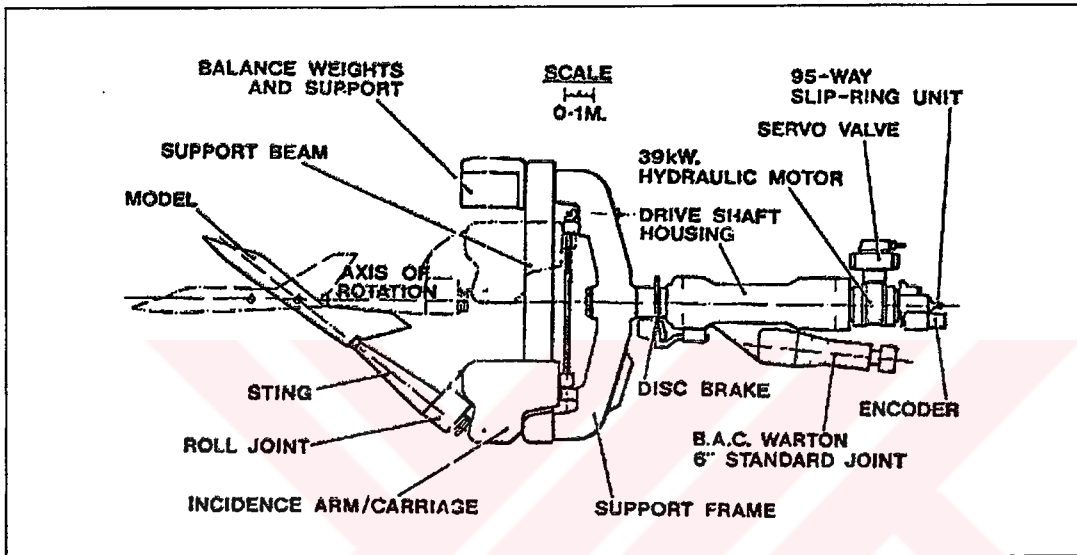


Figure 2.2 Rolling Technique at British Aerospace

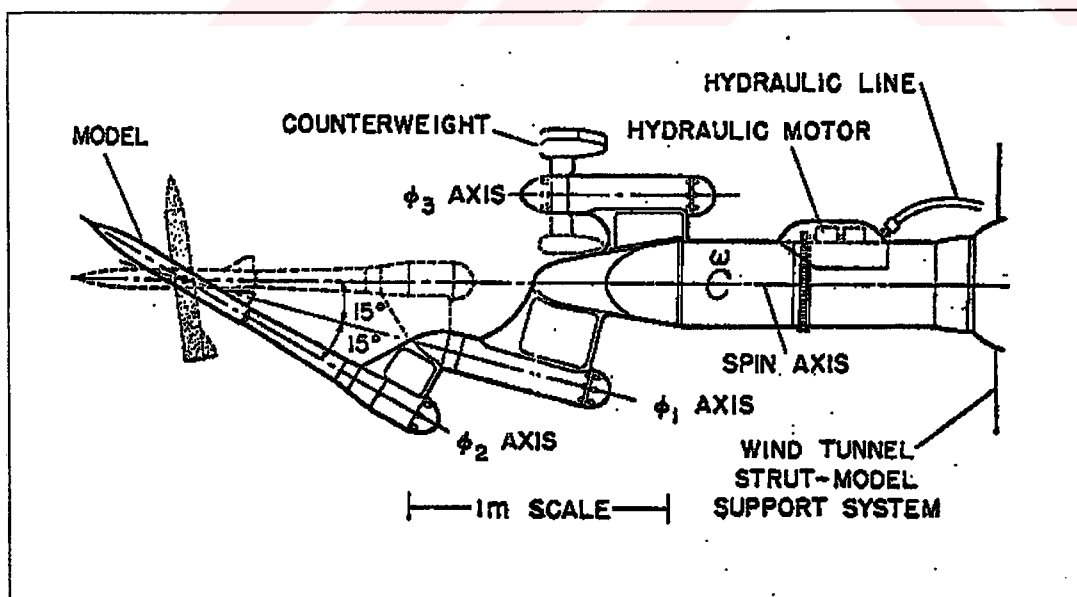


Figure 2.3 Ames Research Center's Large-Scale Rotary Balance (Coning Rig)

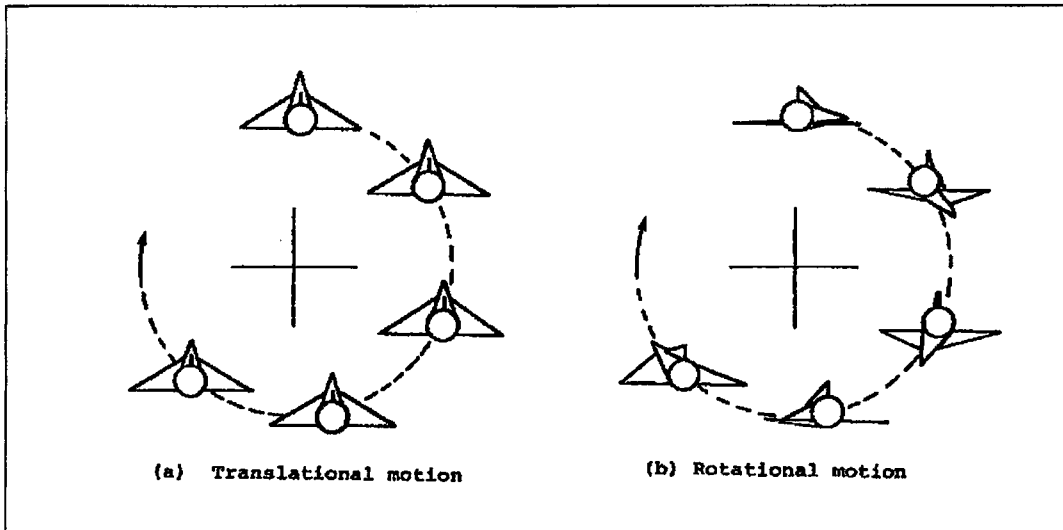


Figure 2.4 Orbital Fixed-Plane Motion

2.1.3 Control Surface Oscillation Techniques

The techniques discussed above are related to dynamic stability testing of full or half models of complete configurations. However, sometimes the dynamics of a component of an aircraft is also of interest. Most often this applies to a control surface such as an aileron. In principle, knowledge of the different effects may be required: (a) the hinge moment derivatives of an oscillating surface, and (b) the derivatives of aerodynamic reactions acting on the model due to the oscillation of a control surface (Figure 2.5). The necessary tests are most conveniently performed using a half model of the aircraft configuration; the hinge moment measurements can be performed with any of the free or forced oscillation methods, whereas the reactions of the model itself can be measured using methods similar to those employed for cross and cross-derivative measurement [5].

2.1.4 Other Techniques

- **Half-Model Technique**

The use of half models for static testing of symmetric configurations at symmetric flow conditions has been a recognized experimental procedure for a long time. This

technique eliminates all interference problems usually associated with the oscillation of a sting, permits the use of models larger than otherwise possible and allows for a more convenient arrangement of the test equipment (outside of the wind tunnel wall). On the other hand, the technique has some problems of its own, such as the possible effect of the gap between the model and the tunnel wall and effect of an interaction between the shock and the wall boundary layer. And, of course, the applications are strictly limited to symmetrical flow conditions [5].

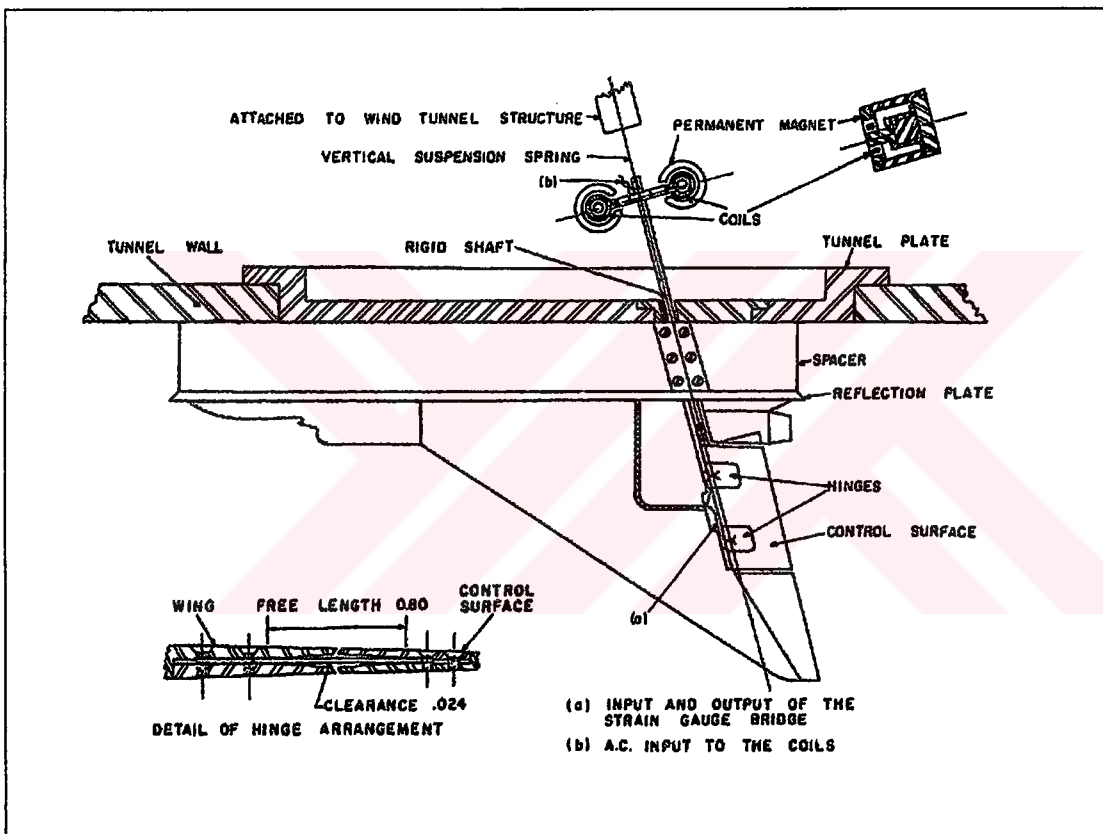


Figure 2.5 Control-Surface Oscillation at NAE

- **Model Free Technique**

In this technique, the model is free to move in a wind tunnel by using cables or magnetic suspensions for the model, dropped from platform into a vertical wind tunnel (Figure 2.6). The main advantage of this method is that the support

interference is minimized in wind tunnel test section. Aircraft controls are deflected by means of remotely controlled servo actuators [4].

- **Free Oscillation Technique**

Free oscillation is one of the first techniques adopted for the measurement of the stability derivatives. The model is suspended to an elastic support (Figure 2.7). The measurements of model oscillation displacements, after pre-load released during wind on runs, provide an estimation of aerodynamic damping. This technique is quite simple and low cost but repeatability of results may be questionable. Loads are measured and the derivatives are only identified from angular displacements and model inertial data [4].

- **Curved Flow Technique**

In curved flow technique, which can be seen in Figure 2.8, the effect of aircraft angular rates on aerodynamic loads is obtained with the superposition of curved flow in an unconventionally shaped wind tunnel test section [4].

- **Ballistic Tests Technique**

The model is launched in a closed space with some kind of propelling system and it is recovered after a soft impact. Onboard accelerometers provide the trajectory parameters and the response to control inputs [4].

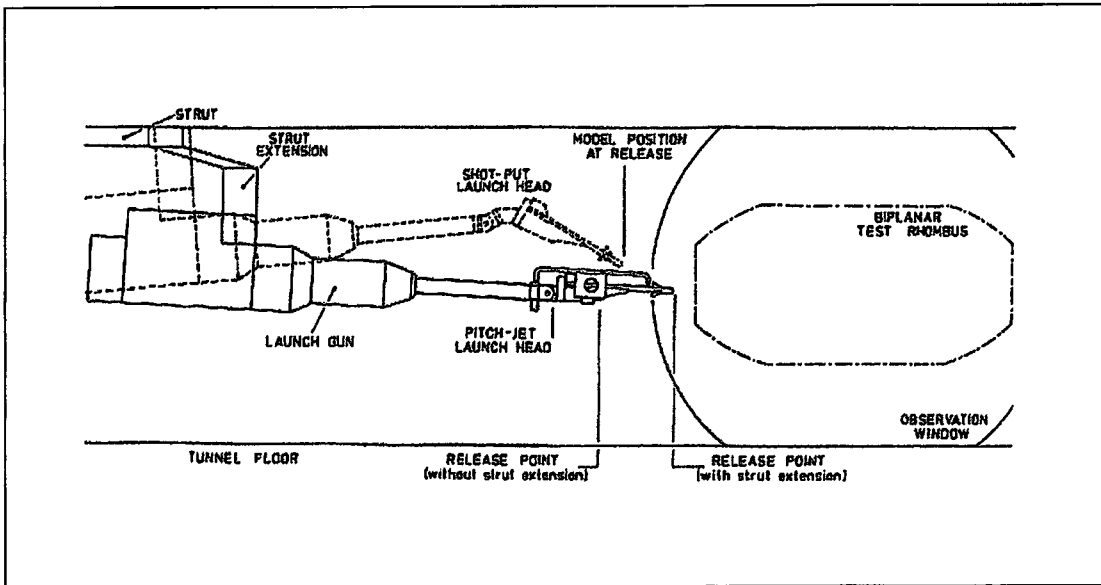


Figure 2.6 Model Free Technique

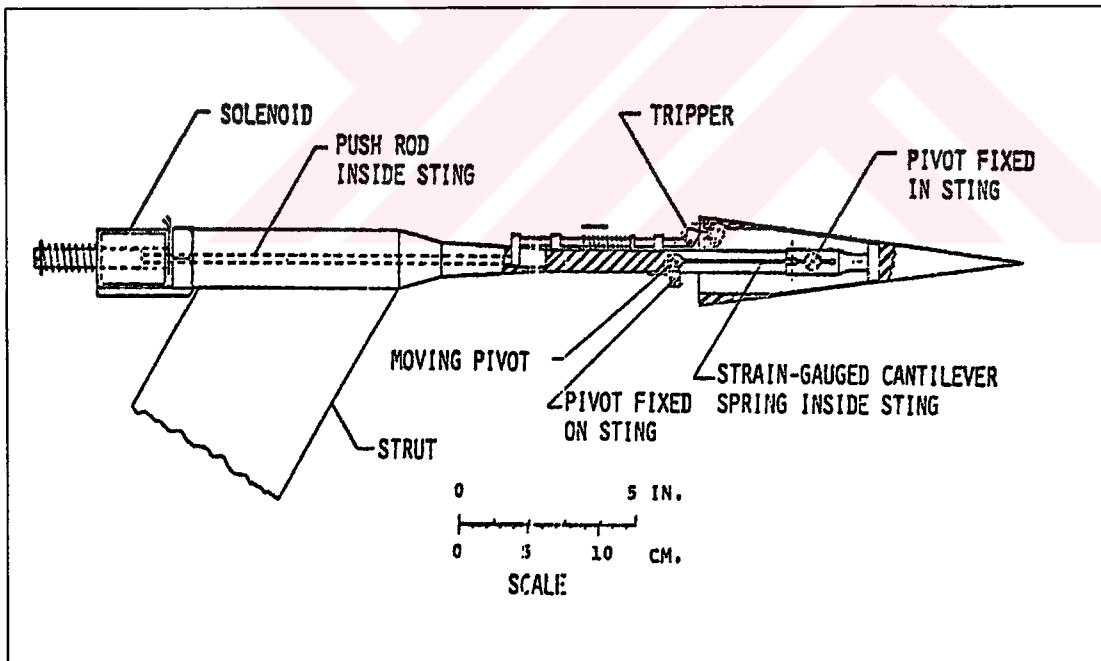


Figure 2.7 Free-Oscillation Pitch Apparatus at NAE

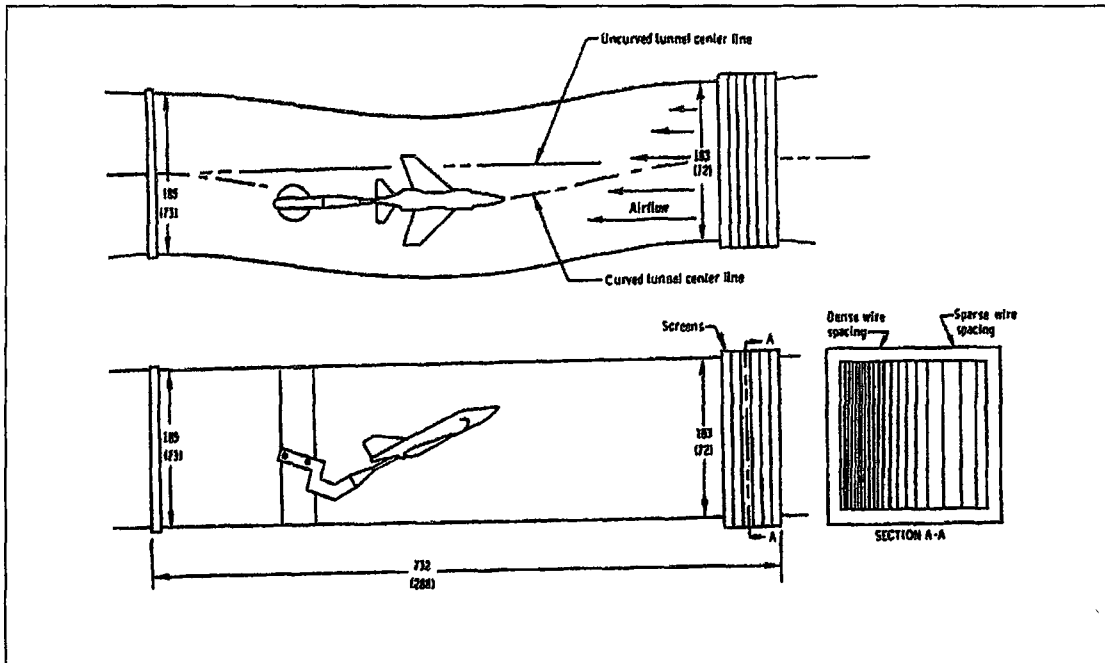


Figure 2.8 Sketch of the Curved-Flow Test Section of the Stability Tunnel

2.2 Examples of Facilities

In this part, the members of the participating organizations to the AGARD working group 16 are reviewed briefly and their facilities and test programs are given.

2.2.1 Aermacchi (AEM), Italy

In Aermacchi, tests were made on both static and rotary balances. The static balance is a rear sting support mounted on a vertical strut and allows angle of attack variation in the range 0° to 45° . Tests on rotary balance were made on the standard Aermacchi rotary balance. A rear cranked sting was used for $\alpha \leq 40^{\circ}$ and a top sting for $\alpha > 40^{\circ}$ (Figure 2.9). The AEM wind tunnel used for tests of WG16 A and B models is a low speed, open jet, 2 m diameter circular test section tunnel with a closed, single return circuit. Tests can also be made with a closed test section by fitting removable transparent walls. A fixed pitch five bladed fan, driven by a 820 hp direct current

motor, gives a wind tunnel speed up to 85 m/s but usual test speeds are 50 and 60 m/s. The contraction ratio is 5.18 and turbulence level is below 1% RMS.

Static balance tests were made on model WG16B in different configurations and have been used for comparison with rotary balance results at zero rotation and with similar static results from other wind tunnels. Rotary balance tests were made in open and closed wind tunnel test sections with both models WG16A and WG16B. Different model supports were used, allowing evaluation of wind tunnel wall and model support interference effects. Effects of nose strakes, boundary layer transition tripping, Reynolds number and angle-of-sideslip were also investigated. In this facility, water tunnel tests were also performed by using rotary rig [3].

2.2.2 Defence Research Agency (DRA), United Kingdom

The main component of the rig shown in Figure 2.10 is a model support sting, which can be oscillated in five degrees of freedom, i.e. pitch, heave (plunge), yaw, sideslip and roll. The slot is aligned horizontally for pitch and plunge motion and vertically for yaw and sideslip motion. Change of alignment is accomplished by rotating the whole assembly through 90° . The sleeve mounting for the swinging arms fits over the shaft housing and the base plate is bolted to the support structure in either of the two positions. For translational motion, i.e. heave and sideslip, the swinging arms are parallel. For pitch and yaw motion the rear stationary pivots of the swinging arms are moved further apart as shown in Figure 2.10.b. The center of oscillation coincides with the balance axis. The angle-of-attack range is normally 0° to 42° .

Tests were made in 4 m x 2.7 m Low Speed Wind Tunnel at DRA Bedford. This is a closed circuit wind tunnel with a very low turbulence level of 0.025% longitudinal at maximum speed of 90 m/s. The present tests were made at 25 m/s for longitudinal tests and 30 m/s for lateral tests. Model WG16A was tested in order to investigate the following effects,

Nose strakes and forebody grit strips

Leading edge root extension (LEX)

Oscillation frequency

Tests were made in five degrees of freedom to obtain a complete set of small amplitude longitudinal and lateral stability derivatives. For rotary balance, a diagram of the apparatus in the 13ft x 9ft Low Speed Wind Tunnel is shown in Figure 2.11. A five component balance (axial force excluded) is machined on to the end of the sting which can be axially rotated by means of a worm and wheel mechanism in the sting carrier (crank). The root end of the sting fits into a socket in the carrier and is clamped with pinch bolts. The sting can be traversed along the rotor to vary angle of attack in 1° increments. Weights can be fixed to the ends of the rotor to maintain static balance [3].

2.2.3 Deutsche Forschungsanstalt Für Luft und Raumfahrt (DLR), GERMANY

The rotary balance and working section of the 3.25m x 2.8m low speed wind tunnel are shown in Figure 2.12. The present test arrangement allows rotary coefficients to be determined in the horizontal wind tunnel by means of a measuring system similar to that used for steady force and moment measurements. Using three different interchangeable stings covers the specified total range of angle of pitch between 10° and 90° . The angle of sideslip is manually adjusted by rotating the front part of the sting about its axis, which is the longitudinal or vertical body axis of the model, depending on the sting being used. The rotary rig has the capability of changing the angle of pitch remotely within a range of 30° , even during rotation and wind-on conditions. This capability allows the engineer to set the angle of pitch continuously, to increase the test efficiency and to better investigate hysteresis effects in the stall and post-stall regimes of rolling or spinning aircraft [3].

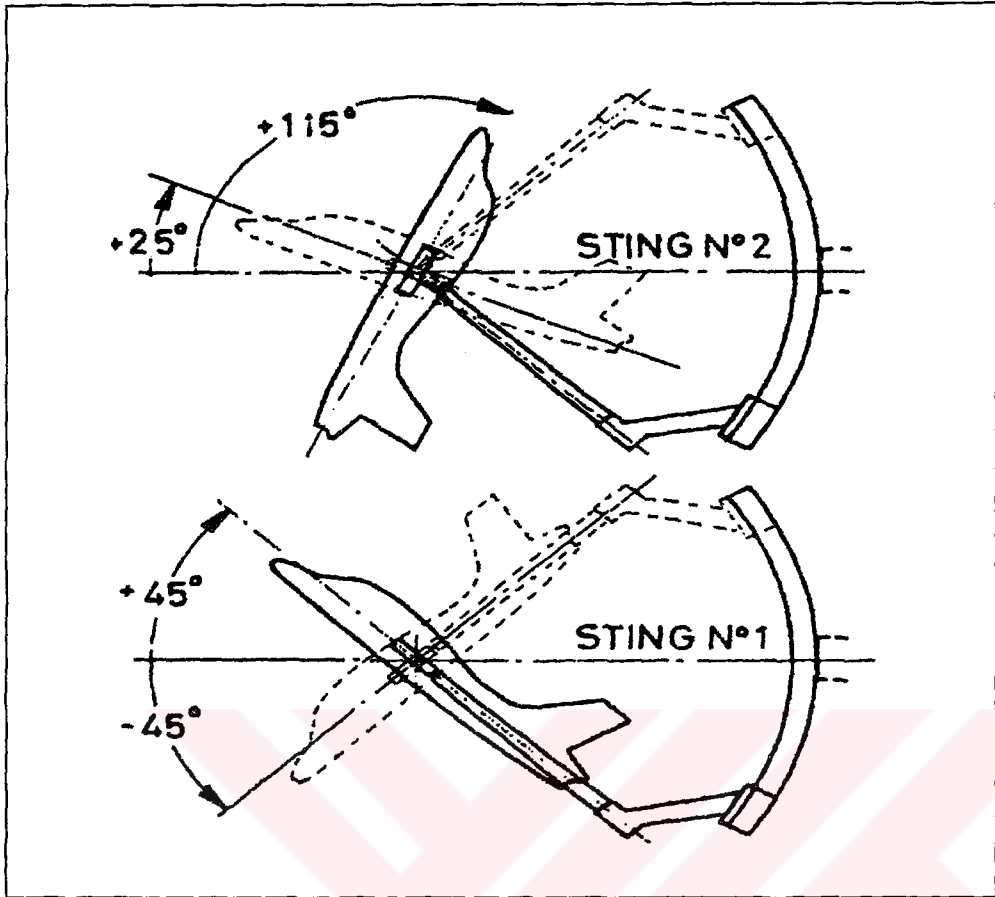


Figure 2.9 AEM Rotary Balance Stings

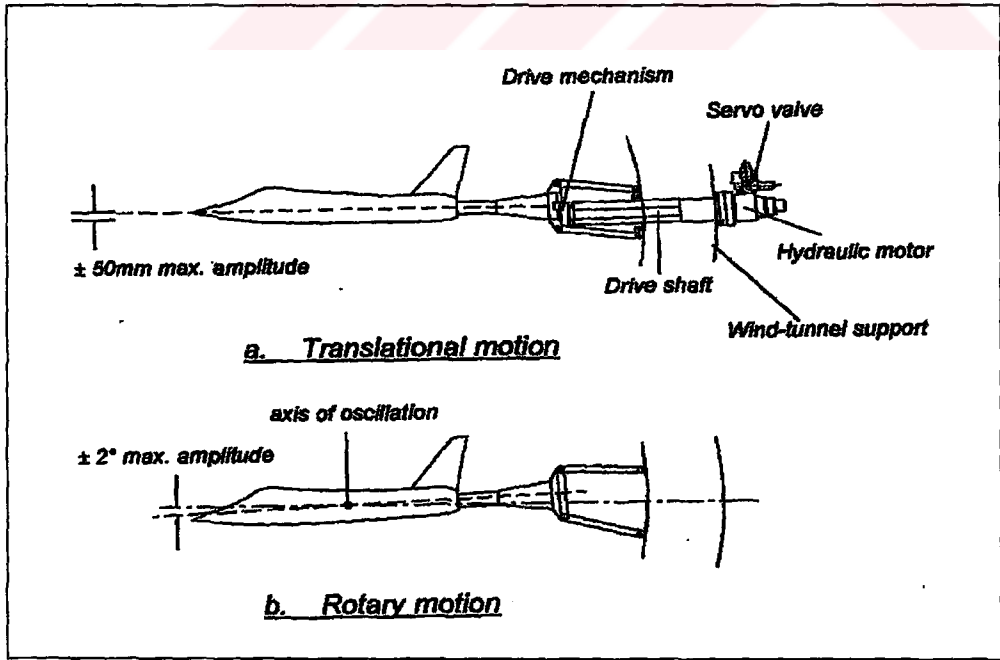


Figure 2.10 DRA Inexorable Drive Rig

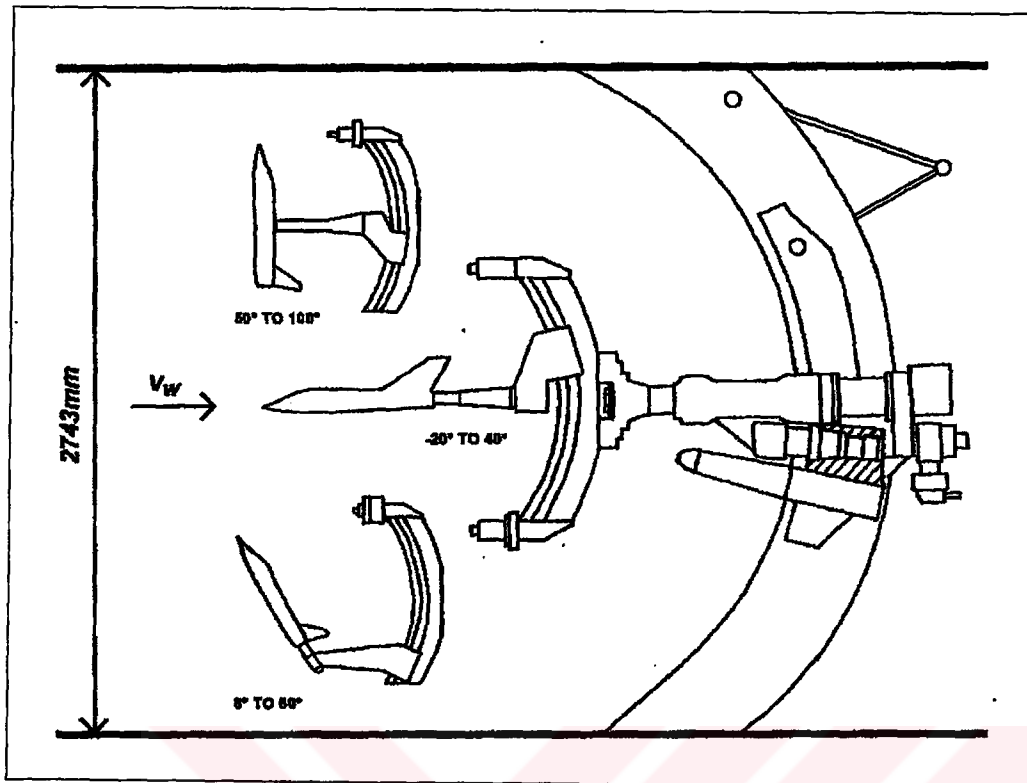


Figure 2.11 DRA Rotary Balance

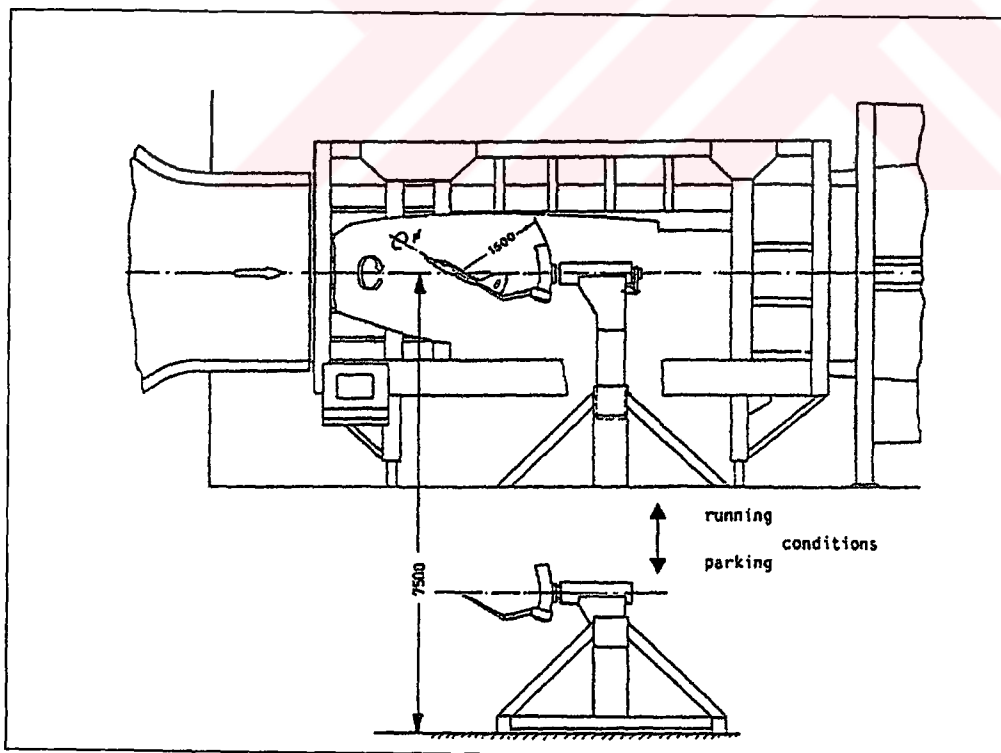


Figure 2.12 DLR Rotary Balance

2.2.4 Eidetics International/NASA Ames (EI), USA

The Eidetics/Ames rotary-balance apparatus is a modified rig developed originally at NASA-Ames and last used in 1983. It is driven by a hydraulic pump and motor system with a tachometer used as feedback to a servo-valve for speed control. New hardware to support the model was recently designed by Eidetics International and constructed for tests with an F/A-18 model to investigate forebody vortex control techniques under rotating conditions. The same hardware was used for this test. The maximum rotation speed for the new hardware is 350 rpm. Figure 2.13 shows the new apparatus as installed in the 7 ft x 10 ft wind tunnel, including a C-strut, strut arm and sting. The angle of attack is adjusted with discrete positions of the sting/clevis on the C-strut (0° to 60° in 3° increments) and rolling the sting in the strut arm sets sideslip angle. Most of the model configurations were tested at three different free stream velocities, 200 ft/sec (60 m/s), 150 ft/sec (45 m/s), and 100 ft/sec (30 m/s) in order to assess Reynolds number effects. All of the various configurations from body alone to full configuration were tested at angles of attack of 24° , 39° , and 51° and only the full configuration at 60° . Some of the configurations, primarily those without strakes, were tested only at the high and low Reynolds numbers [3].

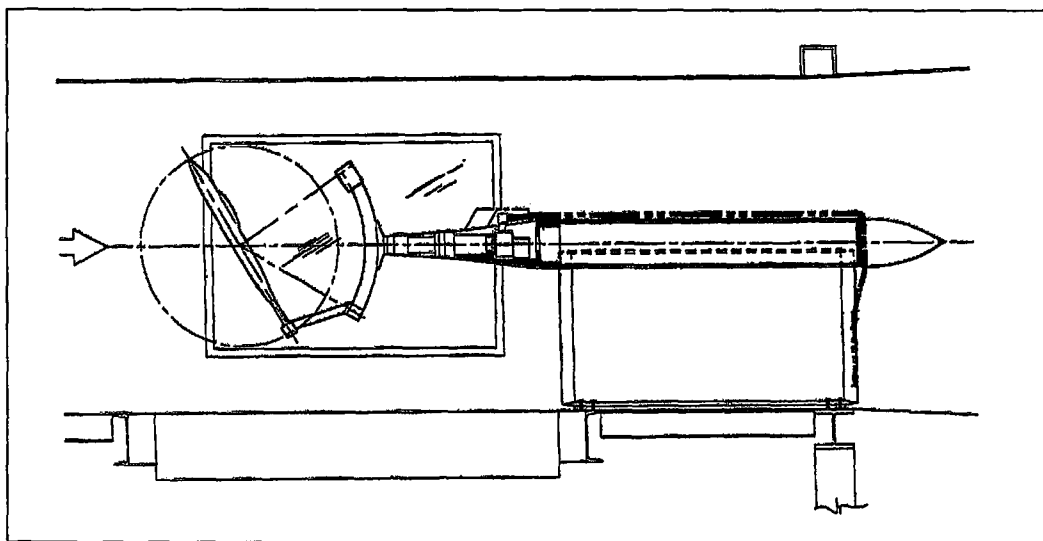


Figure 2.13 General Arrangements of NASA Ames/Eidetics Rotary Balance and Support System in 7 ft x 10 ft Wind Tunnel

2.2.5 Institute for Aerospace Research (IAR), Canada

The tests were conducted in the IAR 2m x 3m Low Speed Wind-Tunnel, a continuous flow facility operating at ambient test section pressures and temperatures in the speed range up to 120 m/s. The model was sting-mounted in the wind tunnel. The sting protruded from a strut cantilevered through the wind tunnel floor. A moving section of the floor travels with the strut and connects with roll-up mechanisms on either side of the test section. When the strut moves in an arc with a center on the model rotation axis the pitch angle of the model could be changed in the range $-40^\circ \leq \sigma \leq 40^\circ$. Higher pitch angles, up to a maximum of $\sigma = 54^\circ$, could be attained by offsetting the sting. The layout of the asymmetric support system is shown in Figure 2.14. The 15000 N pitch / yaw forced-oscillation apparatus was developed to investigate the dynamic characteristics of aircraft models at high angles of attack. The apparatus comprises a driving / positioning system (aft end), and an oscillating mechanism and dynamic balance (front end). The driving system provides precise harmonic motion. The operating frequencies are in the range 0-15 Hz. A clutch-operated mechanism with a precise angular encoder is used for remote adjustment of roll angle in the range -150° to 180° . Combining roll angles with pitch angles permits testing at arbitrary angles of sideslip.

The BWLHV, BWLHVST and BWHV configurations were tested in the IAR at the following test conditions. In these notations, B stands for the body (fuselage), W for the wing, L for the leading edge extension, H for the horizontal tail, V for the vertical tail, S for the forebody strakes and T for the transition fixing.

Velocity	: 20, 25, 30, 70 m/s
Angle of attack	: 0° to 53°
Angle of sideslip	: 0° , $\pm 5^\circ$, $\pm 10^\circ$
Tail deflection	: 0° , $\pm 30^\circ$
Mode of motion	: Static, pitching/yawing oscillation

Oscillation amplitude : 1.2° , 0.5°

Frequency : 5 Hz

Various factors were investigated that influence the static aerodynamic coefficients and the dynamic force and moment derivatives. These factors were tip geometry, Reynolds number, configuration, sideslip angle, amplitude, horizontal tail deflection and support asymmetry [3].

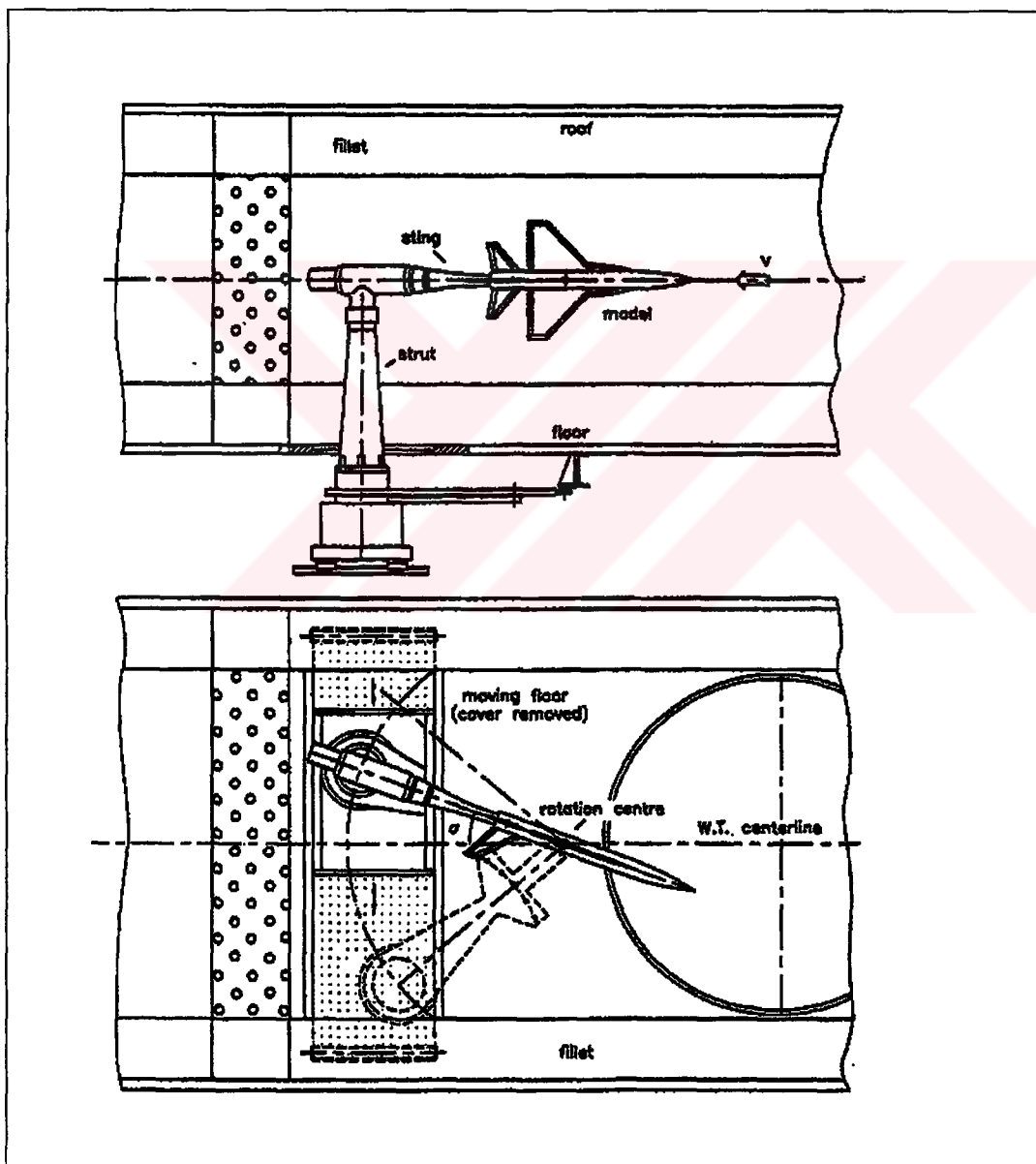


Figure 2.14 IAR Asymmetric Support System for Oscillatory Tests

2.2.6 ONERA-IMFL, France

Oscillatory Rig

The system is installed in the IMFL's horizontal wind tunnel, which is 2.4m in diameter and has an open test section. The experimental set up used in wind tunnel allows kinematic representation of the Euler degrees of freedom commonly used in flight mechanics. The model is mounted on a rear sting and the rig is designed so that the bulky elements remain outside the airstream during tests (Figure 2.15)

In static mode, measurements can be made through a very wide range of incidence ($-100^{\circ} < \alpha < 100^{\circ}$) for sideslip angles of less than 20° . Slow α and β sweeps can be performed for static data with no significant rig interference. Dynamic terms like pitching moment damping coefficient ($C_{mq} + C_{m\dot{\alpha}}$), yawing moment damping coefficient ($C_{nr} - C_{n\beta} \cos \alpha$) can be calculated for different angles of attack by applying harmonic type motions of moderate amplitude.

The emphasis of the tests was on demonstrating different types of test data obtainable for a complete combat configuration rather than on testing a variety of model configurations. Hence the model WG16A was tested with and without forebody strakes/grit strips. The test program included,

Slow α -sweeps at sideslip for static data

Small amplitude pitch and yaw tests to measure derivatives

Large amplitude pitch oscillations

α -ramps at various pitch rates.

Rotary Balance

The installation of the rotary balance in the vertical wind tunnel offers the specific conditions for direct simulation of developed steady spins. An important advantage

of this approach is the elimination of the mechanical load variations produced by the gravitational forces which would occur in a horizontal-type tunnel. The wind tunnel has an open working section, 4 m in diameter and the maximum speed is 45 m/s.

As for the tests with the apparatus, the aim was to investigate the effects on data of test technique rather than configuration. The test program included:

Slow α -sweeps for static data.

Coning tests at low and high α and with sideslip

Oscillatory coning tests for measurement of derivatives

Large-amplitude oscillatory coning tests [3].

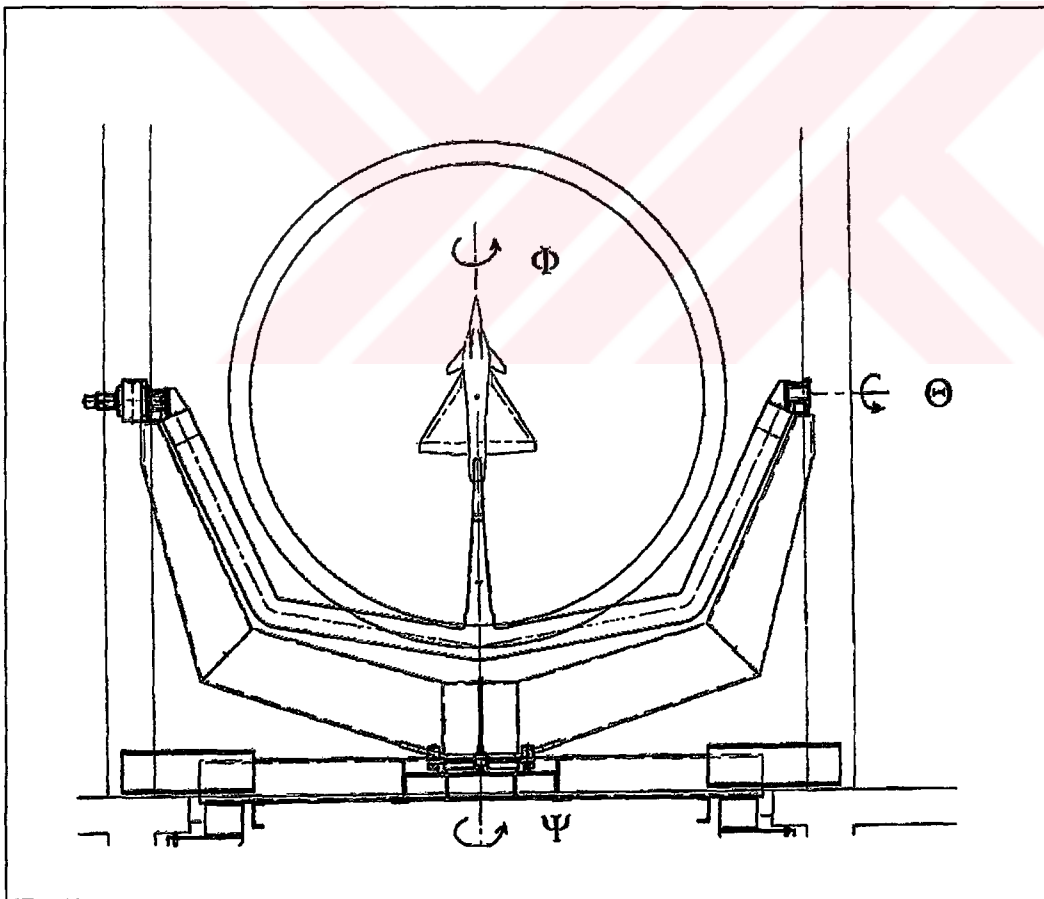


Figure 2.15 ONERA-IMFL Rig

2.2.7 Politecnico di Torino, Italy

The apparatus (Fig 2.16) was designed for static and small amplitude pitch and roll oscillatory tests on aircraft models in the Politecnico di Torino D3M low speed wind tunnel. It is of the direct forced oscillation type with servo-mechanical operation. A vertical strut supports the model and strain gauge balance, which is connected by links and levers to an oscillating vertical rod. The linkage can be changed to drive the model in either pitch or roll. The aerodynamic loads acting on the model are measured with a 5 component internal strain gauge balance (axial force excepted).

Oscillatory motion of the model is excited by means of a driving unit placed under the floor of the wind tunnel test section. The unit is powered by a DC motor and is linked to the main rod, which drives the model, by a gearbox connected to an adjustable flywheel. The oscillation amplitude of the model is set by adjusting the flywheel radius in the range ± 50 mm which corresponds to a pitch or yaw amplitude of $\pm 3.5^\circ$. The oscillation frequency (maximum 5 Hz for lighter models) is set by the rotation speed of the DC motor. Angle-of-attack and sideslip are varied using stepper-motors to drive the lever at the rear of the model for angle-of-attack and to rotate the vertical strut for sideslip. The range of adjustment is -7° to 45° for α and -13° to 13° for β . Experiments were conducted in the D3M low speed wind tunnel, which is a closed circuit wind tunnel with a contraction ratio of 5.44. The test section is circular with a diameter of 3 m. The turbulence level is 0.3%, at $V_\infty = 50$ m/s. Static, pitch and roll tests were made to investigate the following effects,

- Longitudinal transition fixing on forebody,
- Forebody strakes,
- Leading edge root extension

The primary dynamic derivatives are measured and cross-coupling derivatives can also be measured [3].

2.2.8 Aeronautical Research Institute of Sweden (FFA)

The low speed wind tunnel LT1 is an atmospheric, continuous, closed circuit tunnel with a test section diameter of 3.6 m and a length of 8 m. Maximum wind speed is 85 m/s. There are two interchangeable test sections. The rotary balance rig was constructed and built in the mid 1980s (Fig 2.17). It is driven by a hydraulic pump and motor. An electrical motor is used to set the angle of attack (α) remotely. Angles of attack up to $\pm 150^\circ$ can be set by using different sting mountings, The rotation speed range is 15 to 360 rpm at a wind speed of 60 m/s and a model weight of 8 kg. The rig is designed to accommodate models of fighters in the scale range: 1/10 to 1/15. Static and rotary tests were made on model WG16B. The following effects were investigated over an angle-of-attack range of 0° - 69° degrees.

Angle of attack, configuration build up, Reynolds number, forebody longitudinal transition fixing, type of model support, rotary rig interference, forebody nose strakes, nose strake asymmetries, repeatability [3].

2.2.9 NASA Langley/Bihrlle Applied Research/DRA

As part of a NASA/DRA Joint Aeronautical Programme an experimental study was made of the effects of Reynolds number on forces generated by wind-axis rotation of simple fuselage bodies. Rotary balance experiments, including force and moment and surface pressure measurements, were conducted on circular and rectangular section aftbodies with hemispherical and ogive noses at the DRA Bedford 13ft x 9ft atmospheric wind tunnel and the 8ft x 6ft pressurized wind tunnel at DRA Farnborough in the United Kingdom. The bodies were tested at 60° and 90° angle of attack for a wide range of Reynolds numbers in order to observe the effects of laminar, transitional, and turbulent flow separation on the forebody characteristics when rolling about the velocity vector.

The tests were conducted over a range of Reynolds numbers (based on diameter) from about 0.08 to 2.25 million, a Mach number range of 0.024 to 0.21, and at angles

of attack of 60 and 90 degrees. The rotation rate varied from $\Omega b/2V=0.0$ to 0.4 in both positive (clockwise) and negative (counter-clockwise) directions. Pressure data were taken concurrently with force and moment data during each run [3].

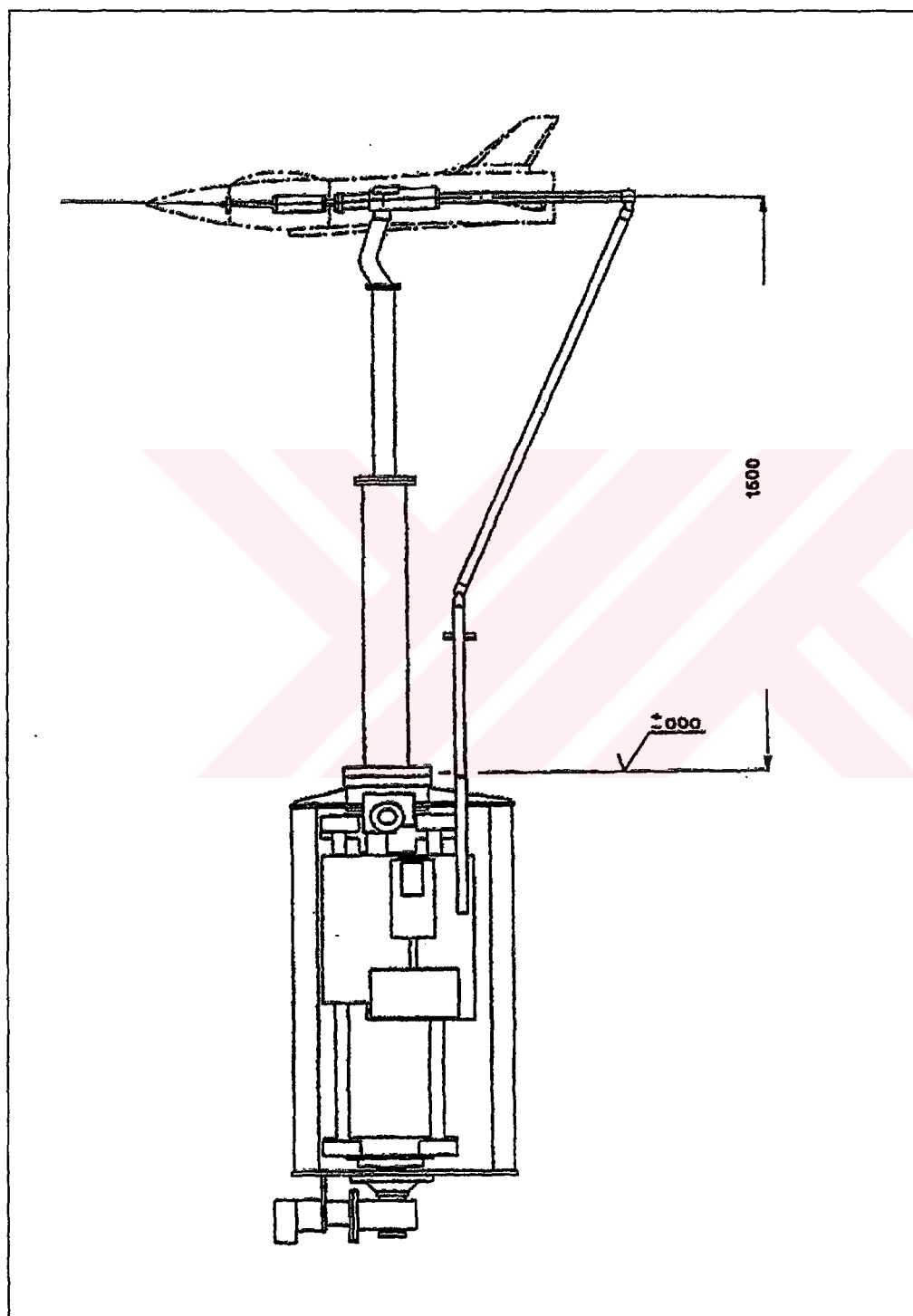


Figure 2.16 The TPI oscillatory balance

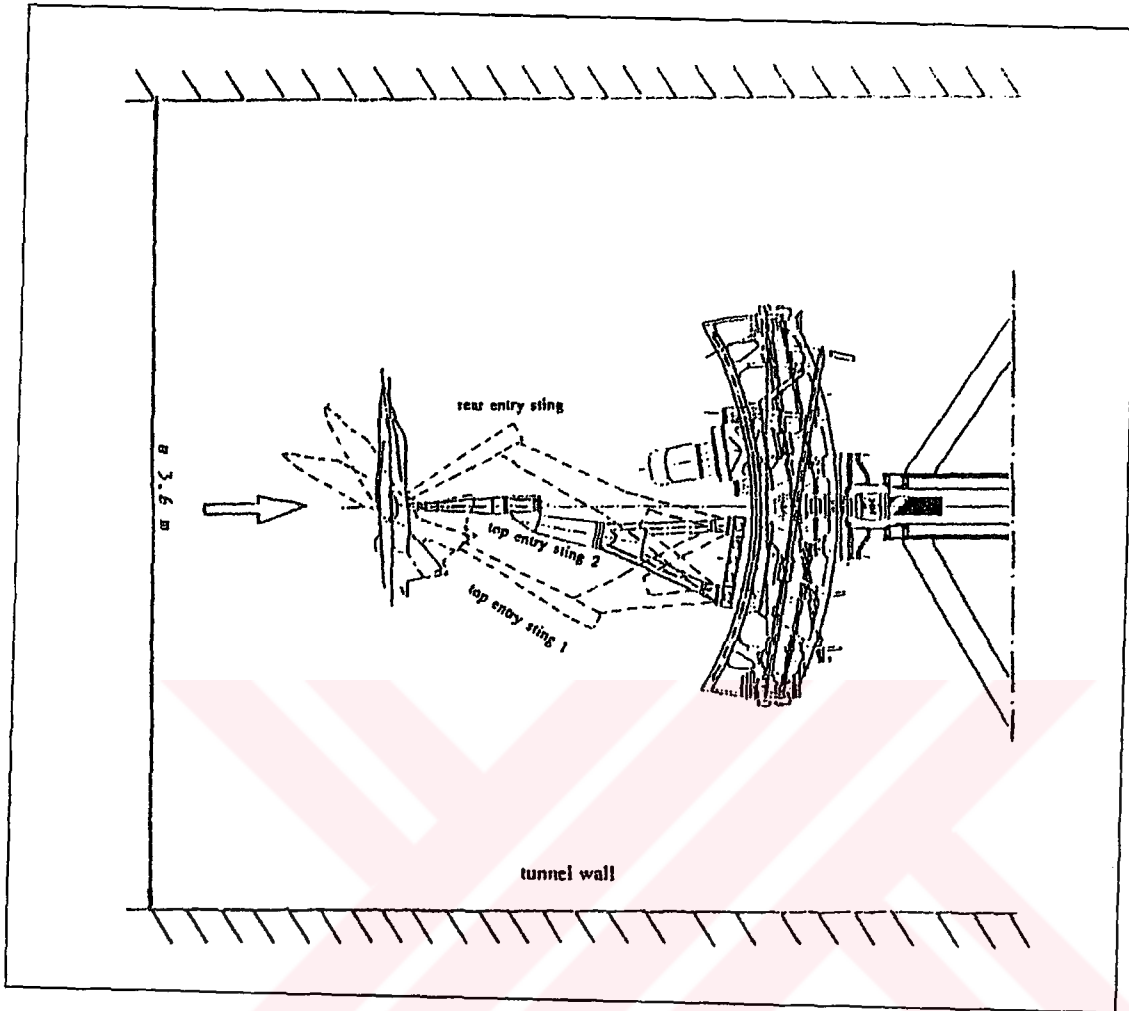


Figure 2.17 FFA Rotary balance

CHAPTER 3

EXPERIMENTAL SET UP

In this chapter, a brief description of the experimental set-up, the generic combat aircraft model which is also called the standard dynamic model, the data acquisition system, and its interface to the measuring sensors and the computer, the internal balance system with its force transducers are given. Their details can be found in Altun's thesis [2].

3.1 Description of the Apparatus

In order to perform the static and the dynamic tests on the model a servo mechanical system is designed and manufactured for the Ankara Wind Tunnel (AWT). At present, this system generates simple harmonic oscillatory motions for the Standard Dynamic Model (SDM) in the pitch plane only with one rotational degree of freedom.

Table 3.1 gives the parts list and Figure 3.1 shows the general perspective view of the experimental set-up. The driving unit placed under the floor of the wind tunnel test section generates the oscillatory harmonic motion of the model. It is powered by means of a DC servomotor and is linked to the oscillating vertical push rod (11) that oscillates the model from the rear of its fuselage by a crank-rod mechanism (16).

The amplitude of oscillations for the model is adjusted by setting the flywheel's (16) eccentricity radius, which can be changed within a range of 50 mm causing $\pm 5^\circ$ of

pitch oscillations in amplitude for the model. The oscillation frequency of the model, whose upper limit is 5 Hz, is set by the rotational speed of the DC servomotor.

The angle of attack range of the experimental apparatus is between -15° and $+45^\circ$. The sideslip angle of the model can be adjusted ranging from -45° to $+45^\circ$. Angle of attack and sideslip angle adjustments are made manually.

Table 3.1 Parts List of the Experimental Set-Up Given in Figure 3.1

Part Number	Part Name
1	Platform Ceiling Plate
2	Supporting Pipe of the Vertical Strut
3	Side Slip (β) Plate
4	Side Slip (β) Indicator
5	Lower End Part of the Vertical Strut
6	Middle Part of the Vertical Strut
7	Upper Part of the Vertical Strut
8	Adapter Connection Part of the Main Strut
9	The Model Adapter
10	The Extension Bar of the Model Adapter
11	Oscillating Vertical Push Rod
12	Support Assembly
13	Adjustable Arm
14	α_{mean} Adjustment Assembly
15	Servo Motor Flange
16	Crank-Rod Mechanism
17	Servo Motor and Crank Rod Connector

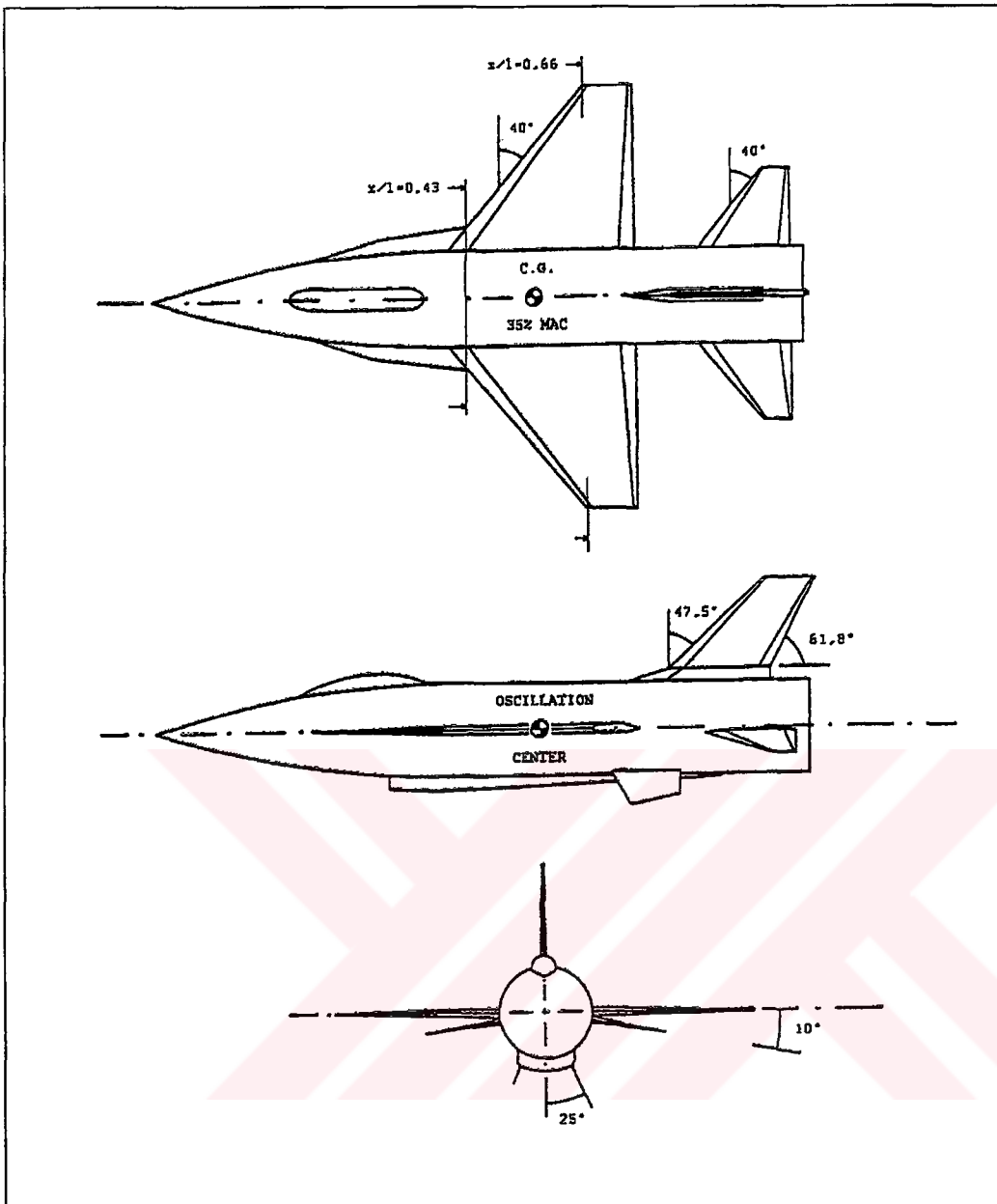


Figure 3.2 The geometry of the Standard Dynamic Model used in the tests.

3.2 The Standard Dynamic Model (SDM)

The standard dynamic model (SDM) used in the tests is shown in Figure 3.2. This is a calibration model which was first introduced by the National Research Council of Canada (NRC) / Institute for Aerospace Research (IAR) in 1978, specifically designed for dynamic tests [6].

The material used for the model an aluminum alloy and the wing surface is trapezoidal in form with a 40⁰ sweep angle. The main geometrical dimensions of the SDM can be seen in Table 3.2.

The experiments were conducted in the AWT low speed wind tunnel whose test section dimensions are 3.05 x 2.44 x 6.10 m. The ratio of span to tunnel width is;

$$\frac{b}{w} = \frac{0.609}{3.05} = 0.199 \quad (3.1)$$

The fuselage length to height ratio is;

$$\frac{l}{h} = \frac{0.943}{2.44} = 0.386 \quad (3.2)$$

Wall interference is, therefore, expected to be negligible, except at high angles of attack [7].

The ratio of wing to test section area is;

$$\frac{S}{S_{WT}} = \frac{0.117}{3.05 \times 2.44} = 0.015 \quad (3.3)$$

With respect to the models previously tested in other facilities, The TPI and also AWT model is larger, because of the dimensions of test section, that reduce the blockage effects to negligible values; The wake blockage influence on the static coefficients of the model has been corrected at high angles of attack in the TPI and was shown to be small. Therefore, the model wake blockage is negligible for $\alpha < 30^0$ because of the ratio, $S/S_{WT}=0.015$ is quite low [7], [8].

Table 3.2 Main Dimensions of the SDM

Length	0.943 m
Span	0.609 m
Mean Aerodynamic Chord	0.220 m
Wing Area	0.117 m ²
Fuselage Diameter	0.135 m
Ogive Ratio	3:1
Weight(without balance and adaptor)	8 kg.

3.3 Data Acquisition System (DAQ)

In this part, components of the data acquisition system and the description of their elements are explained briefly.

3.3.1 Components of DAQ

The function of any data acquisition system is to convert the “real world” (which is the current and voltage produced by physical phenomena such as temperature, pressure, force, flow and level when monitored by the proper transducer) signal into an appropriate digital representation. The purpose of digitizing the signal is to allow the acquired data to be processed by a computer, stored into memory, displayed, or output to some type of controlling device [9].

The data acquisition system used to perform the digitization of data is shown schematically in Figure 3.3. The measurement system installed at AWT in order to measure the stability derivatives is composed of; motion generation and control unit, force transducer, signal conditioning unit, and the data acquisition unit (A/D Conversion). All these units are interfaced to a personnel computer to control, store and display the parameters.

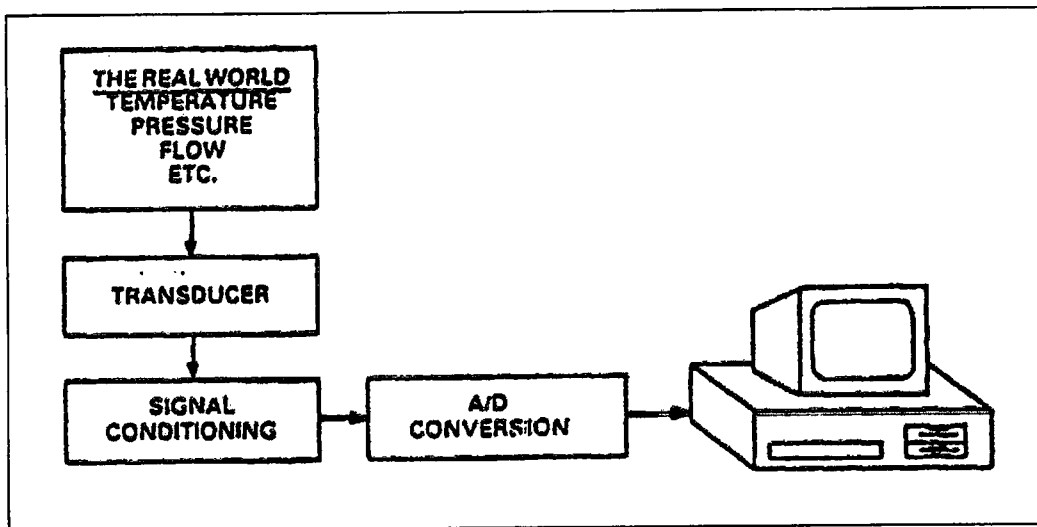


Figure 3.3 Components of a Data Acquisition System

3.3.2 Description and Properties of Components of DAQ System;

- **Motion Generation and Control Unit**

The motion generation and control unit is composed of a DC servomotor and its driver. The servomotor series 6SM57S-3000 is produced by Kollmorgen in Germany. It is linked to the oscillating vertical push rod (11). The revolution of servomotor results in the harmonic motion of the model by means of moving the oscillating vertical push rod.

Some properties of the series 6SM57S-3000 DC servomotor are;

- Standstill torque 4,6 Nm
- Standstill current 2,8 A
- Rated Speed 3000 min⁻¹
- Torque Constant 1,65 Nm/A
- Rotor Moment of Inertia 3,1 kg cm², etc.

The speed of the servomotor is controlled by the driver unit, which is driven by the software written. The frequency of oscillation of the model is set directly by the rotational speed of the DC servomotor.

- **Internal Balance System and Force Transducers**

The internal balance system used to measure the normal and side forces as well as rolling, pitching and the yawing moments of the moving SDM is designed and manufactured by Politecnico di Torino. Technical drawing of the five-component internal balance force transducer system is given in Figure 3.4.

Although the internal balance used is a five component balance designed to measure, pitch, roll and yaw moments as well as the normal and side forces with the exception of the axial force, during the present experiments only three of these components are measured due to limitations in the number of simultaneous sampling channels of the DAQ system. These three channels are used to measure the normal force, the pitch and the roll moments. Hence, the original 5 x 5 calibration matrix of the internal balance is reduced to 3 x 3 matrix to adapt to the present situation. The reduced calibration matrix is given as [2];

$$\begin{bmatrix} L \\ Z \\ M \end{bmatrix} = \frac{2000}{G * V_0} \begin{bmatrix} 0.04558 & -0.00396 & -0.00344 \\ 0.00147 & 0.84753 & -0.01838 \\ 0.00039 & 0.00023 & 0.03897 \end{bmatrix} \begin{bmatrix} VL \\ VZ \\ VM \end{bmatrix} \quad (3.1)$$

where L, Z, M, are the rolling moment, normal force and pitching moment respectively. G is the actual gain of the amplifier, V₀ is the voltage supply of the internal balance. VL, VZ, VM are the balance voltage outputs; rolling moment, normal force and pitching moment respectively.

In the present tests, the actual gain of the amplifier, G, is set to 2000 and the voltage supply of the internal balance, V₀, is set to 9 Volts.

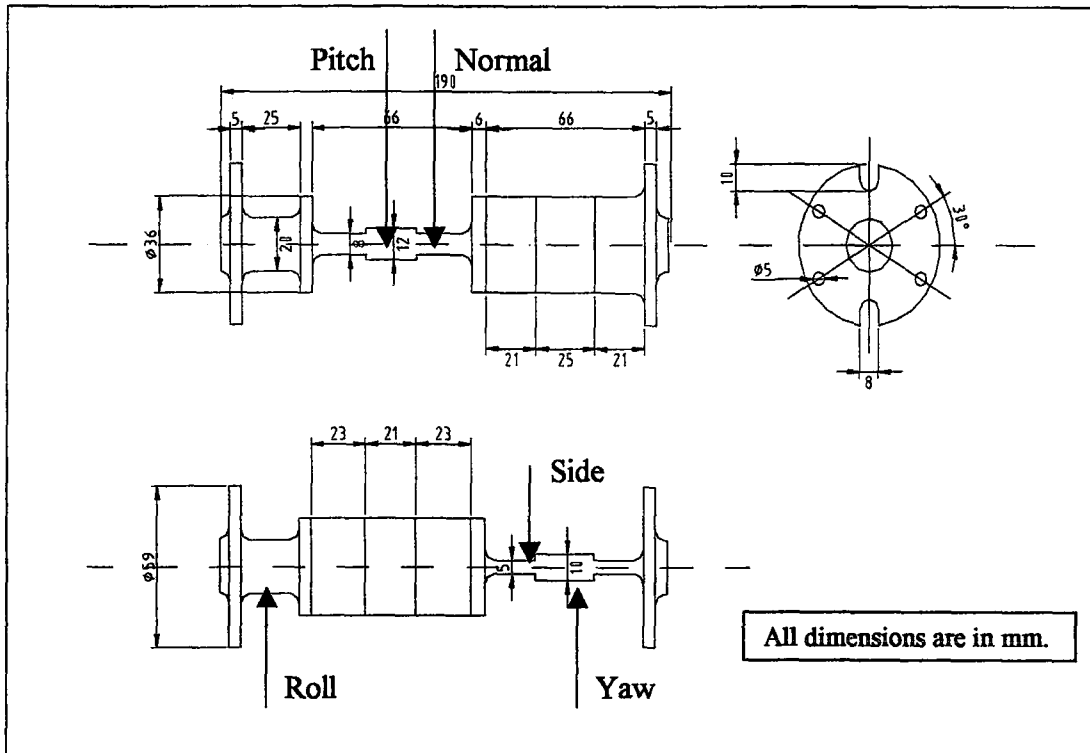


Figure 3.4 Technical drawing of the internal balance

- **Signal Conditioning Unit**

The analog-to-digital conversion process requires clean, high-level voltage inputs to the A/D converter. Signal conditioning unit manipulates the input signals so that the data acquisition board may digitize them properly [9]. The signal conditioning unit used includes amplification, filtering, electrical isolation, multiplexing and completing the bridge of transducers to produce high level signals for the data acquisition device. The National Instrument's SCXI-1120 and SCXI-1140 products are chosen as signal conditioning units for the internal balance measurements. SCXI-1321 and SCXI-1301 terminal blocks are used for SCXI-1121 and SCXI-1140 respectively. These signal conditioning modules are placed in a 12-slot SCXI-1001 chassis.

SCXI-1121 consists of four isolated input channels and four isolated excitation channels. Each channel is isolated and independently configurable via jumpers. The

SCXI-1121 is a module for signal conditioning of strain gauges, RTDs, thermistors, thermocouples, volt and millivolt sources, etc. The module has 250 V_{rms} working isolation, excellent noise immunity, and amplifier gains ranging from 1 to 2000. The analog input range of SCXI-1121 is ± 5 V. Each channel also includes a 3-pole lowpass filter that can be configured for 4 Hz or 10 kHz. SCXI-1321 terminal block is used in conjunction with the SCXI-1121 board, since it facilitates the offset nulling and shunt calibration capability of the strain gage sensor signal going into SCXI-1121 [10].

SCXI-1140 is an 8-channel, simultaneous-sampling differential amplifier module. Each channel contains a high-input impedance instrumentation amplifier with switch-selectable gain followed by a Track/Hold (T/H) amplifier. The T/H amplifiers all sample at the same time, which is useful for preserving interchannel phase relationships. Each analog input channel of the SCXI-1140 has its own instrumentation amplifier with differential inputs. It can be configured such that each channel can be independently adjusted for a gain of 1, 10, 100, 200 or 500. The SCXI-1301 terminal block with 20 screw terminals is also used with the SCXI-1140 module [11].

- **Data Acquisition Card**

Our data acquisition card is the National Instrument's (NI) PCI-6024E card. Some specifications of this card are;

Analog Inputs:

- 16 single-ended, 8 differential channels
- 200 kS/s sampling rate
- 12-bit resolution

Analog Output:

- 2 channels
- 12-bit resolution

Input ranges of channels of PCI-6024E are software programmable with gains of 0.5, 1, 2, 5, 10, 20, 50, 100 and A/D conversion range of ± 5 Volts or 0 to 10 Volts [11].

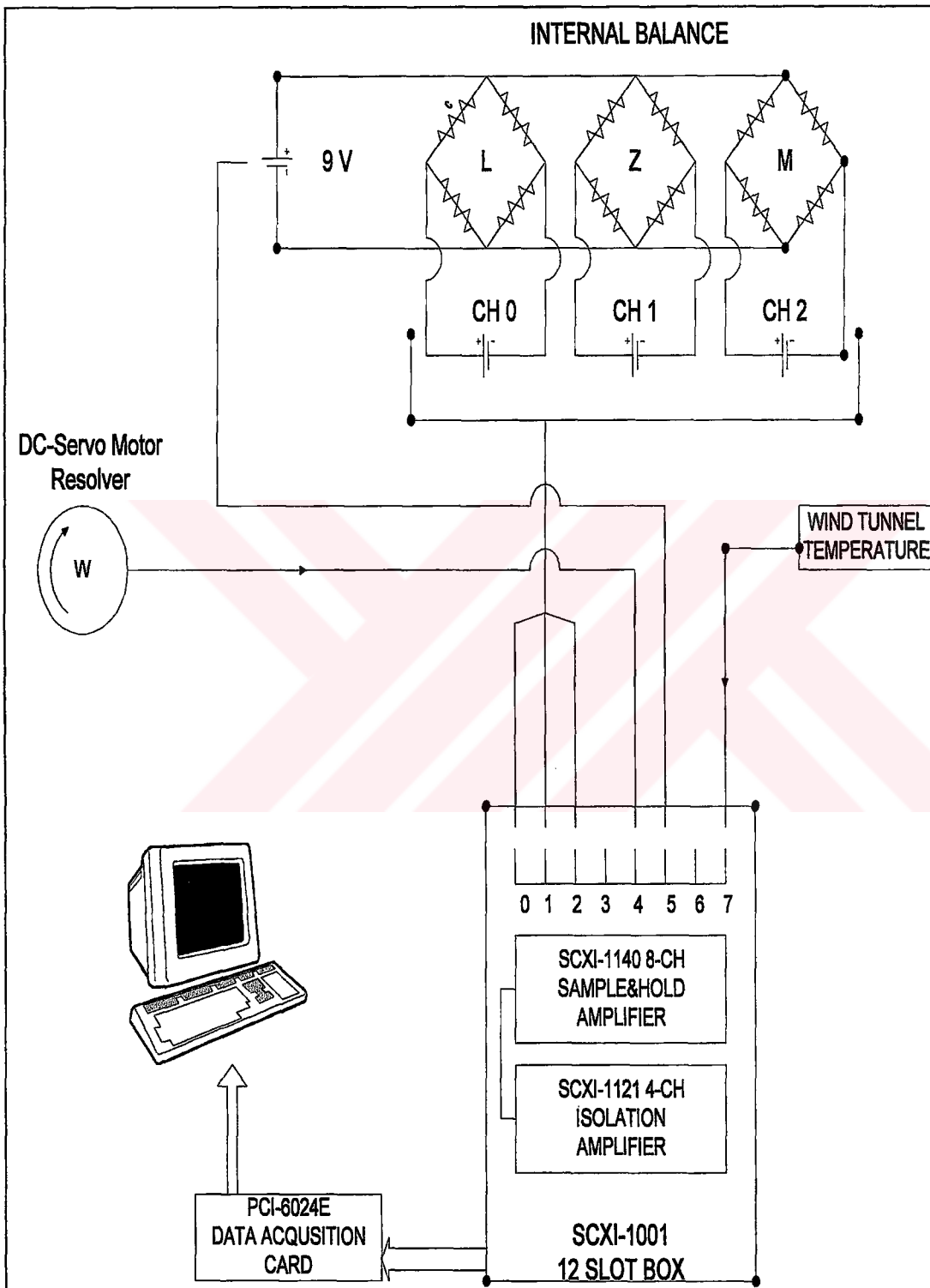


Figure 3.5 The Layout of Hardware and Wiring Connectors

3.4 The Layout of Hardware and Wiring Connectors

The hardware and wiring connectors of the data acquisition system are shown in Figure 3.5. Three outputs of the internal balance; rolling moment, normal force and pitching moment signals, are input to the SCXI-1140 module. Other signals are also input to the remaining channels of SCXI-1140; such as DC servomotor resolver, power supply of internal balance, wind tunnel temperature signals. SCXI-1140 and SCXI-1121 signal conditioning modules are placed in separate slots of the 12-slot chassis available. Signals coming from the conditioner are sent to the data acquisition card where they are converted from analog to digital signal with a 12-bit resolution Analog/Digital (A/D) converter. The conditioned and digitized signals, which are coming from the A/D converter, are then sent to the PC to be stored and analyzed.

3.5 Interface of the Elements of the Experimental Set-up

In order to perform the tests and to get correct measurements, the elements of the experimental set-up must be properly interfaced and this interfacing must be verified. Verification of the present system was performed by Mehmet Altun [2] where he showed that the motion of the model is properly controlled and the forces and moments are accurately measured with the internal balance.

The oscillating vertical push rod (11) supports the fuselage and is connected to the crank-rod mechanism (16). Drive system creates the harmonic motion of the model. The oscillation frequency is set by the rotational speed of the DC servomotor. Adjusting the flywheel's (16) eccentricity radius sets the oscillation amplitude of the model. The amplitude of the oscillations of the model can be adjusted within a range of $\pm 5^\circ$ of pitch amplitude.

The rotation of the motor is controlled by means of a resolver feedback system, which is an advanced type of encoder feedback providing a closed loop control for the rpm control of the motor. The resolver has a sinusoidal signal output, which is simultaneously sent to the data acquisition card with the internal balance outputs in

order to synchronize the measurements of forces and moments with the proper position of the motor. The measurements are started only after attaining the desired frequency of oscillations and stable motion characteristics for the whole system then the voltages read by A/D converter are sent to the PC as mentioned in part 3.4.



CHAPTER 4

DYNAMIC DERIVATIVES

The best way to obtain model-scale dynamic stability information at realistic Reynolds and Mach numbers is through dynamic experiments in a wind tunnel. The concept of a stability derivative is of course related to the traditional form of equations of motion where the result of a small disturbance from the equilibrium flight condition is described by linear superposition of contributions caused by the change in various attitude variables and their time rates of change. With present-day interest in flights at relatively high values of some of the displacement variables (such as α , β and the rate of spin) it is necessary to consider stability derivatives as functions of those variables and to apply the proper local values of the functions for each equilibrium condition. In cases where the variations described by these functions are relatively rapid or where the disturbances are no longer very small, it may also be necessary to replace a particular constant derivative with an analytical expression defining its variation in the vicinity of the equilibrium position [5].

In addition to the familiar damping derivatives (C_{mq} , C_{nr} and C_{lp}) and cross derivatives (C_{np} and C_{lr}), Table 4.1 contains also groups of derivatives labeled cross-coupling derivatives and acceleration derivatives. The first of these cross-coupling derivatives (C_{nq} , C_{lq} , C_{nr} , and C_{mp}) are a direct result of the fact that the modern aircraft often flies in conditions causing significant flow asymmetry. These derivatives relate the longitudinal and the lateral degrees of freedom of an aircraft, providing aerodynamic coupling that does not exist in symmetrical flow conditions. The last group of derivatives is labeled acceleration derivatives and is represented by

moment derivatives due to $\dot{\alpha}$ and $\dot{\beta}$. The word acceleration refers to translational acceleration, which in the first approximation is proportional -from the aerodynamic point of view- to the time rate of change of the angular deflection in the same plane of motion. The aerodynamic reactions due to vertical acceleration, for example, are equivalent to those due to the time rate of change in the angle of attack ($\dot{\alpha}$). Similarly, the lateral acceleration is related to the time rate of change in the angle of sideslip ($\dot{\beta}$). They may also be used to separate the purely-rotary derivatives (such as C_{mq}) from their fixed-axis oscillatory counterparts (such as $C_{mq} + C_{m\dot{\alpha}}$) [5].

Table 4.1 Dynamic moment derivatives [5]

PURE ROTATION	TRANSLATIONAL ACCELERATION	OSCILLATION AROUND FIXED AXIS		
		DAMPING DERIVATIVES	CROSS DERIVATIVES	CROSS-COUPLING DERIVATIVES
C_{lp}, C_{mp}, C_{np} C_{lq}, C_{mq}, C_{nq} C_{lr}, C_{mr}, C_{nr}	$C_{l\dot{\alpha}}, C_{m\dot{\alpha}}, C_{n\dot{\alpha}}$ $C_{l\dot{\beta}}, C_{m\dot{\beta}}, C_{n\dot{\beta}}$	$C_{lp} + C_{l\dot{\beta}} \sin \alpha$	$C_{lr} - C_{l\dot{\beta}} \cos \alpha$	$C_{lq} + C_{l\dot{\alpha}}$
		$C_{mq} + C_{m\dot{\alpha}}$	$C_{np} + C_{n\dot{\beta}} \sin \alpha$	$C_{nr} - C_{n\dot{\beta}} \cos \alpha$
		$C_{nr} - C_{n\dot{\beta}} \cos \alpha$		$C_{mp} + C_{m\dot{\beta}} \sin \alpha$
				$C_{nq} + C_{n\dot{\alpha}}$

The reason why an oscillation around a fixed axis results in a sum of a purely-rotary derivative (such as C_{mq}) and a translational acceleration derivative (such as $C_{m\dot{\alpha}}$) sometimes creates confusion and so a few words of explanation may be in order here. Let us consider, as an example, the longitudinal case. For a free-flying aircraft the variations in the angle of pitch and in the angle of attack can occur independently of each other, and each gives rise to a different longitudinal distribution of the normal velocity. The distribution due to the angle-of-pitch variation (i.e. due to the pitching velocity q) varies along the chord and intersects zero at the axis of rotation, while the distribution due to the angle-of-attack variation is constant along the chord. In the case of an oscillation around a fixed axis both variations occur at the same time and even if the two variables q and $\dot{\alpha}$ are numerically equal, their effects are different

and have to be superimposed. As already indicated, the contribution due to $\dot{\alpha}$ is equivalent to one due to vertical acceleration, since $\dot{\alpha} = \ddot{z}/V$. Similarly, in the lateral case, a rolling (p) or a yawing (r) motion around a fixed axis at an angle of attack causes a simultaneous variation in the rate of change of the angle of sideslip ($\dot{\beta}$). If a system of body axes is used, the resulting composite expressions include a trigonometric function of α , such as in $C_{nr} - C_{n\dot{\beta}} \cos \alpha$ or $C_{np} + C_{n\dot{\beta}} \sin \alpha$ [5].

4.1 Equations of Motion

One of the most difficult problems facing an investigator in the field of flight dynamics is to correctly describe the relationship between the aerodynamic reactions and the motion variables in the inertial equation of motion of an aircraft. The main difficulty in determining the relationship between the instantaneous aerodynamic reactions on a maneuvering aircraft and the motion variables is the fact that this relationship is not solely determined by the instantaneous aerodynamic reactions but depend, in general, on all of the prior states of the motion up to the instant in question [12].

Therefore, before passing to the equations of motion, it is useful that characteristic motions of an aircraft are described in aerodynamic axis and body axis systems.

For nearly rectilinear flight paths, the forces and moments due to an arbitrary motion may be compounded of contributions from four simple motions: steady resultant angle of attack, oscillations in roll and pitch at constant resultant angle of attack, and coning at constant resultant angle of attack. The motions in the aerodynamic axis system are illustrated schematically in Figure 4.1. On the other hand, in the body axis system, the four characteristic motions are steady angle of attack and sideslip, coning at constant angle of attack and sideslip, and the oscillations in pitch and in yaw at constant angles of attack and sideslip. The four motions are illustrated schematically in Figure 4.2 [12].

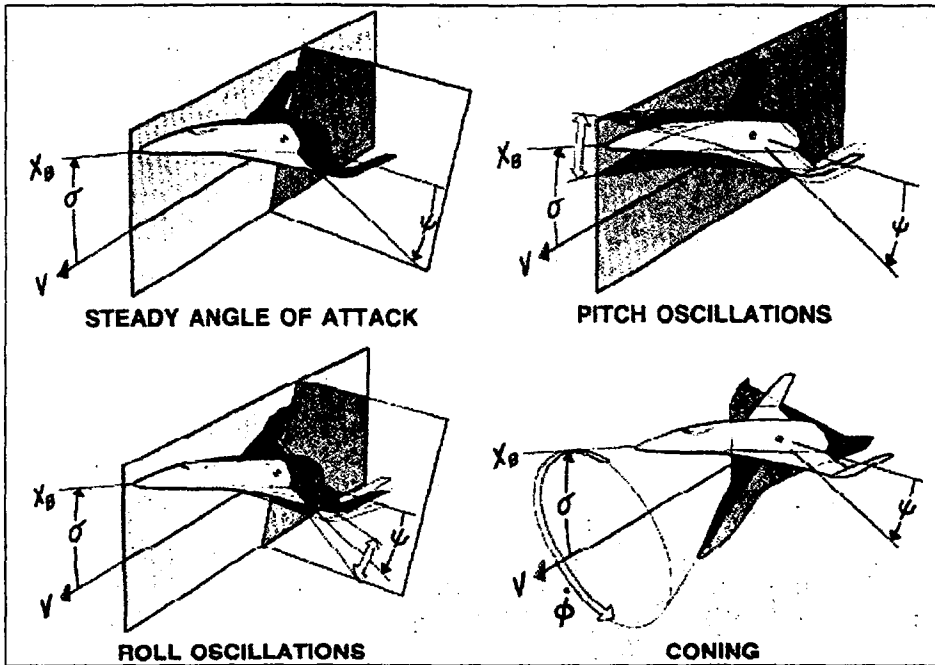


Figure 4.1 Characteristic motions in the aerodynamic axis system.

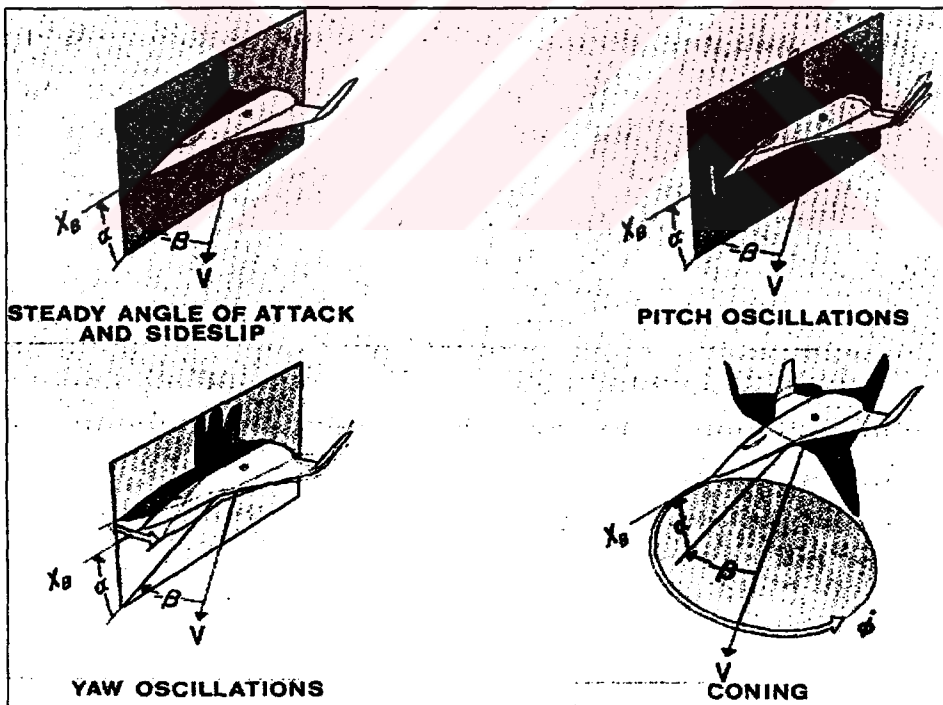


Figure 4.2 Characteristic motions in the body axis system.

Wind tunnel tests conducted in terms of the characteristic motions in the body axis system (Figure 4.2) would require only the coning and oscillation-in-pitch devices. By suitable orientation of the oscillatory device it could be employed to simulate both the planar oscillations in $\hat{\alpha}$ and those in $\hat{\beta}$ as called for by the mathematical model [12].

In what follows, the body axis system (Figure 4.3) is used to compute the dynamic stability derivatives and the equations of motion are given, in general, without any assumptions in the body axis system [13]. They will be used again after making some assumptions for the special conditions in forced oscillation technique part.

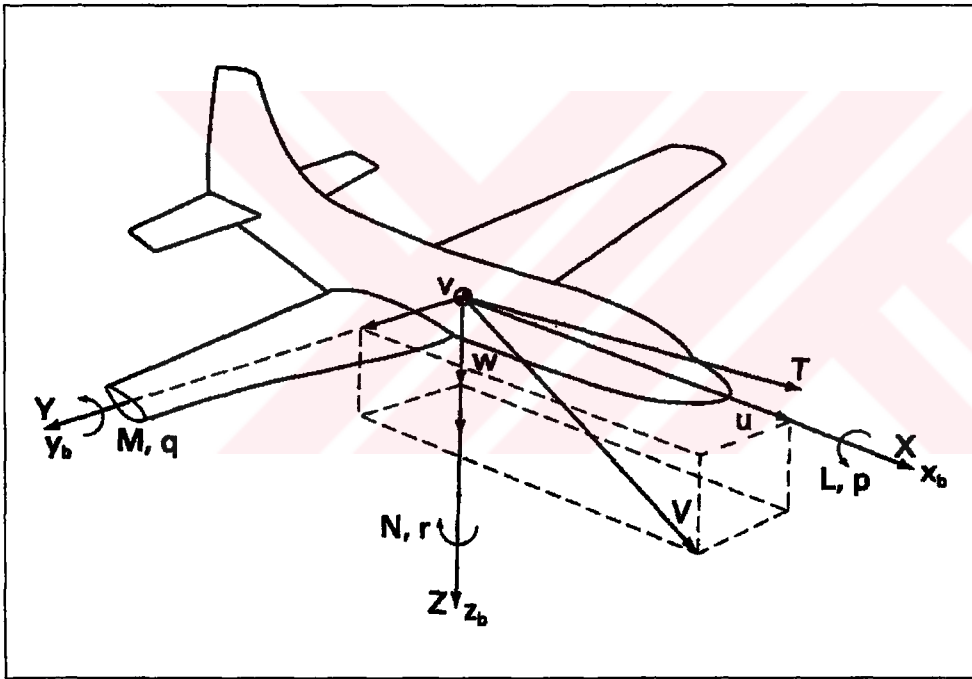


Figure 4.3 Reference Frame: Body Axis

Equations of motion:

$$\dot{u} = \sum F_x / m - qw + rv \quad (4.1)$$

$$\dot{v} = \sum F_y / m - ru + pw \quad (4.2)$$

$$\dot{w} = \sum F_z / m - pv + qu \quad (4.3)$$

$$\dot{p} = [\sum L - (I_z - I_y)qr + I_x(\dot{r} + pq)] / I_x \quad (4.4)$$

$$\dot{q} = [\sum M - (I_x - I_z)rp + I_x(r^2 - p^2)] / I_y \quad (4.5)$$

$$\dot{r} = [\sum N - (I_y - I_x)pq + I_x(\dot{p} - qr)] / I_z \quad (4.6)$$

External Forces and Moments:

$$\sum F_x = T - mg \sin \theta + C_x \bar{q} S \quad (4.7)$$

$$\sum F_y = mg \cos \theta \sin \phi + C_y \beta \bar{q} S \quad (4.8)$$

$$\sum F_z = mg \cos \theta \cos \phi + \left[\begin{array}{l} C_{z_r} + C_{z_\alpha}(\alpha - \alpha_T) + C_{z_q}(q\bar{c}/2V) \\ + C_{z_\dot{\alpha}}(\dot{\alpha}\bar{c}/2V) \end{array} \right] \bar{q} S \quad (4.9)$$

$$\sum L = \left[\begin{array}{l} C_{l_r} + C_{l_\alpha}(\alpha - \alpha_T) + C_{l_\beta}\beta + C_{l_p}(pb/2V) + C_{l_q}(q\bar{c}/2V) \\ + C_{l_\dot{\alpha}}(\dot{\alpha}\bar{c}/2V) + C_{l_r}(rb/2V) + C_{l_\dot{\beta}}(\dot{\beta}b/2V) \end{array} \right] \bar{q} S b \quad (4.10)$$

$$\sum M = \left[\begin{array}{l} C_{m_r} + C_{m_\alpha}(\alpha - \alpha_T) + C_{m_\beta}\beta + C_{m_p}(pb/2V) + C_{m_q}(q\bar{c}/2V) \\ + C_{m_\dot{\alpha}}(\dot{\alpha}\bar{c}/2V) + C_{m_r}(rb/2V) + C_{m_\dot{\beta}}(\dot{\beta}b/2V) \end{array} \right] \bar{q} S \bar{c} \quad (4.11)$$

$$\sum N = \left[\begin{array}{l} C_{n_r} + C_{n_\alpha}(\alpha - \alpha_T) + C_{n_\beta}\beta + C_{n_p}(pb/2V) + C_{n_q}(q\bar{c}/2V) \\ + C_{n_\dot{\alpha}}(\dot{\alpha}\bar{c}/2V) + C_{n_r}(rb/2V) + C_{n_\dot{\beta}}(\dot{\beta}b/2V) \end{array} \right] \bar{q} S b \quad (4.12)$$

Auxiliary Equations:

$$\alpha = \arctan(w/u) \quad (4.13)$$

$$\beta = \arctan(v/u) \quad (4.14)$$

$$\dot{\alpha} = (u\dot{w} - \dot{u}w)/(u^2 + w^2) \quad (4.15)$$

$$\dot{\beta} = (u\dot{v} - \dot{u}v)/(u^2 + v^2) \quad (4.16)$$

$$V = (u^2 + v^2 + w^2) \quad (4.17)$$

The aircraft motion, in its most general terms, is described in six degrees of freedom, (6DOF). The corresponding system of equations of motion, given above, contains as external forces axial, normal and side forces in addition to the motor thrust and the force of gravity, and as the external moments the moments of pitch, yaw and roll. The forces and moments, which are dependent on flight conditions such as angles of attack, yaw, and roll, flight speed, acceleration and the angular velocities of pitch, yaw and roll, may be given as partial derivatives of these variables. In general, the coefficients such as $C_{l\alpha}$, C_{mq} , $C_{n\beta}$ and others, which are included in the equations of motion, are derived from the data obtained from the wind-tunnel experiments or from the flight tests.

The knowledge of certain neglected dynamic stability derivatives until now is becoming recognized by an increasing number of investigators as an important aspect for the design of high performance aircraft and as a consequence a number of experimental techniques are being developed to determine them. One of these techniques is the forced-oscillation technique where the model is sting mounted on an oscillating internal balance. This type of data is used in small-perturbation stability analysis, and is in widespread use today. For example, experience has shown that the damping in roll of current fighters at high- α is usually a function of the

amplitude and frequency of the motion, and any valid mathematical representation of their lateral response at high- α absolutely requires the use of forced oscillation data [14]. In the following section, the forced oscillation technique which is used to determine the dynamic stability derivatives, is described in detail.

4.2 Forced Oscillation Technique

Wind tunnel tests are performed by means of described experimental apparatus during the model's characteristic motions. During those motions, aerodynamic forces and moments are computed using appropriate mathematical model. Several oscillatory experimental testing techniques that have been developed to determine the dynamic stability derivatives were mentioned in chapter 2. One of the largely adopted techniques is the direct forced oscillation technique, which is based on oscillating the aircraft model around its center of gravity with small and constant amplitude in a single degree of freedom. In this way, the relationship between the aerodynamic forces and the primary motion in the plane of motion is established. Experiments, in which the primary oscillation takes place in different degrees of freedom, yield various dynamic stability derivatives.

In AWT, the standard dynamic model is constrained to oscillate at a constant speed and small amplitude about its center of gravity (CG). During calculations of aerodynamic force and moments, body axis coordinate system is used as illustrated in Figure 4.3 and 4.4. The equations of motion can be developed from the rigid body equations using the Newton's second law [15]:

$$\Sigma \text{ Forces in the vertical direction} = m \frac{dw}{dt} \quad (4.18)$$

$$\Sigma \text{ Pitching moments} = \Sigma M_{cg} = I_y \ddot{\theta} \quad (4.19)$$

$$\Sigma \text{ Rolling moments} = I_x \ddot{\phi} \quad (4.20)$$

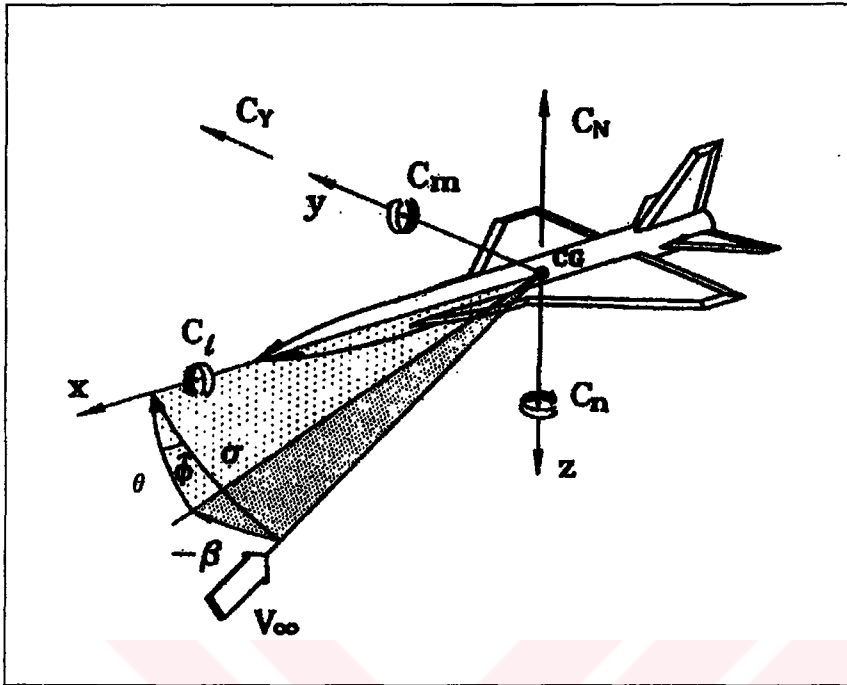


Figure 4.4 The body axes reference system

If the small disturbance theory is applied to the motion of an airplane which consists of small deviations about a steady flight condition, the normal force, Z , the pitching moment, M , the rolling moment, L , the vertical velocity, w , the pitch angle, θ , and the roll angle ϕ can all be expressed in terms of their initial reference values and their perturbed values [15]:

$$Z = Z_0 + \Delta Z \quad (4.21)$$

$$M = M_0 + \Delta M \quad (4.22)$$

$$L = L_0 + \Delta L \quad (4.23)$$

$$w = w_0 + \Delta w \quad (4.24)$$

$$\theta = \theta_0 + \Delta\theta \quad (4.25)$$

$$\phi = \phi_0 + \Delta\phi \quad (4.26)$$

If the initial values are 0, then Equations 4.18, 4.19 and 4.20 reduce to

$$\Delta Z = m \frac{d}{dt} \Delta w \quad (4.27)$$

$$\Delta M = I_y \Delta \ddot{\theta} \quad (4.28)$$

$$\Delta L = I_x \Delta \ddot{\phi} \quad (4.29)$$

The change in aerodynamic forces and moments are functions of the motion variables; Δu , Δw , $\Delta \dot{w}$, Δq , etc. The functional relationship for the normal force, the pitching and the rolling moments are given as follows [15];

$$\Delta Z = \frac{\partial Z}{\partial u} \Delta u + \frac{\partial Z}{\partial w} \Delta w + \frac{\partial Z}{\partial \dot{w}} \Delta \dot{w} + \frac{\partial Z}{\partial q} \Delta q + \frac{\partial Z}{\partial \delta_e} \Delta \delta_e + \frac{\partial Z}{\partial \delta_r} \Delta \delta_r \quad (4.30)$$

$$\Delta M = \frac{\partial M}{\partial u} \Delta u + \frac{\partial M}{\partial w} \Delta w + \frac{\partial M}{\partial \dot{w}} \Delta \dot{w} + \frac{\partial M}{\partial q} \Delta q + \frac{\partial M}{\partial \delta_e} \Delta \delta_e + \frac{\partial M}{\partial \delta_r} \Delta \delta_r \quad (4.31)$$

$$\Delta L = \frac{\partial L}{\partial v} \Delta v + \frac{\partial L}{\partial p} \Delta p + \frac{\partial L}{\partial r} \Delta r + \frac{\partial L}{\partial \delta_r} \Delta \delta_r + \frac{\partial L}{\partial \delta_a} \Delta \delta_a \quad (4.32)$$

Above aerodynamic force and moments can be expressed as a function of all the motion variables that are given in part 4.1; however, in the equations given alone only the terms that are usually the most significant have been retained.

Consider the case in which the model's center of gravity is constrained to move in a straight line at a constant speed but the model is free to pitch about its center of gravity so that it can perform only a pitching motion. For the restricted motion that we are examining, the variables are the angle of attack, pitch angle and the time rate of change of these variables. The pitching moment is not only a function of the pitch angle but also a function of the other variables which can be expressed in a functional form as follows [15]:

$$\Delta M = f(\Delta\alpha, \Delta\dot{\alpha}, \Delta q, \Delta\delta_e) \quad (4.33)$$

Equation 4.28 can be expanded in terms of the perturbation variables by means of Taylor series as;

$$\Delta M = \frac{\partial M}{\partial \alpha} \Delta\alpha + \frac{\partial M}{\partial \dot{\alpha}} \Delta\dot{\alpha} + \frac{\partial M}{\partial q} \Delta q \quad (4.34)$$

If the body frame axis and the fixed frame axis coincide, the change in angle of attack and pitch angle are the same such that;

$$\Delta\alpha = \Delta\theta \quad \text{and} \quad \Delta\dot{\theta} = \Delta\dot{\alpha} = \Delta q$$

Then substituting into equation 4.28 yields;

$$\Delta\ddot{\alpha} - (M_q + M_{\dot{\alpha}})\Delta\dot{\alpha} - M_{\alpha}\Delta\alpha = 0 \quad (4.35)$$

where

$$M_q = \frac{\partial M}{\partial q} / I_y, \quad M_{\dot{\alpha}} = \frac{\partial M}{\partial \dot{\alpha}} / I_y, \quad M_{\alpha} = \frac{\partial M}{\partial \alpha} / I_y$$

Using the similar consideration given above, the aerodynamic normal force acting on the airplane is a function of the angle of attack, pitch angle and the time rate of change of the angle of attack and can be expressed in terms of the stability derivatives as follows:

$$\Delta Z = Z_{\alpha}\Delta\alpha + Z_{\dot{\alpha}}\Delta\dot{\alpha} + Z_q\Delta q \quad (4.36)$$

There is another effect observed on the dynamic stability derivatives which is due to the presence of aerodynamic cross-coupling caused by asymmetric flow conditions. Asymmetric flows occur not only when an aircraft flies at nonzero sideslip but also when it flies at zero sideslip but at high angles of attack. In both cases we may expect the occurrence of secondary lateral aerodynamic forces and moments in response to a primary pitching maneuver and vice versa, the onset of secondary longitudinal reactions in response to a primary lateral maneuver. Because of various time lags, these secondary reactions will consist of components that are both in-phase and out-of-phase with the primary motion, and will give rise, therefore, to both static and dynamic cross-coupling effects [16]. Therefore, under the pitching maneuver consideration, the rolling moment is a function of the angle of attack, pitch angle and the time rate of change of the angle of attack and can be expressed as;

$$\Delta L = L_{\alpha}\Delta\alpha + L_{\dot{\alpha}}\Delta\dot{\alpha} + L_q\Delta q \quad (4.37)$$

Equation (4.35) is a nonhomogenous ordinary second-order differential equation, having constant coefficients. This equation is similar to a torsional spring-mass-damper system with a forcing function. The static stability of the airplane can therefore be thought of as the equivalent of an aerodynamic spring, while the aerodynamic damping terms are similar to a torsional damping device [15].

In forced oscillation technique, the model is connected to an internal balance (multi-axis force transducer) and is forced to oscillate by small amplitudes and frequencies

according to a harmonic forcing motion generated by a mechanical device (i.e. flywheel).

Equivalence can be established with a second order oscillator where the system is excited by a forcing motion of the support system. If the compliance and the structural damping of the balance are negligible, then it can be concluded that $\theta(t) \cong \Delta\alpha(t)$ (Figure 4.5). The oscillating system is considered locally linear i.e. both the forcing function and the force reaction on the balance are similar harmonic functions (small oscillation amplitude and frequency). This method is effective for small amplitudes and frequency of oscillations ($f \leq 3 \text{ Hz}$, $\theta \leq 3^\circ / 5^\circ$) about one of the three reference body axes: X(roll), Y (pitch) and Z (yaw) [8].

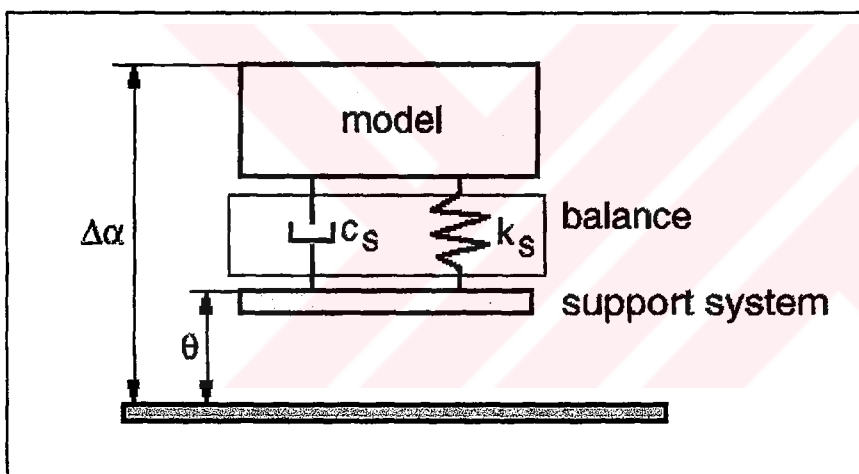


Figure 4.5 Second order oscillator equivalent system for the response of the aircraft model under small oscillations

The aerodynamic loads acting on the model F_i produce minimal proportional displacements of the force transducer that are measured by means of strain gages (connected as four elements Wheatstone bridge for each measured load component). Therefore, the strain of the sensing element is converted into a voltage output E_j [4]:

$$\{F_i\} = [a_{ij}] \cdot \{E_j\} \quad (4.38)$$

The reaction on the balance $M(t)$ is measured as

$$\bar{M}(t) = \sum_{j=1}^n a_{Mj} \cdot \bar{E}_j(t) \quad (4.39)$$

where n is the number of sensing elements of the force transducer and a_{Mj} is one of the rows of the so called calibration matrix (pitching moment component). The elements of the calibration matrix must be properly determined by means of an appropriate calibration procedure.

The forced oscillation test is performed in two phases: tare and wind-on tests.

Tare test: In tare tests the wind is off and the model is oscillated while not being subjected to the aerodynamic loads and hence the forcing function is only due to the inertial coupling between the primary motion and the degree of freedom under study [17].

$$M^T(t) = I_y \Delta \ddot{\alpha} + c_s \Delta \dot{\alpha} + k_s \Delta \alpha \quad (4.40)$$

Wind-on test: In the wind-on measurements the forcing function includes the unknown aerodynamic interactions between the primary motion and the degree of freedom being considered [17].

$$\begin{aligned} M^W(t) &= M^T(t) - M_{aer} = M^T(t) - M_\alpha \Delta \alpha - M_q \Delta q - M_{\dot{\alpha}} \Delta \dot{\alpha} \\ &= M^T(t) - M_\alpha \Delta \alpha - (M_q + M_{\dot{\alpha}}) \Delta \dot{\alpha} \end{aligned} \quad (4.41)$$

where $q = \Delta \dot{\alpha}$ is assumed for rectilinear flight.

The reaction $M(t)$ can be split into “in-phase” and “out-of-phase” components with respect to the simple harmonic oscillatory motion given as;

$$\Delta\alpha(t) = \alpha_0 \cos(\omega t) \text{ (Figure 4.6):} \quad (4.42)$$

$$\bar{M}(t) = \sum_{j=1}^n a_{Mj} [\bar{E}_{IN} + \bar{E}_{OUT}] \quad (4.43)$$

where

\bar{E}_{IN} and \bar{E}_{OUT} can be expressed as the Fourier cosine and sine series expansions respectively while retaining only the first terms of these series;

$$\bar{E}_{IN} = |E_{IN}| \cdot \cos(\omega t) \cdot \vec{j} \quad (4.44)$$

$$\bar{E}_{OUT} = |E_{OUT}| \cdot \sin(\omega t) \cdot \vec{j} \quad (4.45)$$

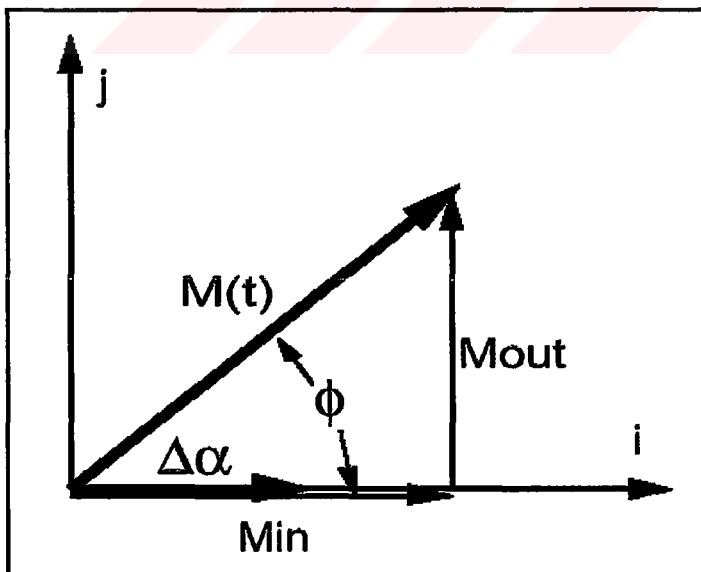


Figure 4.6 In-phase and out-of-phase components of $M(t)$

The vectorial components of the voltage output E_j are computed as the first terms of a Fourier series expansion of $E(t)$ [4]:

The amplitude of the in-phase and out-of-phase components of this series representation is computed as the Fourier cosine and sine series coefficients of the voltage output from the respective sensor of the balance. It has to be noted that the voltage output from the sensor is sinusoidal in nature whose mean value is brought to zero.

$$|E_{IN}|_j = \frac{1}{\pi} \int_0^{2\pi} E_j(t) \cdot \cos(\omega t) \cdot d(\omega t) \quad (4.46)$$

$$|E_{OUT}|_j = \frac{1}{\pi} \int_0^{2\pi} E_j(t) \cdot \sin(\omega t) \cdot d(\omega t) \quad (4.47)$$

From the equilibrium in wind-on conditions we find that:

$$\begin{aligned} \vec{M}_{aer} &= M_\alpha \cdot \alpha_0 \cos(\omega t) - (M_q + M_{\dot{\alpha}}) \cdot \omega \alpha_0 \sin(\omega t) \\ &= \sum_{j=1}^n a_{M_j} \cdot \left[|E_{IN}|^T \cos(\omega t) + |E_{OUT}|^T \sin(\omega t) \right]_j \\ &\quad - \sum_{j=1}^n a_{M_j} \cdot \left[|E_{IN}|^W \cos(\omega t) + |E_{OUT}|^W \sin(\omega t) \right]_j \end{aligned} \quad (4.48)$$

$$\begin{aligned} M_\alpha \cdot \alpha_0 \cos(\omega t) - (M_q + M_{\dot{\alpha}}) \cdot \omega \alpha_0 \sin(\omega t) = \\ \sum_{j=1}^n a_{M_j} \cdot \left[|E_{IN}|^T - |E_{IN}|^W \right]_j \cos(\omega t) + \sum_{j=1}^n a_{M_j} \cdot \left[|E_{OUT}|^T - |E_{OUT}|^W \right]_j \sin(\omega t) \end{aligned} \quad (4.49)$$

Hence :

$$M_{\alpha} = \frac{\sum_{j=1}^n a_{Mj} \cdot [E_{IN}|^T - |E_{IN}|^W]_j}{\alpha_0} \quad (4.50)$$

$$M_{\dot{q}} + M_{\dot{\alpha}} = \frac{\sum_{j=1}^n a_{Mj} \cdot [E_{OUT}|^T - |E_{OUT}|^W]_j}{\omega \cdot \alpha_0} \quad (4.51)$$

where, it is assumed that the amplitude of oscillation α_0 and the frequency of oscillations ω are the same for both the wind-off and wind-on conditions under the forced oscillation technique.

$$\alpha_0^T = \alpha_0^W \text{ and } \omega^T = \omega^W$$

Note that the derivatives $M_{\dot{q}}$ and $M_{\dot{\alpha}}$ cannot be separated, and their combined effect can only be predicted.

Equation 4.50 and 4.51 can also be written in their nondimensional form as;

$$C = \frac{M_{\alpha}}{\alpha_0} \quad (4.52)$$

where $M_q = \frac{\partial M}{\partial q}$ and $M_{\dot{\alpha}} = \frac{\partial M}{\partial \dot{\alpha}}$ are the variation of the pitch moment with angular velocity about pitch axis and with time rate of change of angle of attack respectively. In addition,

$$C_{mq} = \frac{\partial C_m}{\partial \left(\frac{qc}{2V_\infty}\right)} \quad \text{and} \quad C_{m\dot{\alpha}} = \frac{\partial C_m}{\partial \left(\frac{\dot{\alpha}c}{2V_\infty}\right)}$$

Physical meanings of these coefficients are:

C_{mq} : The stability coefficient C_{mq} represents the change in the pitching moment coefficient with respect to the pitching velocity q . The pitching motion of the airplane affects the aerodynamic characteristics of both the wing and the horizontal tail. The wing contribution is usually quite small in comparison to that produced by the tail. A common practice is to compute the tail contribution and then increase it by 10 percent to account for the effect of the wing.

$C_{m\dot{\alpha}}$: The stability coefficient $C_{m\dot{\alpha}}$ arises because of the lag in the wing downwash in getting to the tail. As the wing angle of attack changes, the circulation around the wing will be altered. The change in circulation alters the downwash at the tail; however, it takes a finite time for the alteration to occur.

Similar considerations on the data reduction procedure can be repeated for the calculation of normal force and rolling moment dynamic derivatives. Hence:

$$C_{z\alpha} = \frac{Z_\alpha}{\frac{1}{2}\rho V^2 S} \tag{4.54}$$

where $Z_\alpha = \frac{\partial Z}{\partial \alpha}$ and is the variation of normal force with angle of attack

$$C_{zq} + C_{z\dot{\alpha}} = \frac{Z_q + Z_{\dot{\alpha}}}{\frac{1}{4} \rho V S c} \quad (4.55)$$

where $Z_q = \frac{\partial Z}{\partial q}$ and $Z_{\dot{\alpha}} = \frac{\partial Z}{\partial \dot{\alpha}}$ are the variations of normal force with angular velocity about pitch axis and with time rate of change of angle of attack respectively. In addition,

$$C_{zq} = \frac{\partial C_z}{\partial \left(\frac{qc}{2V_\infty} \right)} \quad \text{and} \quad C_{z\dot{\alpha}} = \frac{\partial C_z}{\partial \left(\frac{\dot{\alpha}c}{2V_\infty} \right)}$$

$$C_{l\alpha} = \frac{L_\alpha}{\frac{1}{2} \rho V^2 S b} \quad (4.56)$$

where $L_\alpha = \frac{\partial L}{\partial \alpha}$ and is the variation of roll moment with angle of attack

$$C_{lq} + C_{l\dot{\alpha}} = \frac{L_q + L_{\dot{\alpha}}}{\frac{1}{4} \rho V S c b} \quad (4.57)$$

where $L_q = \frac{\partial L}{\partial q}$ and $L_{\dot{\alpha}} = \frac{\partial L}{\partial \dot{\alpha}}$ are the variations of roll moment with angular velocity about pitch axis and with time rate of change of angle of attack respectively. In addition,

$$C_{lq} = \frac{\partial C_l}{\partial \left(\frac{qc}{2V_\infty} \right)} \quad \text{and} \quad C_{l\dot{\alpha}} = \frac{\partial C_l}{\partial \left(\frac{\dot{\alpha}c}{2V_\infty} \right)}$$

CHAPTER 5

STATIC AND DYNAMIC TESTS RESULTS

This chapter deals with the results of the static and dynamic tests and their correlation with results obtained from other test facilities. The results are presented as functions of angle of attack. The effects of oscillation frequency, oscillation amplitude and wind speed were also investigated as well as the repeatability of data. The test matrices for static and dynamic tests are shown in Table 5.1 and Table 5.2 respectively.

All aerodynamic coefficients presented in the figures are referred to body axes according to the definition shown in Figures 4.3 and 4.4 in chapter 4.

Table 5.1 The Test Matrix for Static Tests

α -range (deg)	Step (deg)	β (deg)	V (m/s)	Model Configuration
$-6^{\circ} \div 30^{\circ}$	3°	0°	20	BWLVH
$-6^{\circ} \div 30^{\circ}$	"	"	30	"
$-6^{\circ} \div 30^{\circ}$	"	"	40	"

Table 5.2 Test Matrix for Oscillatory Tests – pitch mode

α -range (deg)	Step (deg)	β (deg)	V (m/s)	f (Hz)	θ (deg)	Model Configuration
$0^0 \div 30^0$	5^0	0^0	30	1	$\pm 1^0$	BWL VH
$0^0 \div 30^0$	"	0^0	"	1	$\pm 2^0$	BWL VH
$0^0 \div 30^0$	"	0^0	"	2	$\pm 1^0$	BWL VH
0^0		0^0	20	1	$\pm 1^0$	BWL VH
"		"	"	2	"	"
"		"	"	1	$\pm 2^0$	"
"		"	"	2	"	"
20^0		0^0	20	1	$\pm 1^0$	BWL VH
"		"	"	2	"	"
"		"	"	1	$\pm 2^0$	"
"		"	"	2	"	"
0^0		0^0	30	1	$\pm 1^0$	BWL VH
"		"	"	2	"	"
"		"	"	1	$\pm 2^0$	"
"		"	"	2	"	"
20^0		0^0	30	1	$\pm 1^0$	BWL VH
"		"	"	2	"	"
"		"	"	1	$\pm 2^0$	"
"		"	"	2	"	"
0^0		0^0	40	1	$\pm 1^0$	BWL VH
"		"	"	2	"	"
"		"	"	1	$\pm 2^0$	"
"		"	"	2	"	"
20^0		0^0	40	1	$\pm 1^0$	BWL VH
"		"	"	2	"	"
"		"	"	1	$\pm 2^0$	"
"		"	"	2	"	"

5.1 Static Test Results and Comparison with Other Facilities

The results of static coefficients of C_l , C_z , and C_m are presented in Figures 5.1 to 5.9 for 20, 30 and 40 m/s wind velocities including data repeatability. In order to check the repeatability of tests, measurements were repeated three times for each case. Figure 5.9 has to be interpreted with precaution since these experiments are not repeated after a certain time interval. These data are collected one after the other for a given angle of attack setting. Therefore these results show a much better agreement than the others. In general, agreement between the three sets of data was good except for the rolling moment, C_l . The values for the rolling moments are very small as can be seen in Figures 5.1, 5.2 and 5.3 and differences between the three data sets might be due to the asymmetry or very small values of the rolling moment.

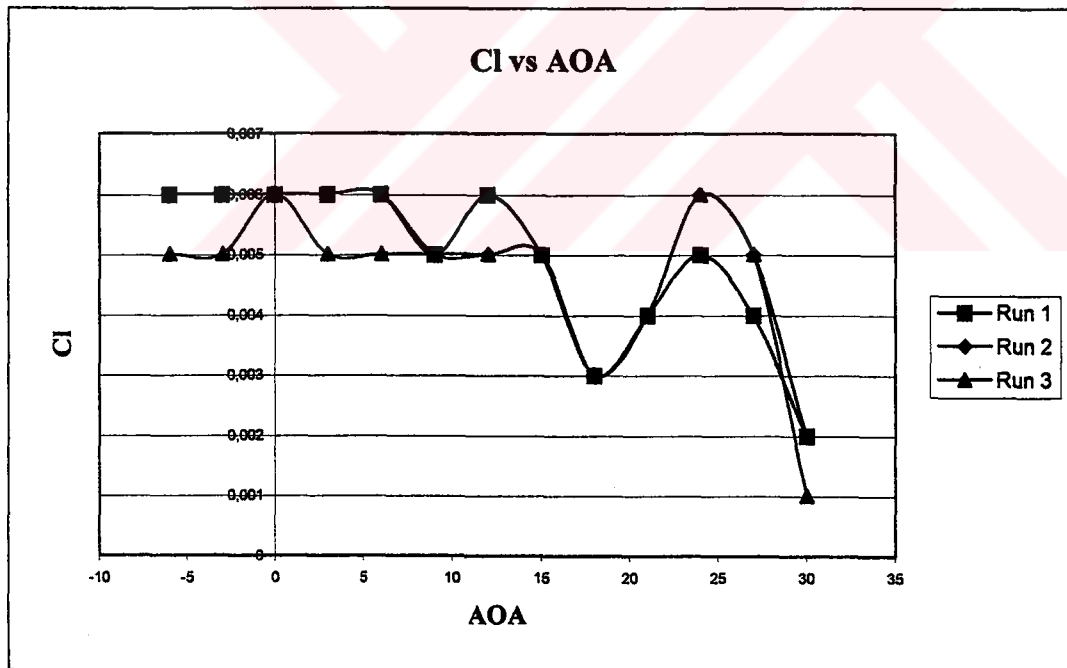


Figure 5.1 The static values for roll moment coefficient C_l for $V=20$ m/s (data repeatability)

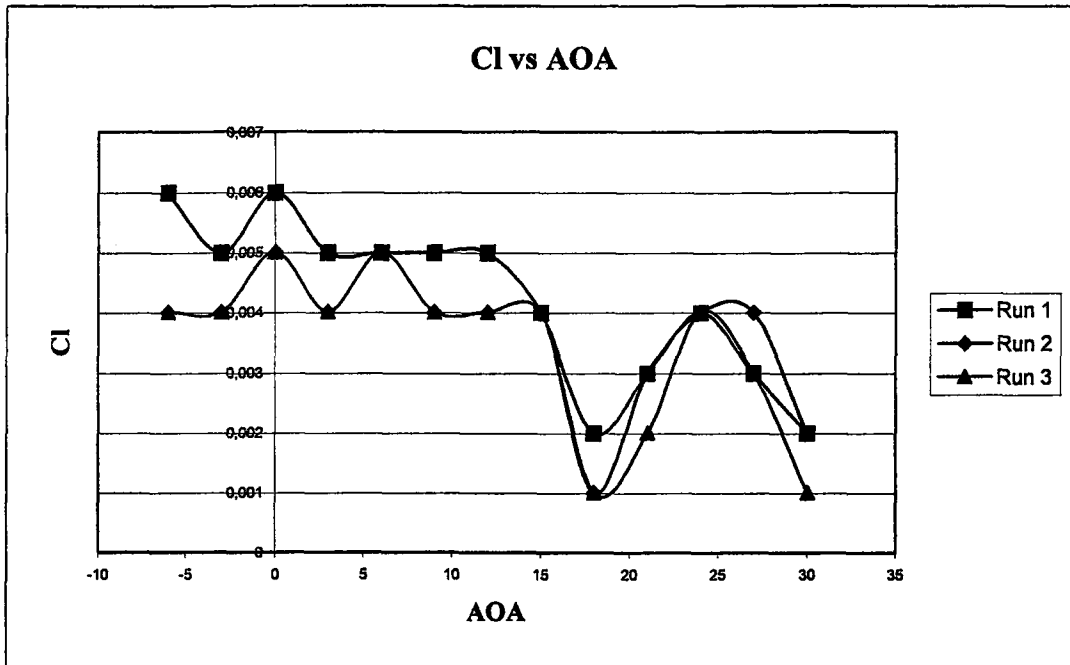


Figure 5.2 The static values for roll moment coefficient C_l for $V=30$ m/s (data repeatability)

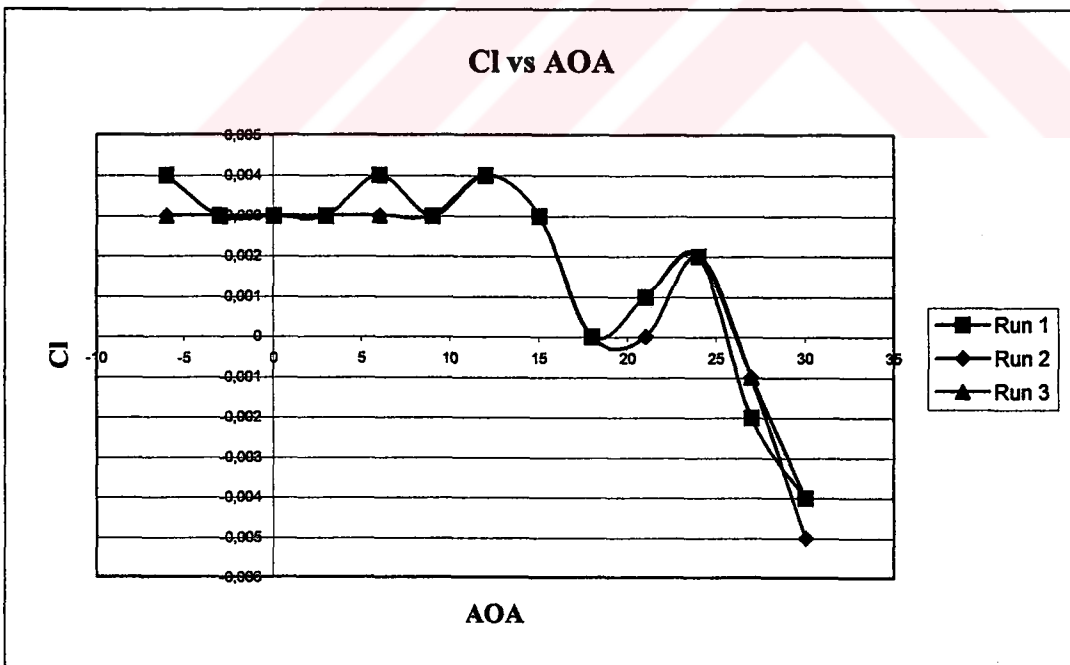
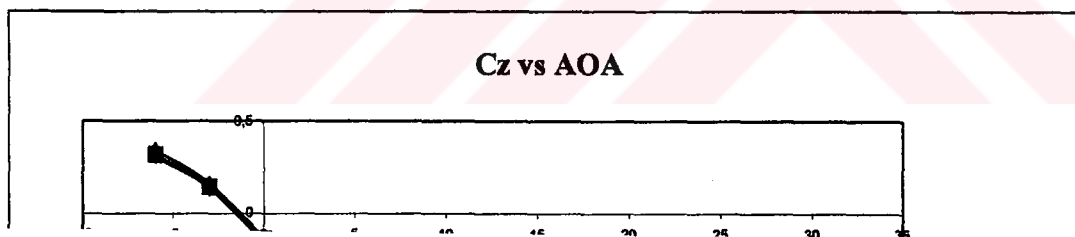


Figure 5.3 The static values for roll moment coefficient C_l for $V=40$ m/s (data repeatability)

The trend of normal force, C_z , is presented in Figures 5.4, 5.5 and 5.6 for 20, 30 and 40 m/s respectively. From the figures it is clear that the normal force curves are extended linearly up to $\alpha=18^\circ$, where the wing-stall occurs. The resulting loss of lift due to this stall is observed with the kink observed in the C_z curve around $\alpha=18^\circ$.

The trend of pitching moment, C_m , can be seen in Figures 5.7, 5.8 and 5.9 for 20, 30 and 40 m/s respectively. The pitching moment curve increases linearly with angle of attack range from -6° to -3° and decreases in the interval of -3° to 0° . The pitching moment curve is linear from $\alpha=5^\circ$ up to $\alpha=15^\circ$. Between 0° and 5° the pitching moment coefficients goes through a minimum value. At $\alpha=15^\circ$, the pitching moment coefficient C_m attains a peak value for all of the velocities tested. After this peak, C_m starts to decline linearly with angle of attack up to $\alpha=30^\circ$. It appears that separation on the horizontal stabilizer is delayed by the downwash of the wing so that the normal force slope of the stabilizer is kept at relatively high values due to the effectively lower angle of attack. Thus, when the wing C_z is reduced by tip stalling above $\alpha=18^\circ$, a stabilizing pitching moment results. The favorable effect of the wing downwash is maintained up to about 30° which was also the case observed in ref. [7].



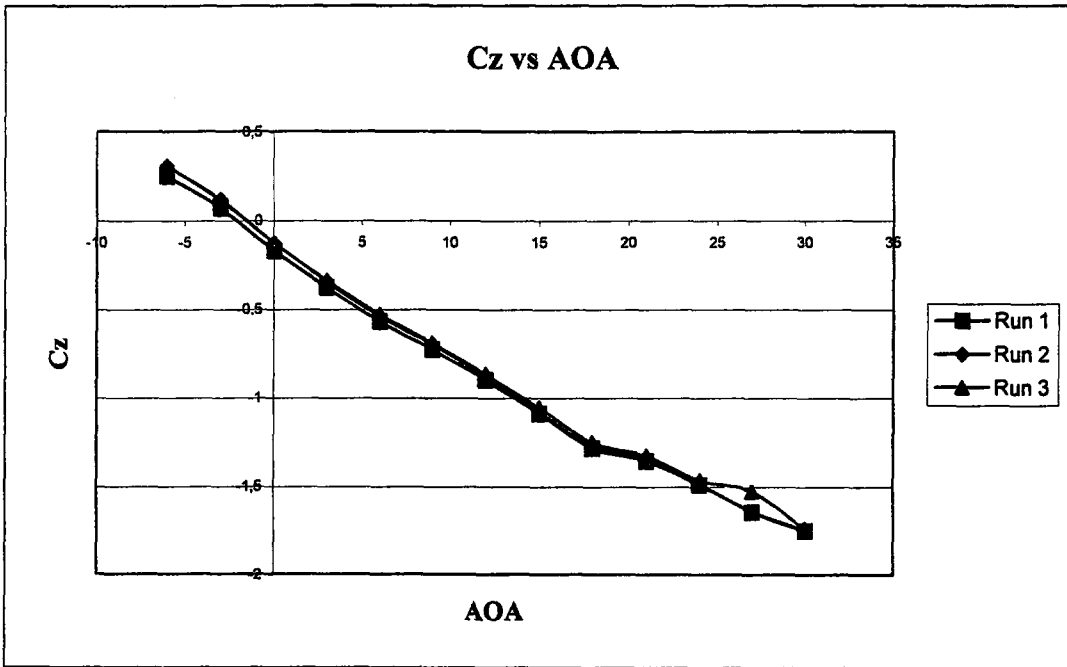


Figure 5.5 The static values for normal force coefficient C_z for $V=30$ m/s (data repeatability)

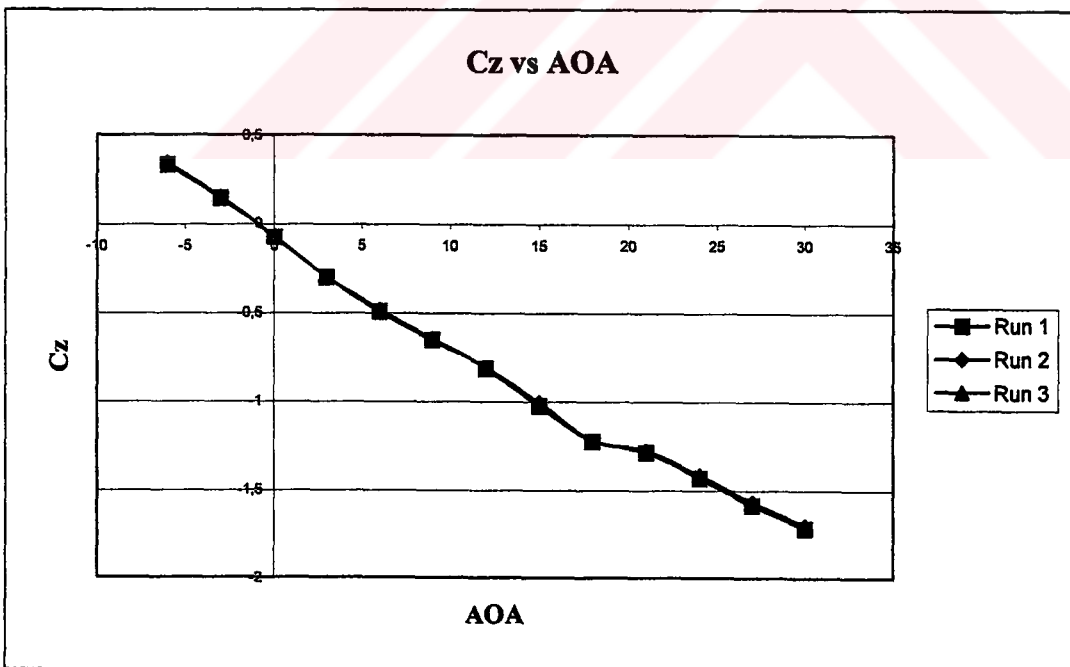


Figure 5.6 The static values for normal force coefficient C_z for $V=40$ m/s (data repeatability)

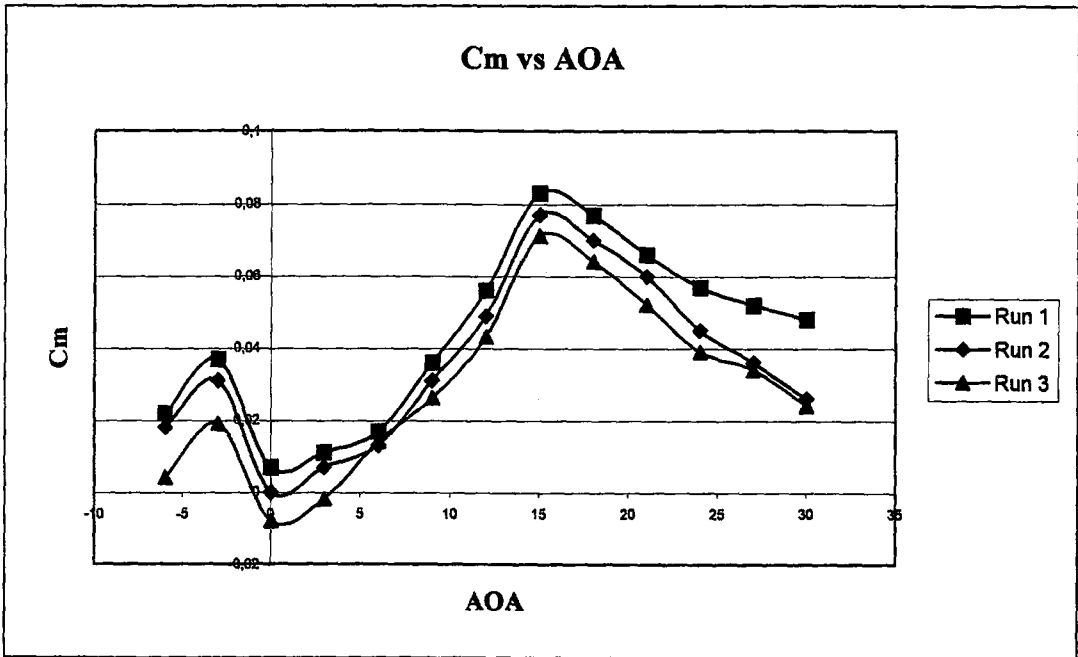


Figure 5.7 The static values for pitching moment coefficient C_m for $V=20$ m/s (data repeatability)

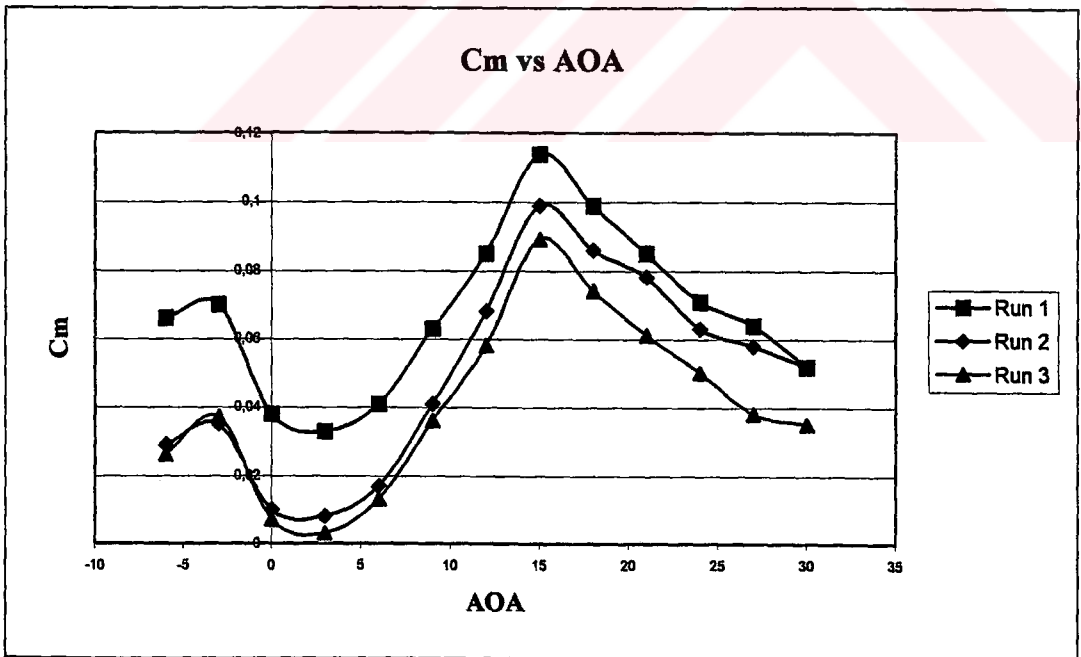


Figure 5.8 The static values for pitching moment coefficient C_m for $V=30$ m/s (data repeatability)

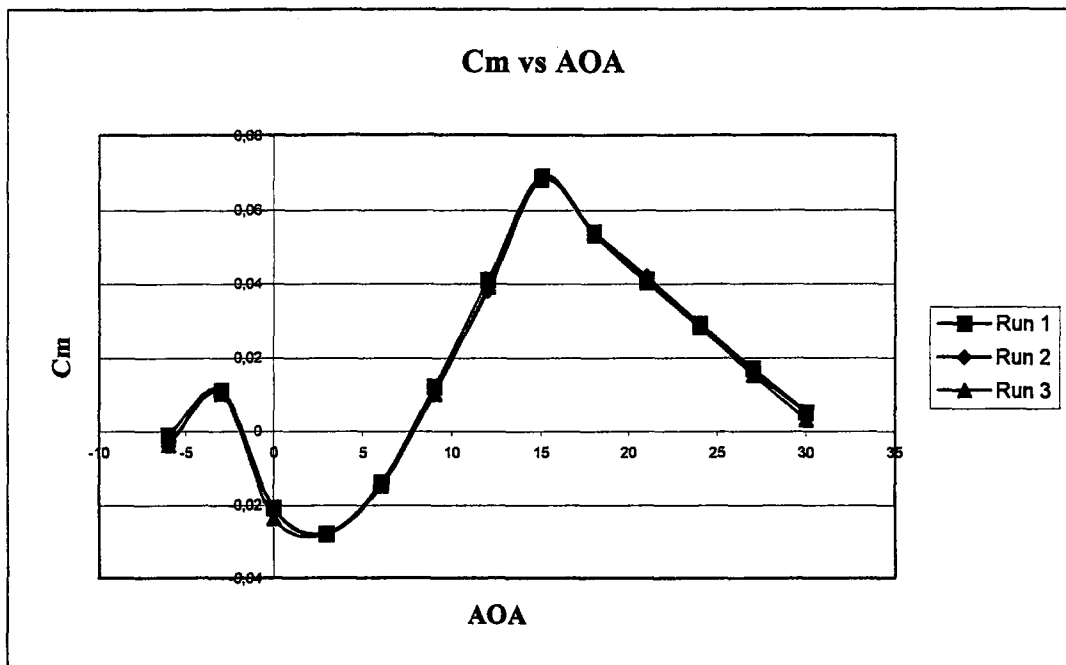


Figure 5.9 The static value for pitching moment coefficient C_m for $V=40$ m/s (data repeatability)

The effects of velocity on the rolling moments are depicted in Figure 5.10. Since the rolling moments are very small at zero sideslip, over the complete α range, the differences between the three data set at $V=20,30$ and 40 m/s are largely within the experimental uncertainty. In Figure 5.11, the effect on the normal force, C_z , of changing the velocity from 20 to 40 m/s is negligible as might be expected for this configuration. In the case of the pitching moment as shown in Figure 5.12, the velocity effects are, in general, also small, but measurable differences are observed through α range.

The primary aim of the correlation is to evaluate the reliability of tests done with the same model configuration in different wind tunnel test facilities. The static results of the AWT tests are generally in good agreement with those of other facilities (TPI, NAE) and can be seen in Figures 5.13, 5.14 and 5.15 for rolling moment, normal force and pitching moment respectively. Differences become evident at α larger than 25° for the longitudinal coefficients C_z and C_m (Figure 5.14 and 5.15).

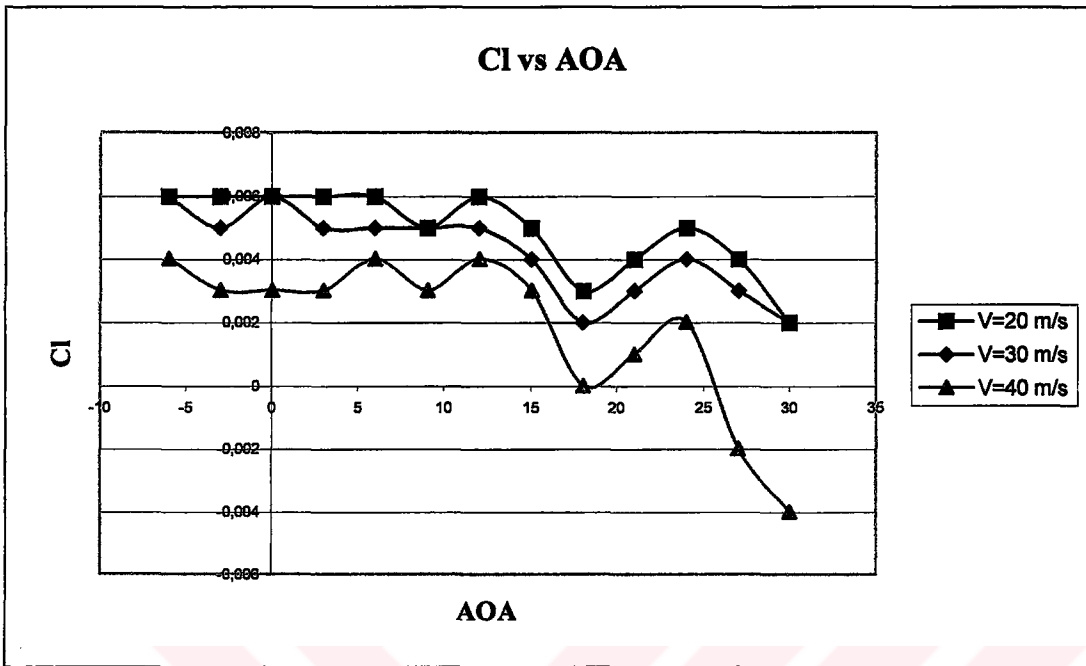


Figure 5.10 The Effect of Velocity on C_l

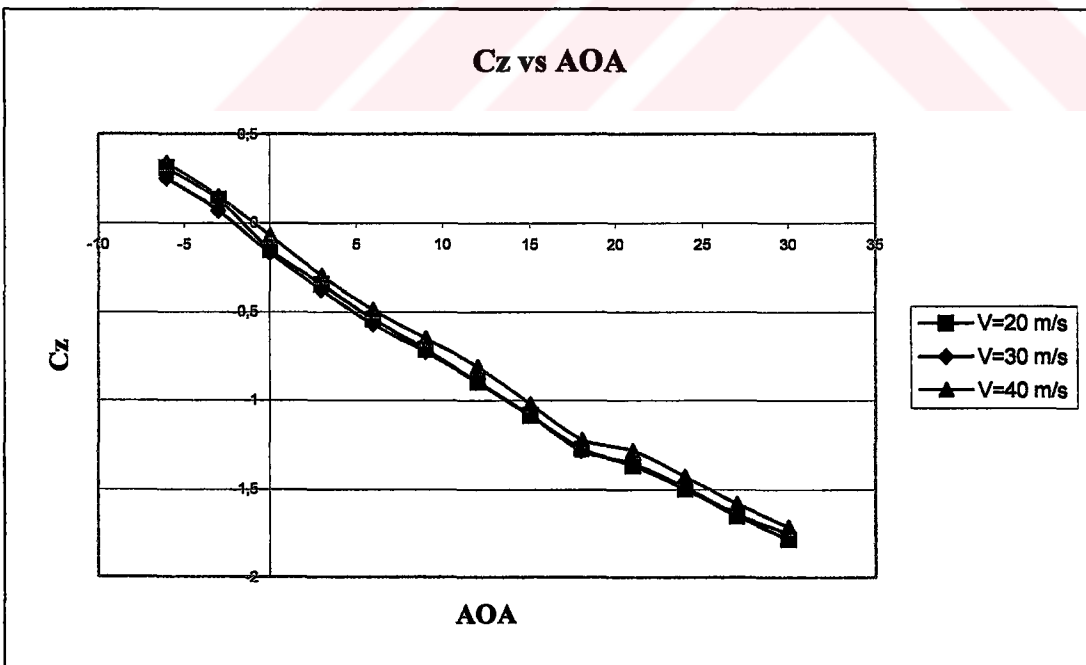


Figure 5.11 The Effect of Velocity on C_z

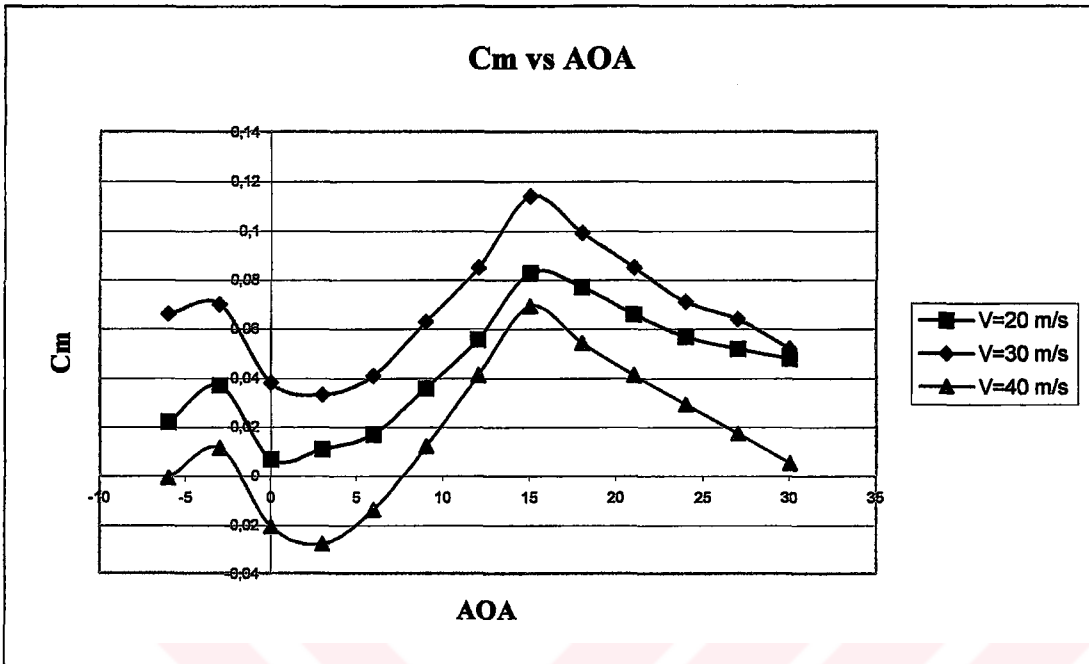


Figure 5.12 The Effect of Velocity on C_m

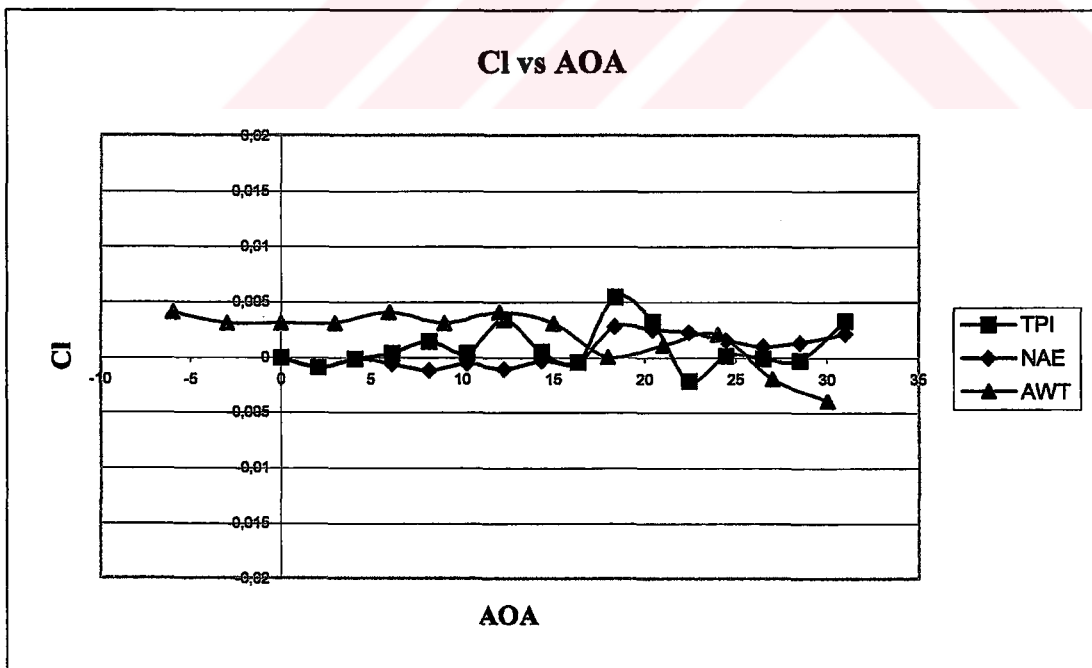


Figure 5.13 The facility comparison for the static coefficient C_l variation with angle of attack

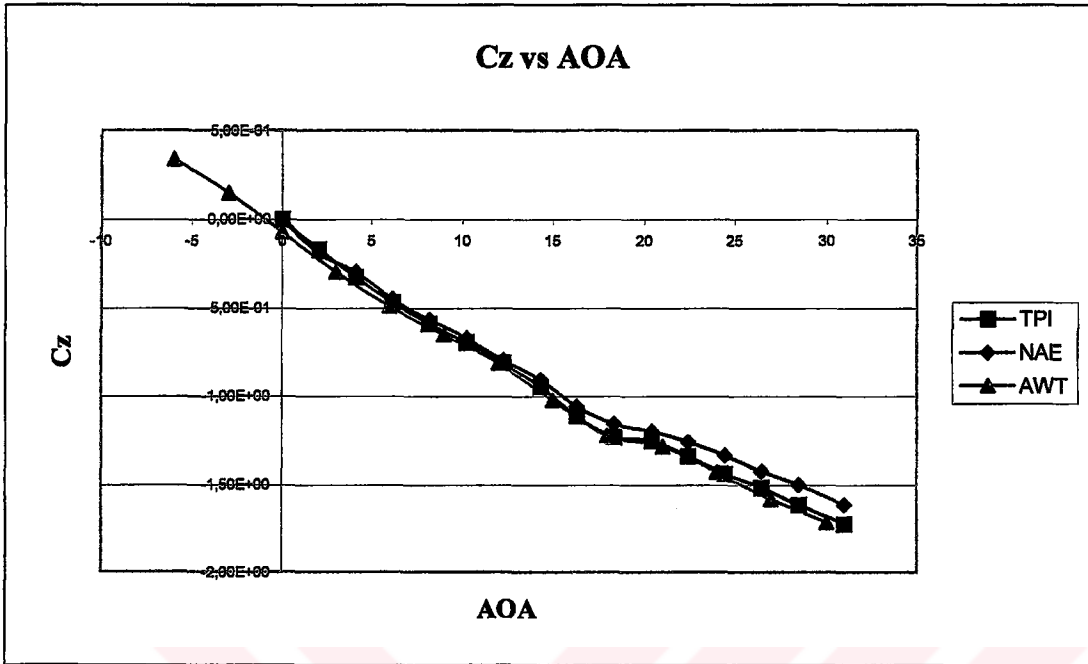


Figure 5.14 The facility comparison for the static coefficient C_z variation with angle of attack

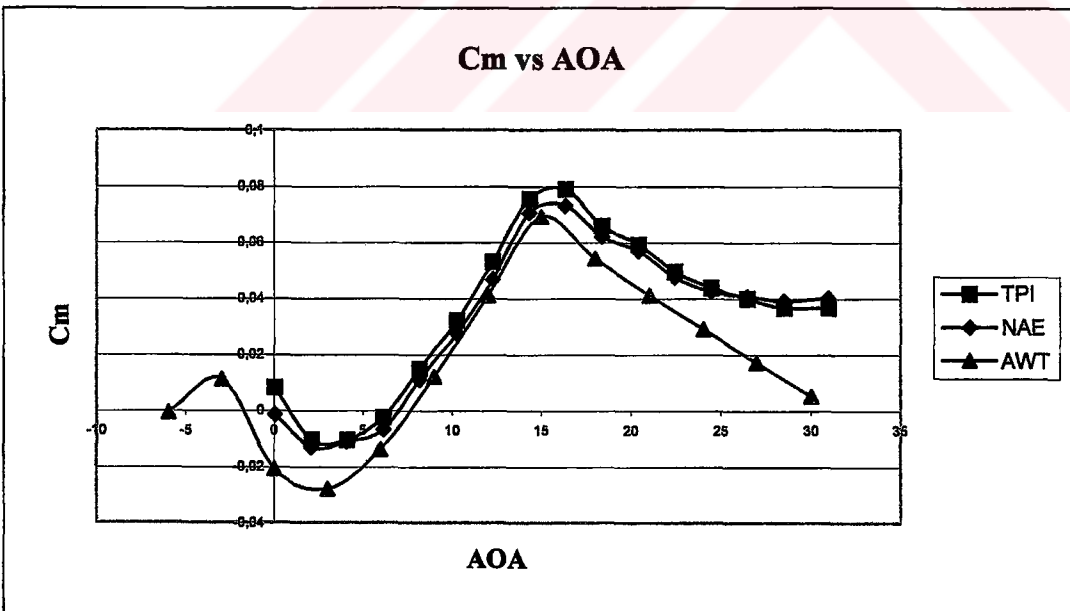


Figure 5.15 The facility comparison for the static coefficient C_m variation with angle of attack

5.2 Dynamic Test Results and Comparison with Other Facilities

As mentioned in chapter 4, the goal of the oscillatory tests using forced oscillation technique is to get the stiffness and the damping derivatives of rolling moment, C_l , normal force, C_z , and pitching moment, C_m . The oscillatory tests made in pitch mode show that the repeatability of different tests is good except two cases of the rolling moment damping derivatives, $C_{lq} + C_{l\dot{\alpha}}$, in the linear range of α (Figures 5.16 to 5.33). In order to check the repeatability of test data, each test case run was repeated three times.

The stiffness derivative $C_{l\alpha}$ (Figures 5.16, 5.17, 5.18) is mostly small in the linear range of angle of attack and remains around zero in the angle of attack range. A similar behavior is characterized for the damping derivative $C_{lq} + C_{l\dot{\alpha}}$ (Figures 5.19, 5.20, 5.21). As might be expected for pitch oscillations, the rolling moment derivatives, which is a cross-coupling derivative for pitch oscillations, are very small at zero sideslip over the complete α range.

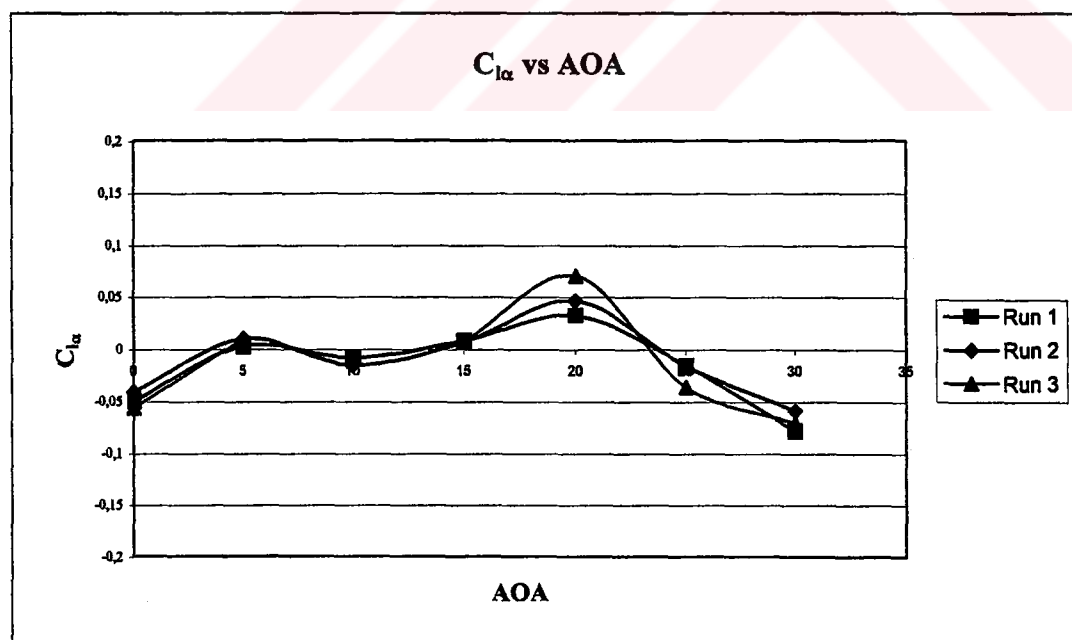


Figure 5.16 The Stiffness Derivative $C_{l\alpha}$ for $V = 30m/s$, $f = 1Hz$, $\theta = \pm 1^\circ$ (data repeatability)

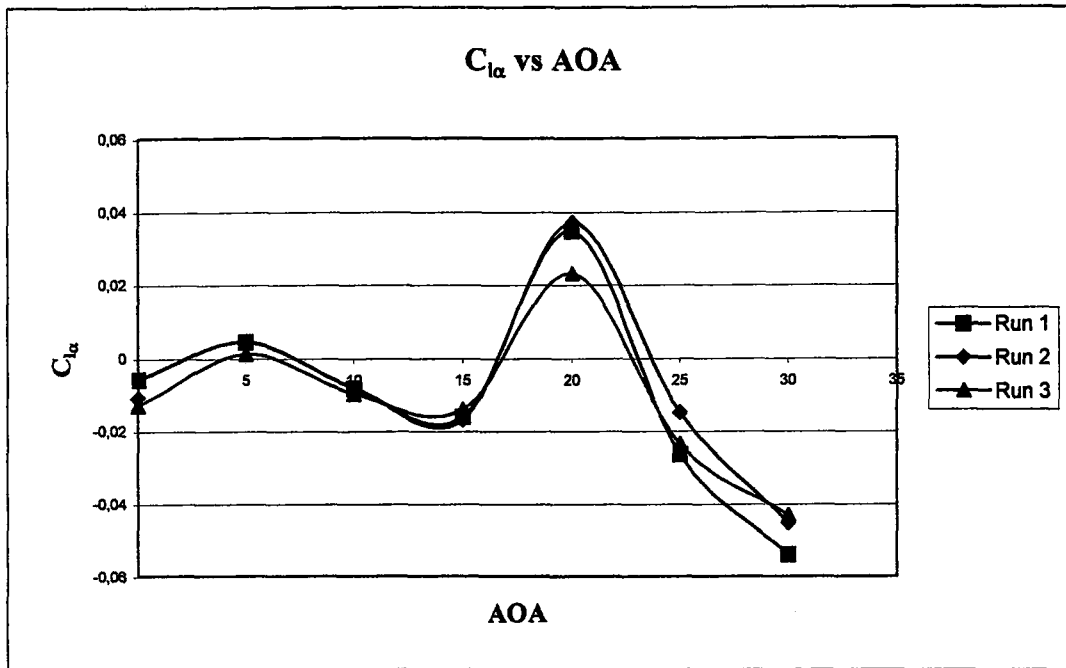


Figure 5.17 The Stiffness Derivative $C_{l\alpha}$ for $V = 30\text{m/s}$, $f = 1\text{Hz}$, $\theta = \pm 2^\circ$ (data repeatability)

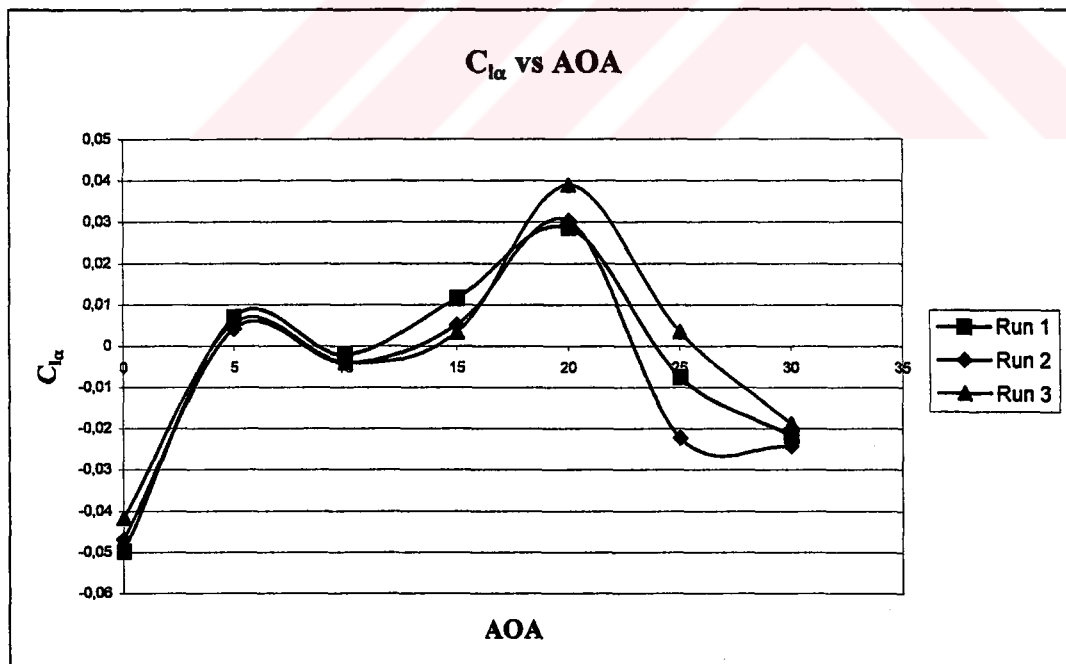


Figure 5.18 The Stiffness Derivative $C_{l\alpha}$ for $V = 30\text{m/s}$, $f = 2\text{Hz}$, $\theta = \pm 1^\circ$ (data repeatability)

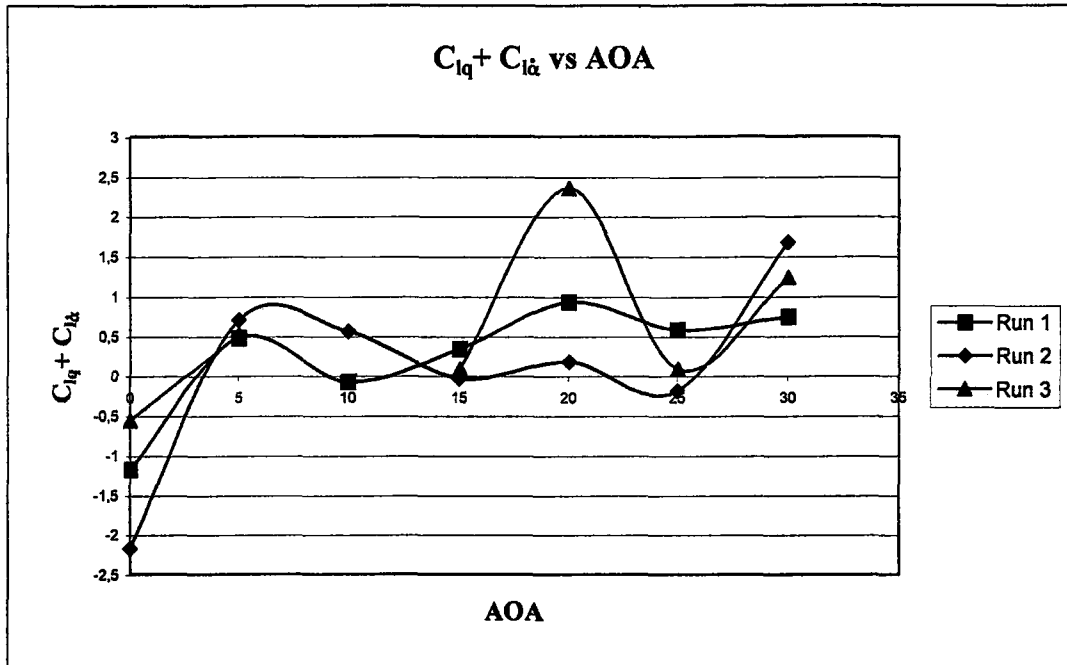


Figure 5.19 The Damping Derivative $C_{lq} + C_{l\dot{\alpha}}$ for $V = 30m/s$, $f = 1Hz$, $\theta = \pm 1^\circ$ (data repeatability)

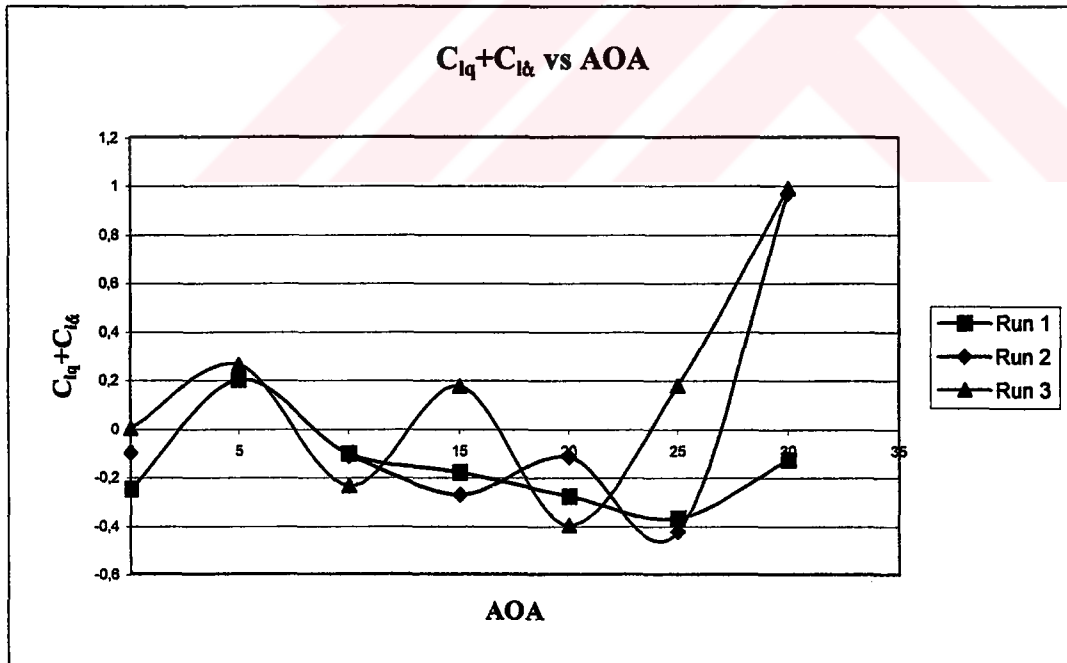


Figure 5.20 The Damping Derivative $C_{lq} + C_{l\dot{\alpha}}$ for $V = 30m/s$, $f = 1Hz$, $\theta = \pm 2^\circ$ (data repeatability)

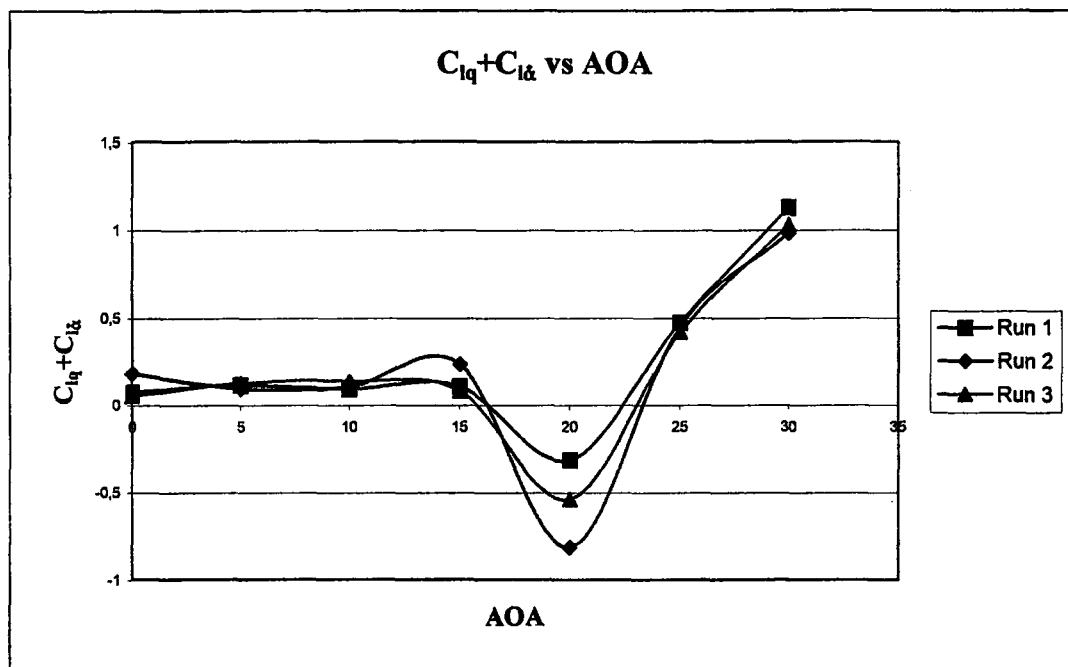


Figure 5.21 The Damping Derivative $C_{lq} + C_{l\dot{\alpha}}$ for $V = 30m/s$, $f = 2\text{ Hz}$, $\theta = \pm 1^\circ$ (data repeatability)

Figures 5.22, 5.23 and 5.24 show the trend of the stiffness derivative $C_{z\alpha}$ and figures 5.25, 5.26 and 5.27 show the trend of the damping derivative $C_{zq} + C_{z\dot{\alpha}}$. The normal force damping derivative $C_{zq} + C_{z\dot{\alpha}}$ at zero sideslip initially peaks at $\alpha=15^\circ$, after which a sharp drop occurs, to reach a minimum value at $\alpha=20^\circ$ as can be seen from Figure 5.27. Beyond this point the damping rises to a steady level at $\alpha=25^\circ$ and higher. It should be noted that, in figures 5.25 and 5.26, the values of damping derivatives $C_{zq} + C_{z\dot{\alpha}}$, for test runs made at $f=1\text{ Hz}$, are observed to be much larger than according to the damping derivative values of Figure 5.27, for test runs made at $f=2\text{ Hz}$. Probable cause of these very large values is discussed in chapter 6 and is attributed to fact that the center of gravity and the oscillation center for the model did not coincide. The behavior of the damping derivative, $C_{zq} + C_{z\dot{\alpha}}$, is reflected in an opposing trend in the stiffness derivative $C_{z\alpha}$, with its negative and positive peaks at the same angles of attack as in the damping case, namely $\alpha=15^\circ$ and 20° respectively.

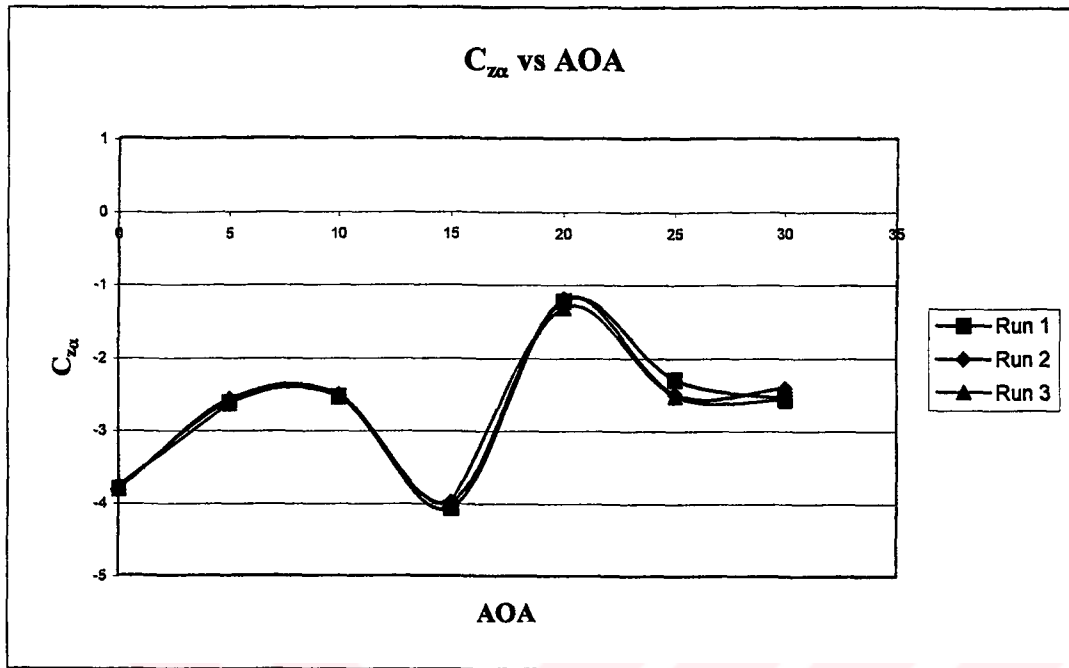


Figure 5.22 The Stiffness Derivative $C_{z\alpha}$ for $V = 30\text{m/s}$, $f = 1\text{Hz}$, $\theta = \pm 1^\circ$ (data repeatability)

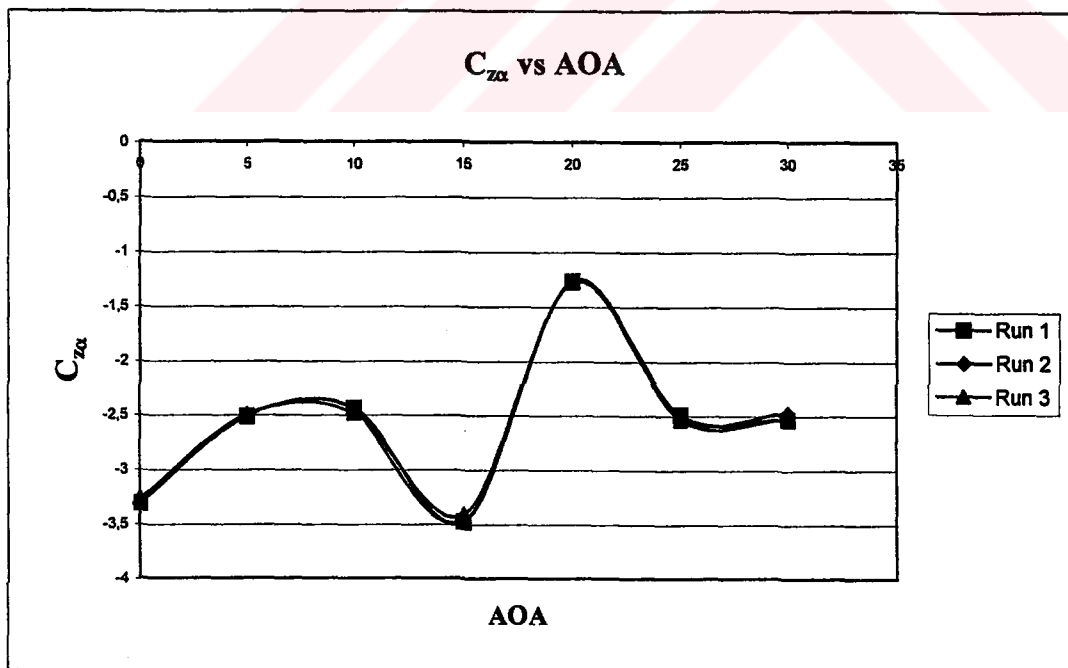


Figure 5.23 The Stiffness Derivative $C_{z\alpha}$ for $V = 30\text{m/s}$, $f = 1\text{Hz}$, $\theta = \pm 2^\circ$ (data repeatability)

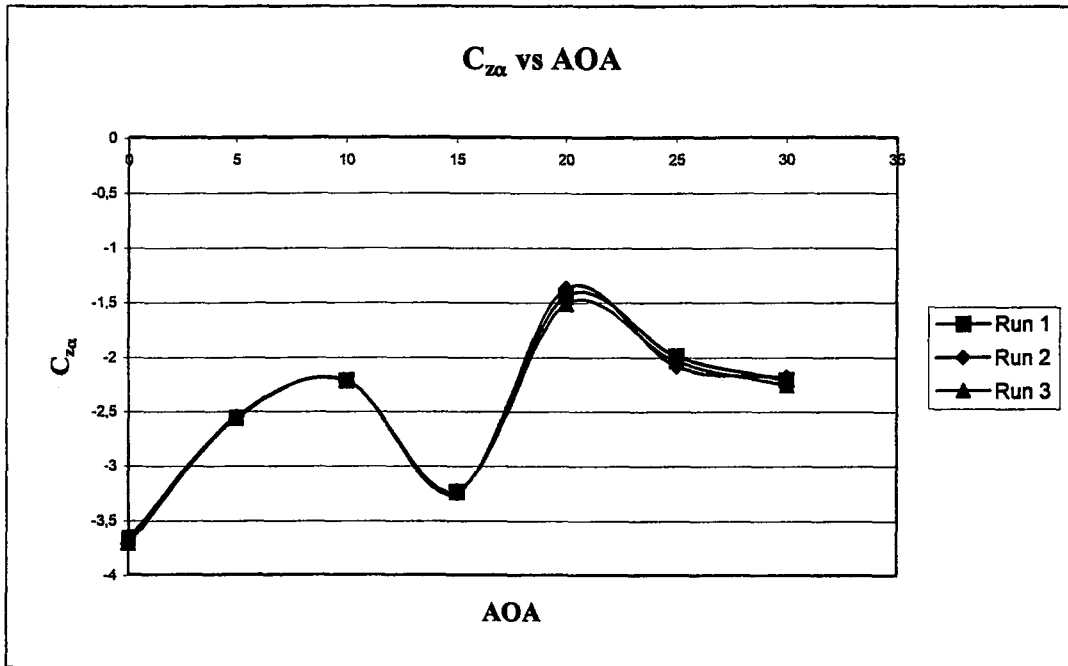


Figure 5.24 The Stiffness Derivative $C_{z\alpha}$ for $V = 30m/s$, $f = 2 Hz$, $\theta = \pm 1^\circ$ (data repeatability)

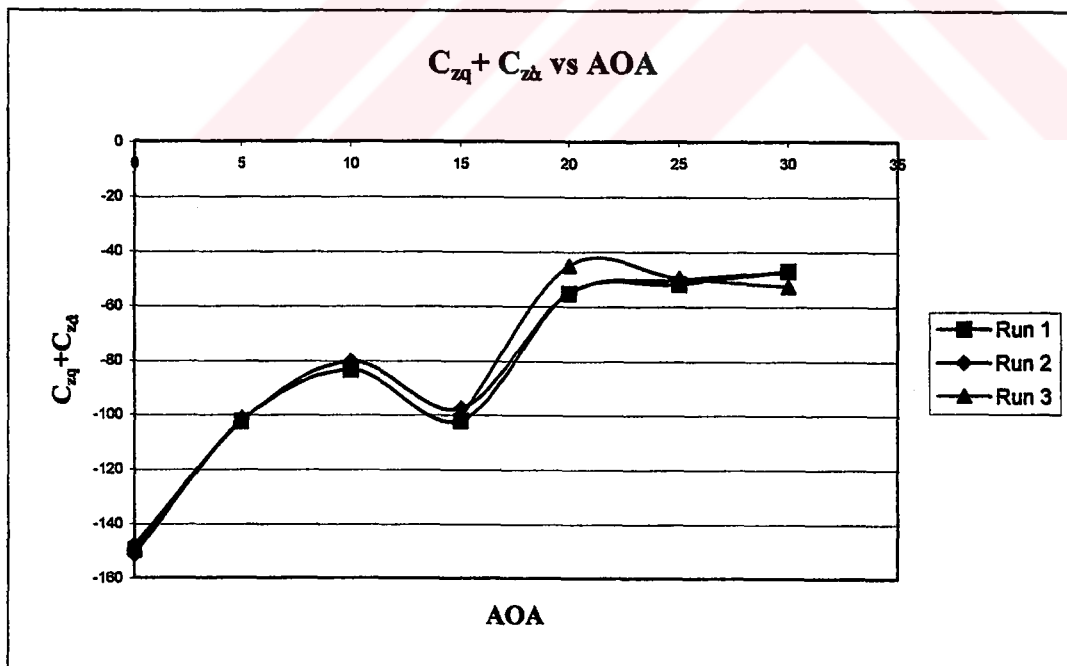


Figure 5.25 The Damping Derivative $C_{zq} + C_{z\dot{\alpha}}$ for $V = 30m/s$, $f = 1 Hz$, $\theta = \pm 1^\circ$ (data repeatability)

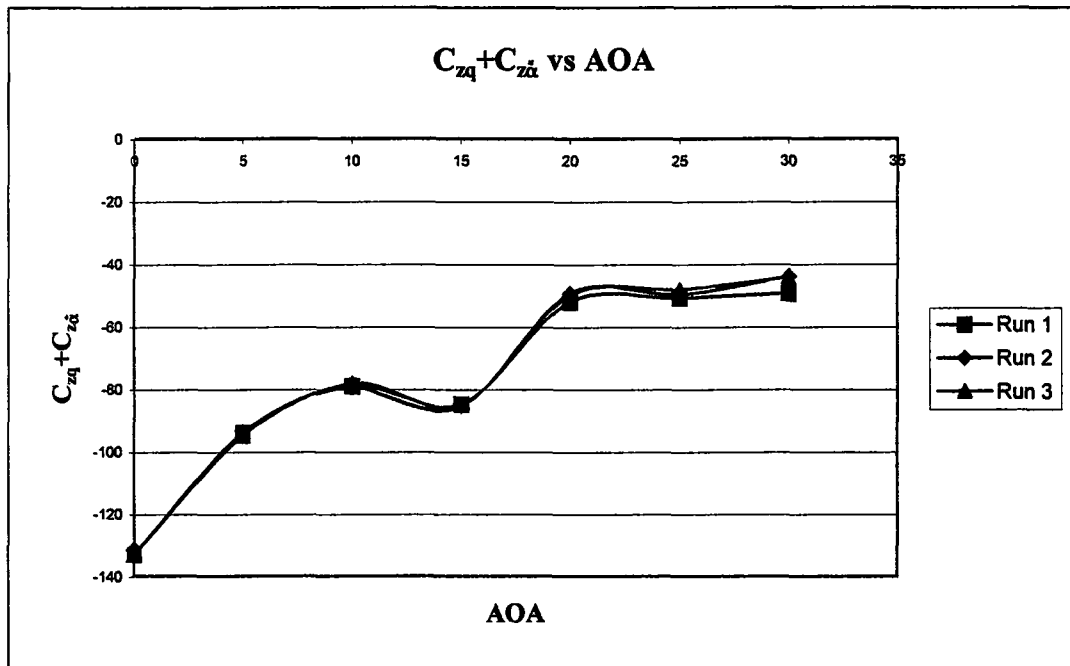


Figure 5.26 The Damping Derivative $C_{zq} + C_{z\dot{\alpha}}$ for $V = 30 \text{ m/s}, f = 1 \text{ Hz}, \theta = \pm 2^\circ$ (data repeatability)

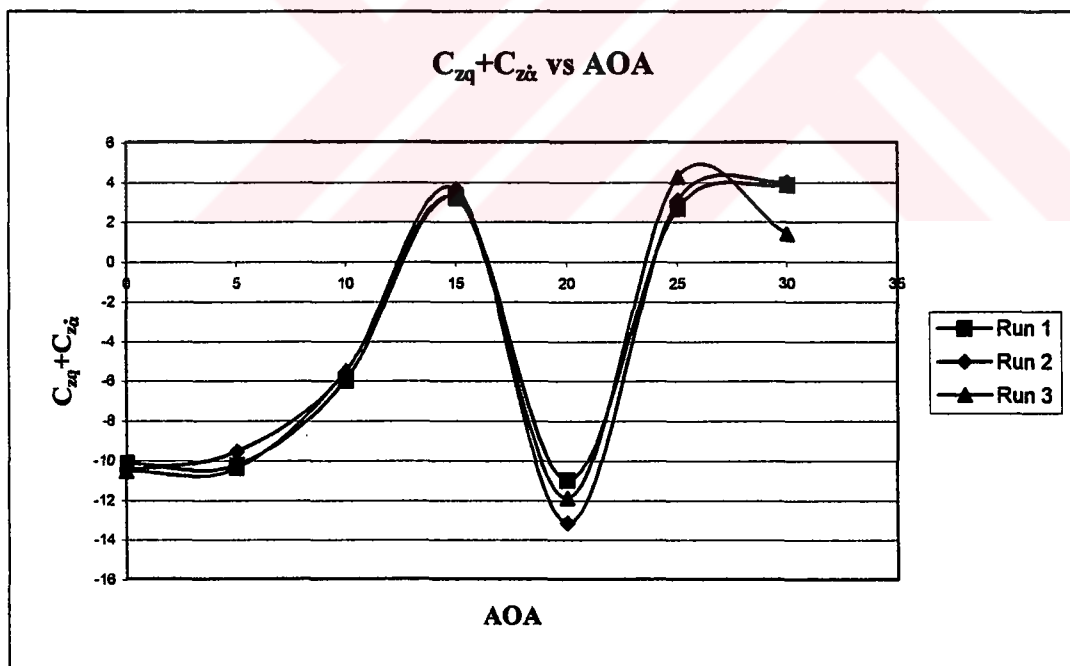


Figure 5.27 The Damping Derivative $C_{zq} + C_{z\dot{\alpha}}$ for $V = 30 \text{ m/s}, f = 2 \text{ Hz}, \theta = \pm 1^\circ$ (data repeatability)

The trend of $C_{m\alpha}$ is presented in Figures 5.28, 5.29 and 5.30. The stiffness derivative $C_{m\alpha}$ rises linearly and peaks at $\alpha=10^\circ$. Then it reaches a minimum value at $\alpha=20^\circ$. After this angle of attack, $C_{m\alpha}$ slightly rises to a steady level. The damping derivative $C_{mq} + C_{m\dot{\alpha}}$ is presented in Figures 5.31, 5.32 and 5.33. The damping derivative $C_{mq} + C_{m\dot{\alpha}}$ slightly rises and peaks at $\alpha=10^\circ$ and reaches a minimum value at $\alpha=20^\circ$, after which, rises slowly again (see Figure 5.33).

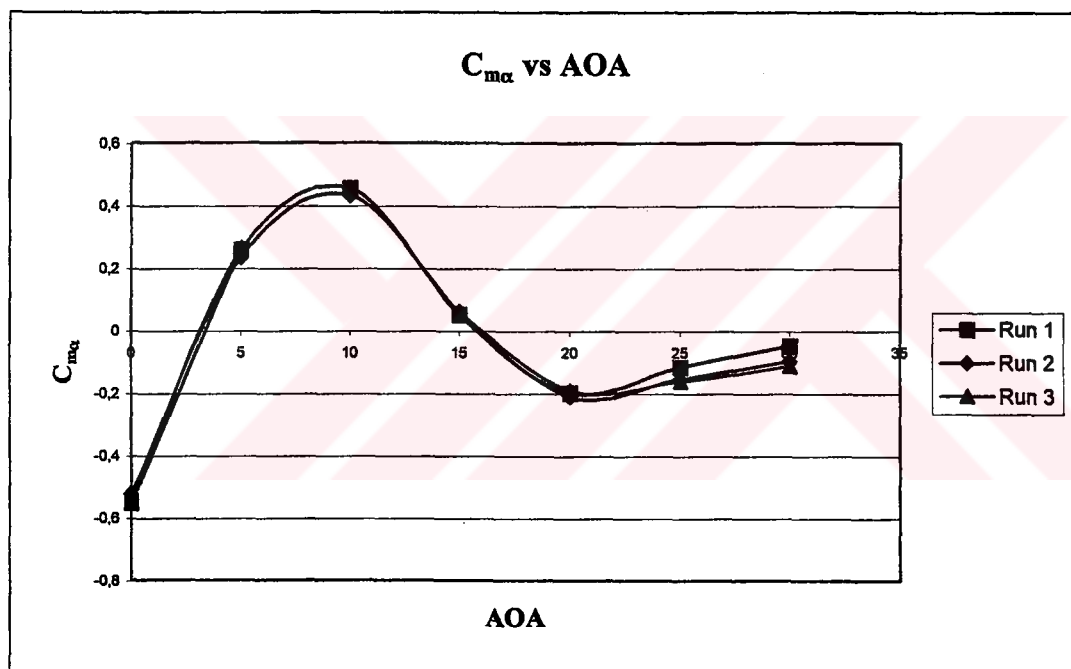


Figure 5.28 The Stiffness Derivative $C_{m\alpha}$ for $V = 30m/s$, $f = 1Hz$, $\theta = \pm 1^\circ$ (data repeatability)

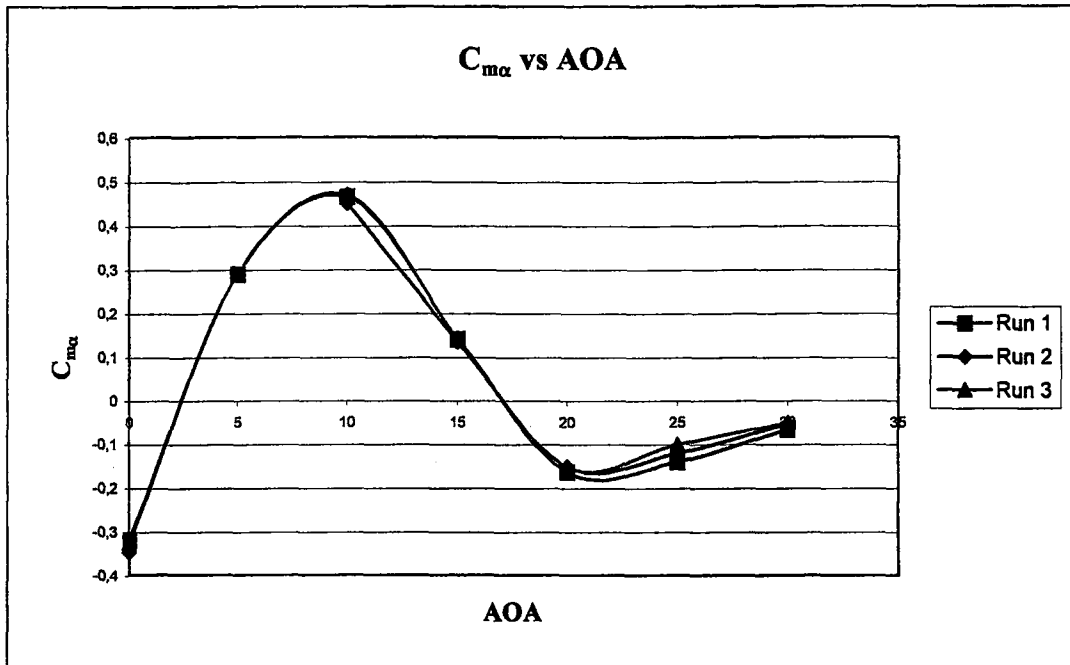


Figure 5.29 The Stiffness Derivative $C_{m\alpha}$ for $V = 30\text{ m/s}, f = 1\text{ Hz}, \theta = \pm 2^\circ$ (data repeatability)

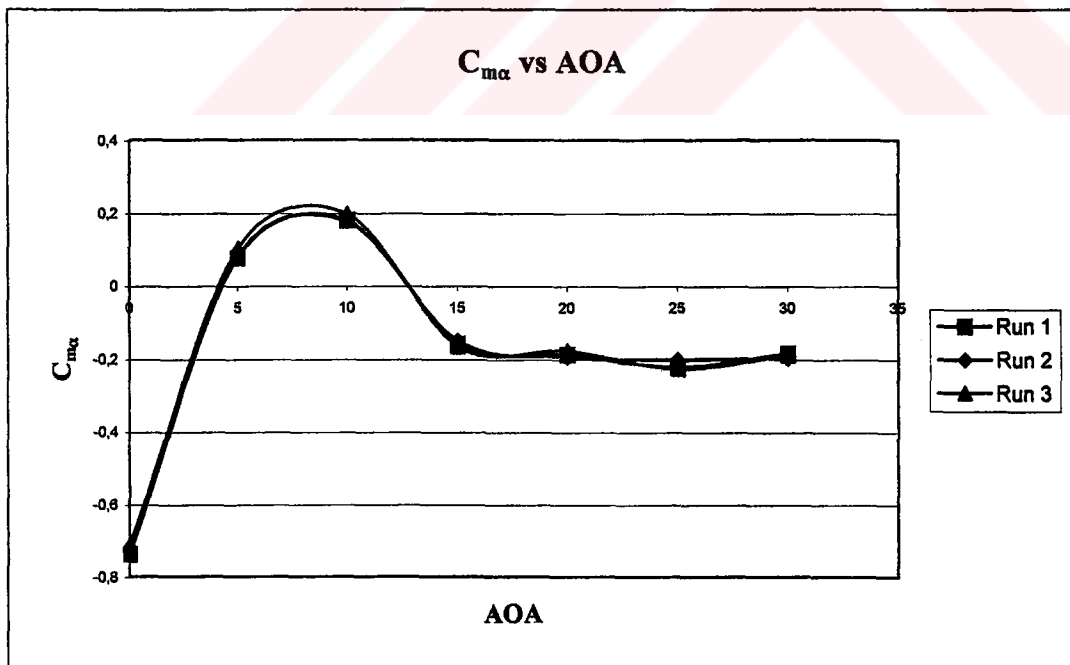


Figure 5.30 The Stiffness Derivative $C_{m\alpha}$ for $V = 30\text{ m/s}, f = 2\text{ Hz}, \theta = \pm 1^\circ$ (data repeatability)

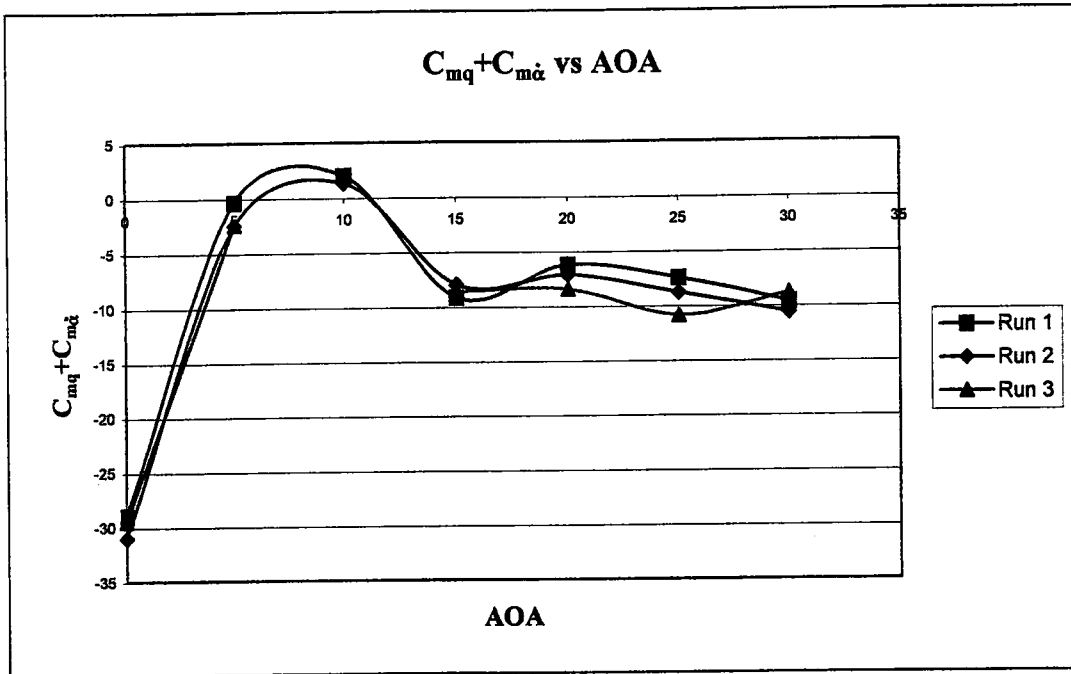


Figure 5.31 The Damping Derivative $C_{mq} + C_{m\dot{\alpha}}$ for $V = 30m/s$, $f = 1Hz$, $\theta = \pm 1^\circ$
(data repeatability)

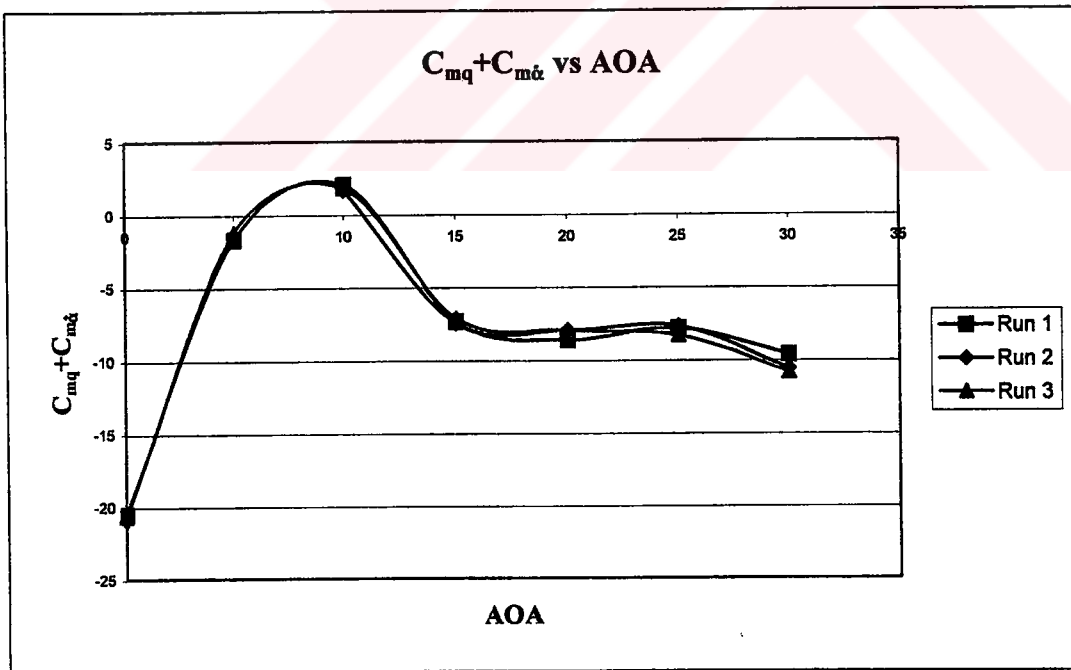


Figure 5.32 The Damping Derivative $C_{mq} + C_{m\dot{\alpha}}$ for $V = 30m/s$, $f = 1Hz$, $\theta = \pm 2^\circ$
(data repeatability)

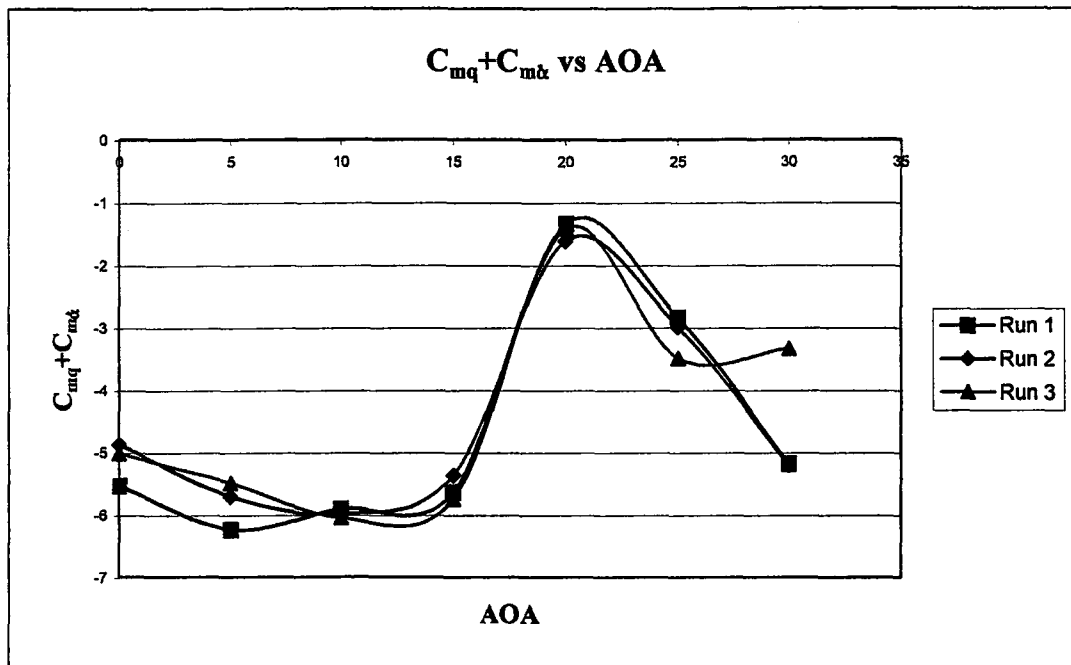


Figure 5.33 The Damping Derivative $C_{mq} + C_{m\dot{\alpha}}$ for $V = 30m/s$, $f = 2 Hz$, $\theta = \pm 1^\circ$ (data repeatability)

The effect of the amplitude of the oscillation on the rolling moment stiffness derivative $C_{l\alpha}$ is shown in Figure 5.34. Differences in the variation of $C_{l\alpha}$ due to amplitude variation are quite small. However, differences in the variation of the rolling moment damping derivative $C_{lq} + C_{l\dot{\alpha}}$ are noticeable and the trend of the variation of derivatives with angle of attack is quite different (Figure 5.35).

The effect of amplitude on normal force stiffness derivative $C_{z\alpha}$ and damping derivative $C_{zq} + C_{z\dot{\alpha}}$ can be seen from Figures (5.36) and (5.37) respectively. The amplitude effect on $C_{z\alpha}$ and $C_{zq} + C_{z\dot{\alpha}}$ are small but noticeable at $\alpha = 15^\circ$.

Similar trends for the effect of oscillation amplitudes are observed in Figures 5.38 and 5.39 for $C_{m\alpha}$ and $C_{mq} + C_{m\dot{\alpha}}$ variation with respect to angle of attack.

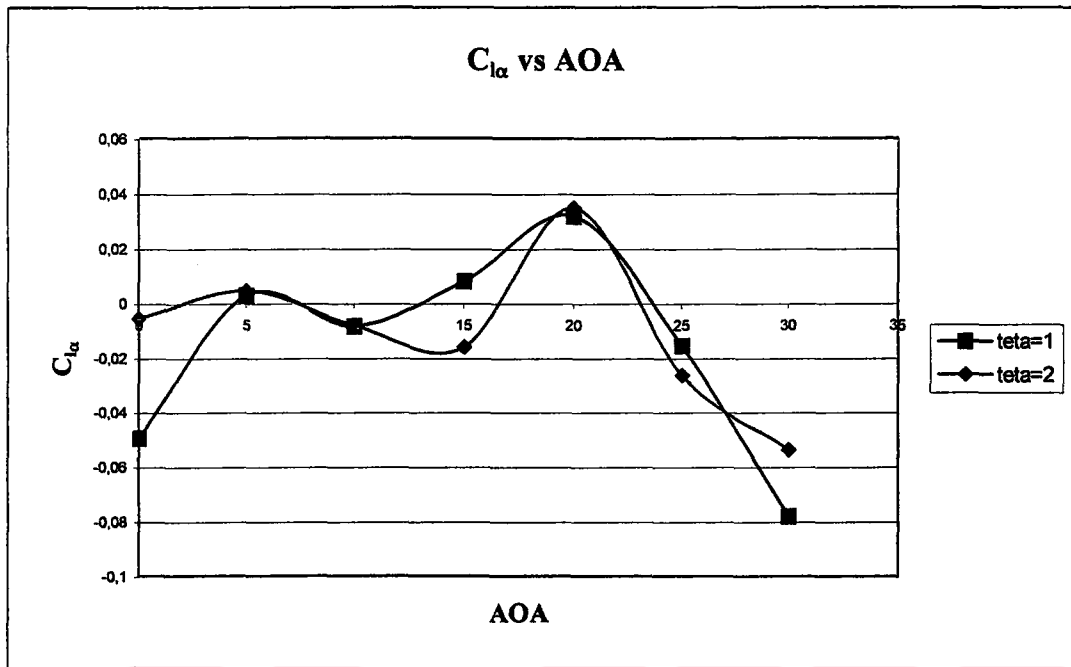


Figure 5.34 The Effect of Amplitude on $C_{l\dot{\alpha}}$ for $V = 30 \text{ m/s}$, $f = 1 \text{ Hz}$

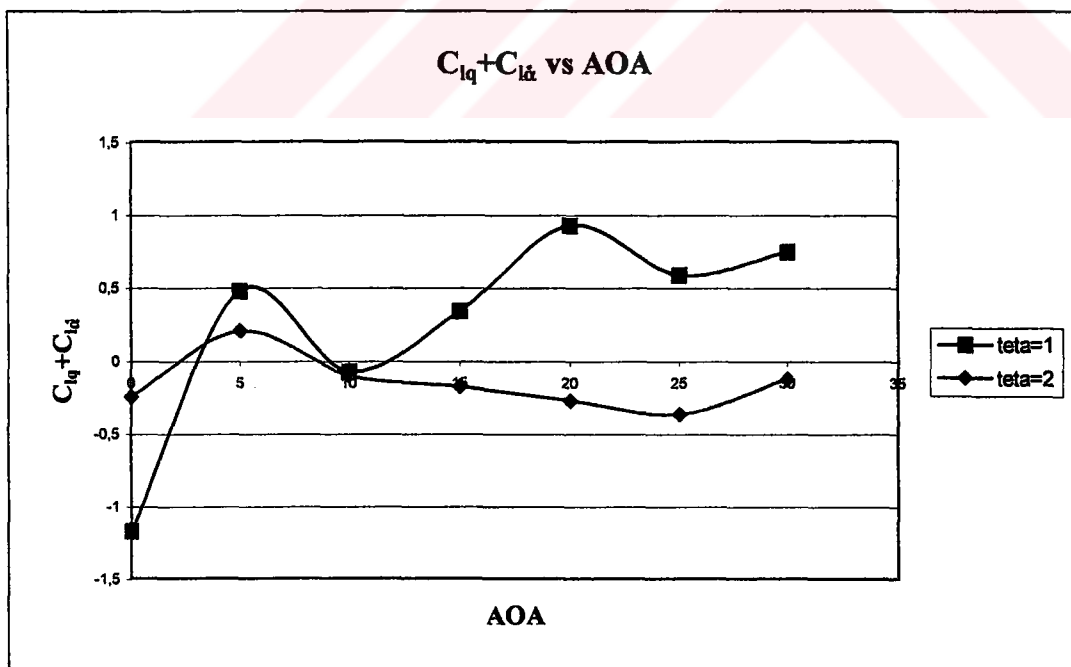


Figure 5.35 The Effect of Amplitude on $C_{lq} + C_{l\dot{\alpha}}$ for $V = 30 \text{ m/s}$, $f = 1 \text{ Hz}$

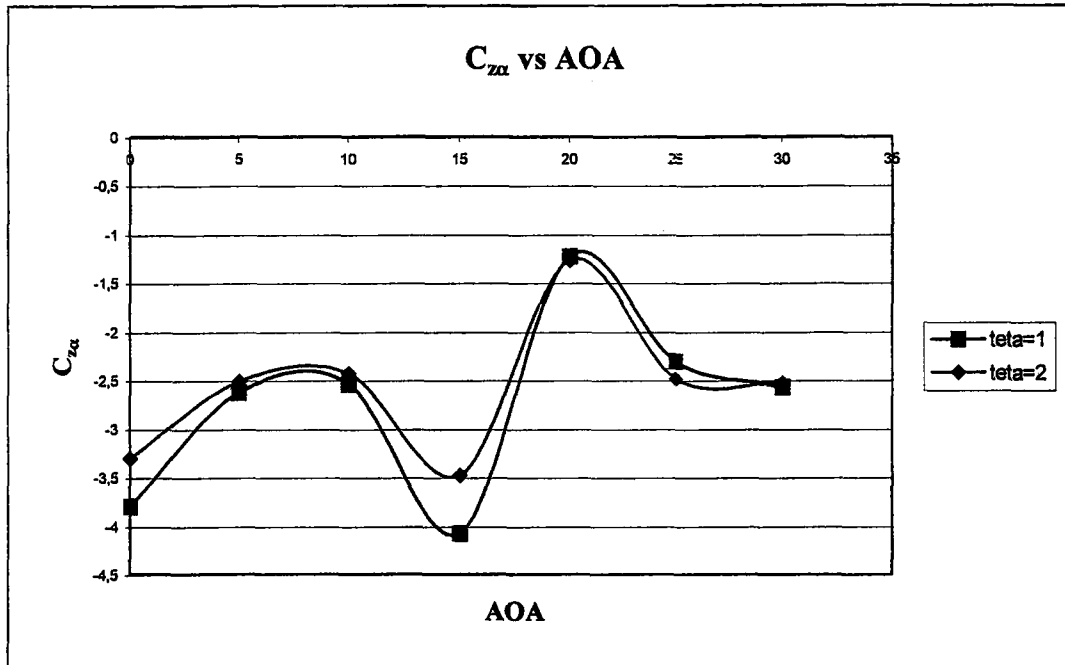


Figure 5.36 The Effect of Amplitude on $C_{z\alpha}$ for $V = 30 \text{ m/s}$, $f = 1 \text{ Hz}$

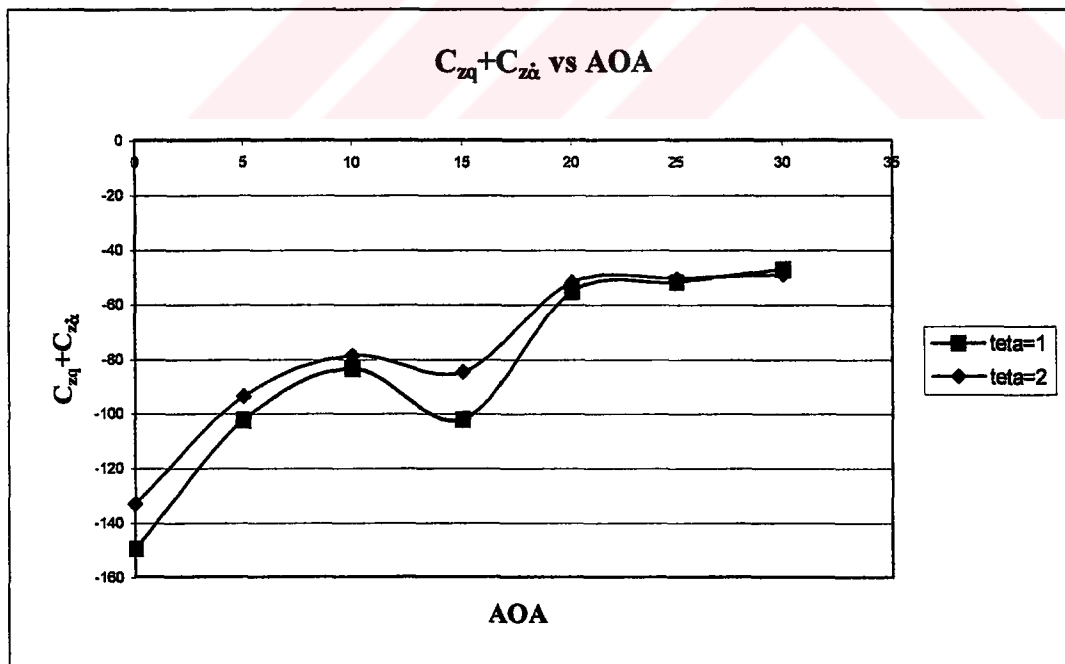


Figure 5.37 The Effect of Amplitude on $C_{zq} + C_{z\alpha}$ for $V = 30 \text{ m/s}$, $f = 1 \text{ Hz}$

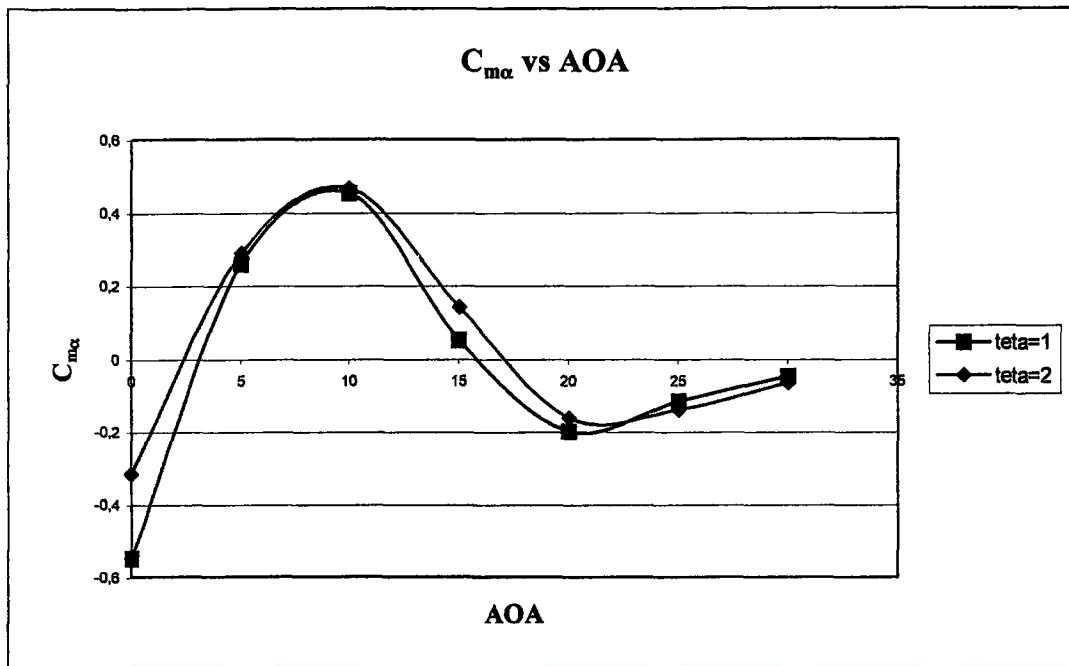


Figure 5.38 The Effect of Amplitude on $C_{m\alpha}$ for $V = 30 \text{ m/s}$, $f = 1 \text{ Hz}$

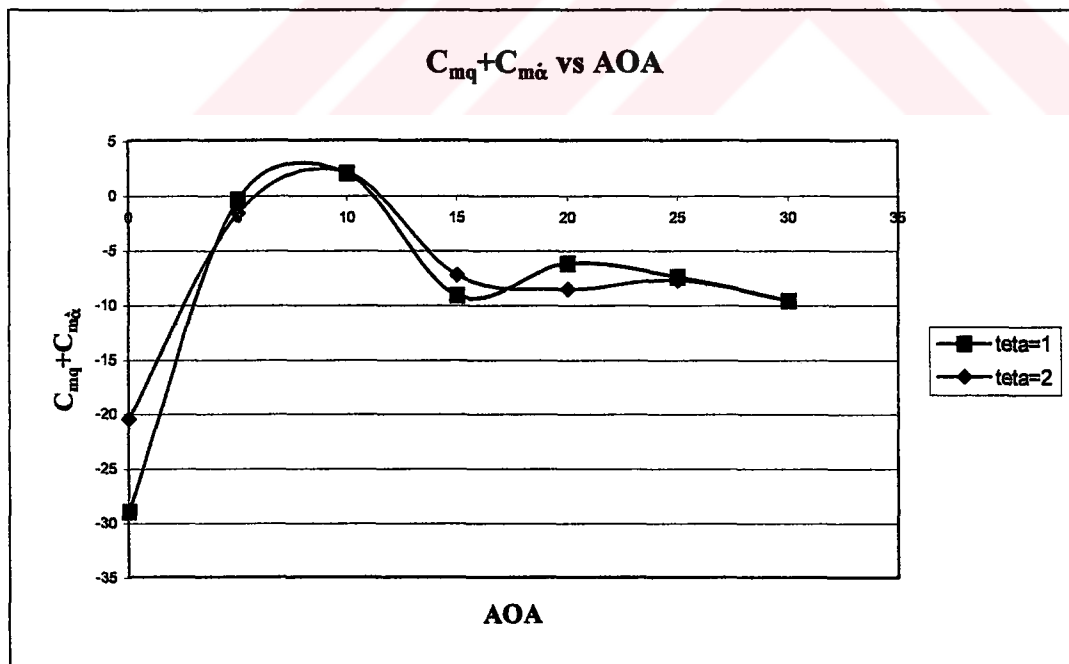


Figure 5.39 The Effect of Amplitude on $C_{mq} + C_{m\alpha}$ for $V = 30 \text{ m/s}$, $f = 1 \text{ Hz}$

Results from pitch oscillation tests at two different frequencies, $f=1$ Hz ($K=0.023$) and 2 Hz ($K=0.046$) for $V = 30\text{ m/s}$, $\theta = \pm 1^\circ$ are shown in figures 5.40 to 5.45. Although the effect of frequency on rolling moment stiffness derivative $C_{l\alpha}$ (Figure 5.40) is small, the effect on the rolling moment damping derivative $C_{lq} + C_{l\dot{\alpha}}$ is large as observed in Figure 5.41.

Although there are some differences in the variation of normal force stiffness derivative $C_{z\alpha}$ with frequency the variation with angle of attack has the same trend (Figure 5.42). However the effects of frequency on the normal force damping coefficient $C_{zq} + C_{z\dot{\alpha}}$ is more pronounced (Figure 5.43). The levels of damping Coefficient $C_{zq} + C_{z\dot{\alpha}}$ are not of the same order of magnitude for different frequencies and show different trends for the variation with angle of attack. The variation of pitching moment stiffness derivative $C_{m\alpha}$ with frequency is small but still noticeable (Figure 5.44). Whereas, the effect of oscillation frequency becomes clearly evident for the pitching moment damping coefficient $C_{mq} + C_{m\dot{\alpha}}$ as shown in Figure 5.45.

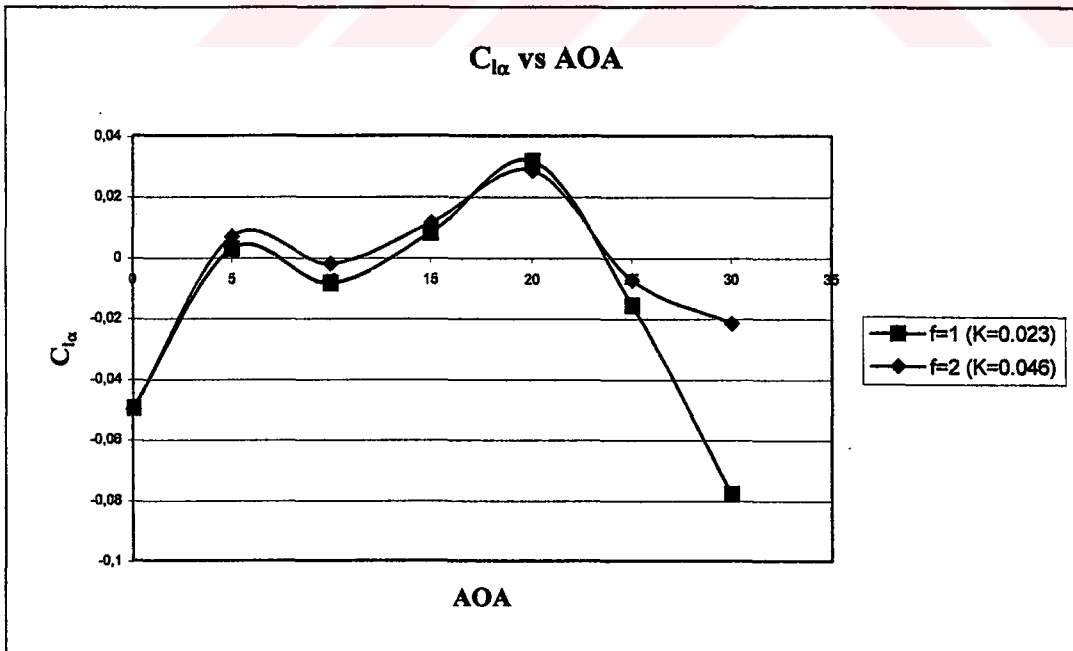


Figure 5.40 The Effect of Frequency on $C_{l\alpha}$ for $V = 30\text{ m/s}$, $\theta = \pm 1^\circ$

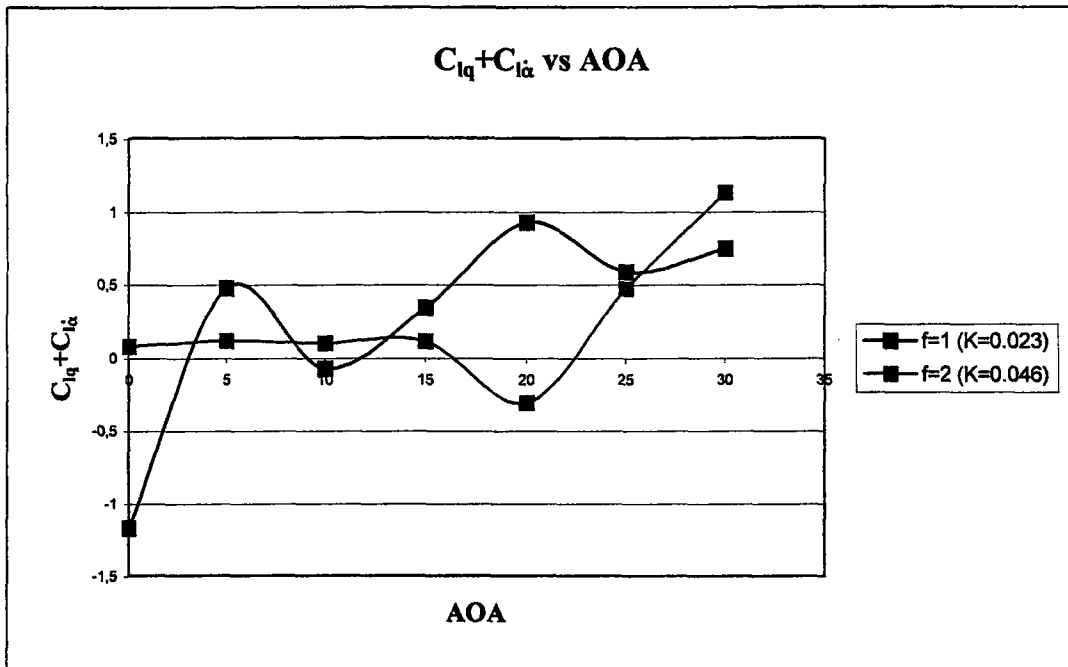


Figure 5.41 The Effect of Frequency on $C_{lq} + C_{l\dot{\alpha}}$ for $V = 30 \text{ m/s}$, $\theta = \pm 1^\circ$

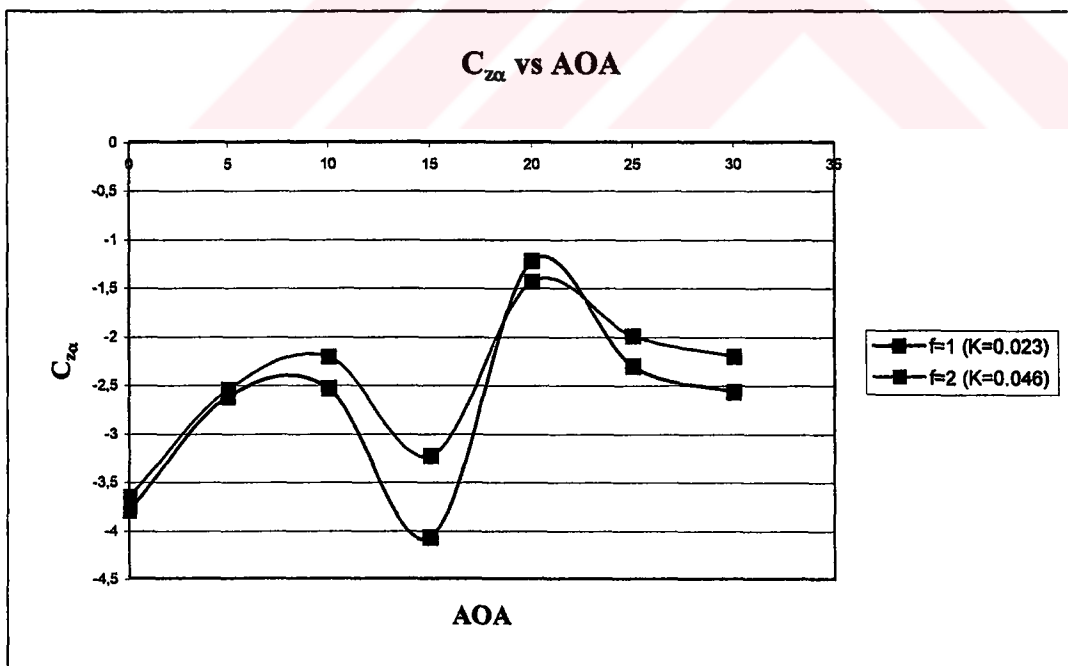


Figure 5.42 The Effect of Frequency on $C_{z\alpha}$ for $V = 30 \text{ m/s}$, $\theta = \pm 1^\circ$

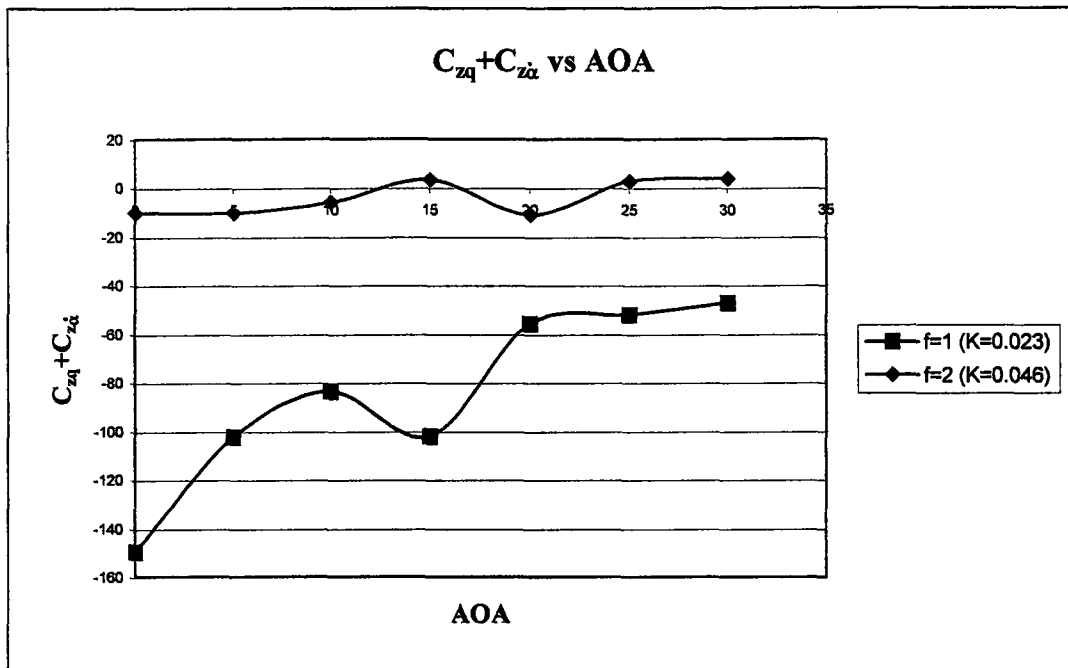


Figure 5.43 The Effect of Frequency on $C_{zq} + C_{z\dot{\alpha}}$ for $V = 30 \text{ m/s}$, $\theta = \pm 1^\circ$

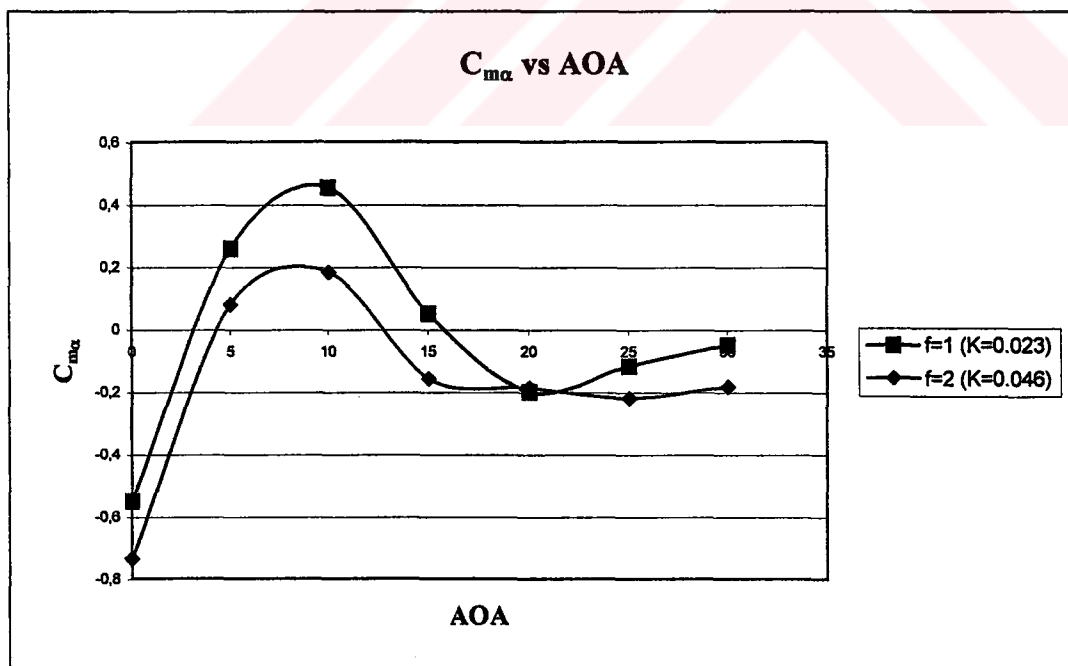


Figure 5.44 The Effect of Frequency on $C_{m\alpha}$ for $V = 30 \text{ m/s}$, $\theta = \pm 1^\circ$

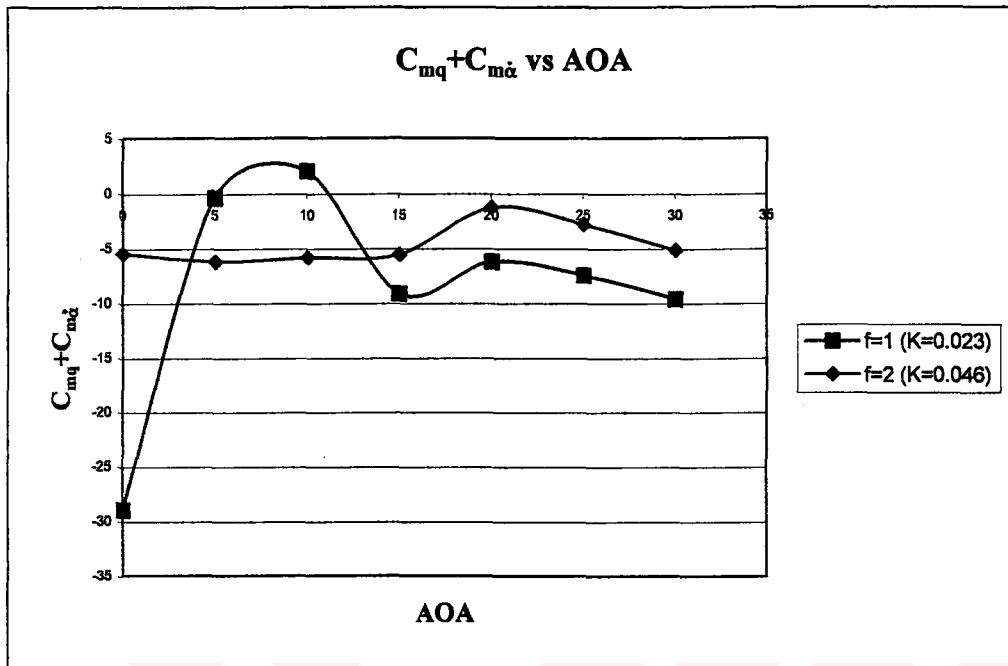


Figure 5.45 The Effect of Frequency on $C_{mq} + C_{m\dot{\alpha}}$ for $V = 30 \text{ m/s}$, $\theta = \pm 1^\circ$

Comparison of the rolling moment stiffness and damping coefficient variations with respect to angle of attack with those obtained in other wind tunnel facilities can be seen in Figures 5.46 and 5.47 respectively. The value of the stiffness coefficient $C_{l\alpha}$ (Figure 5.46) is very small and remains around zero in the complete range of angle of attack studied. A similar behavior is also observed in the damping derivative $C_{lq} + C_{l\dot{\alpha}}$ variation with respect to angle of attack (Figure 5.47).

In Figures 5.48 and 5.49 the normal force stiffness and damping coefficient variation with angle of attack are compared with the results obtained in Politecnico di Torino (TPI) and National Aeronautical Establishment (NAE). The results exhibit similar trends but for values of α larger than 20° the damping coefficients measured in AWT and TPI show different behavior.

The stiffness and the damping coefficients for the pitching moment are compared with those obtained in TPI and NAE in Figures 5.50 and 5.51 respectively. Differences in the measured values are evident in the whole range of angle of attack considered. However the trends are observed to be similar. The experimental results of the AWT tests are generally in good agreement with those of the other facilities. The differences observed between the present test results and those of the other test facilities can be attributed to the particular characteristics of the facilities used; such as the differences in suspension systems, wind tunnel characteristics, model blockage and interference effects, flow asymmetries caused by the support systems, etc.

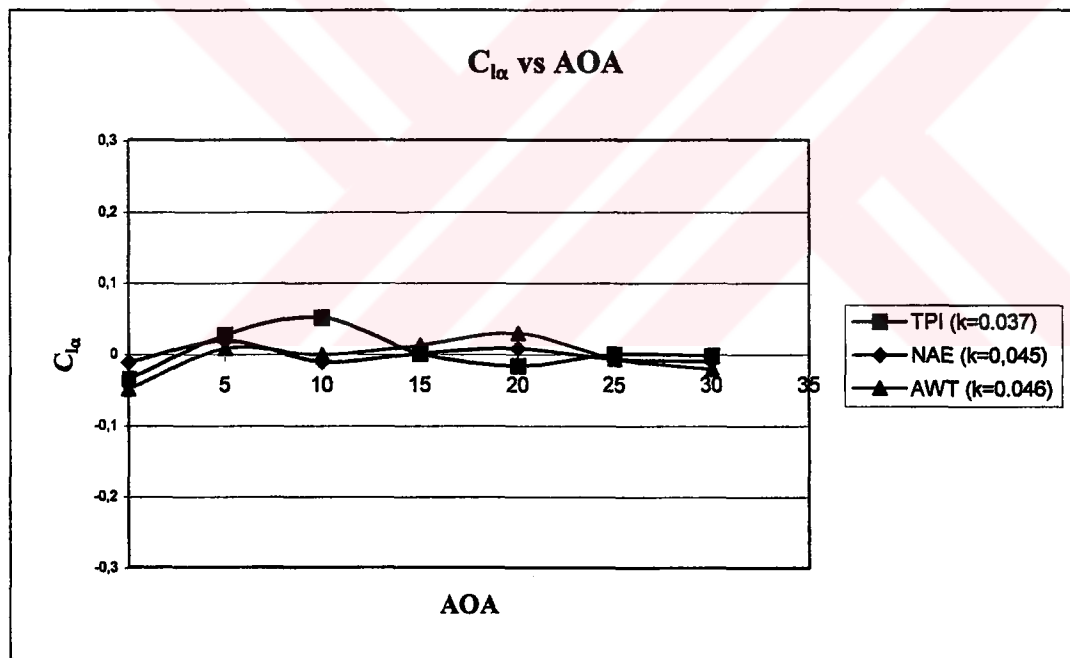


Figure 5.46 Comparisons of $C_{l\alpha}$ coefficient measurements with results obtained in other test facilities

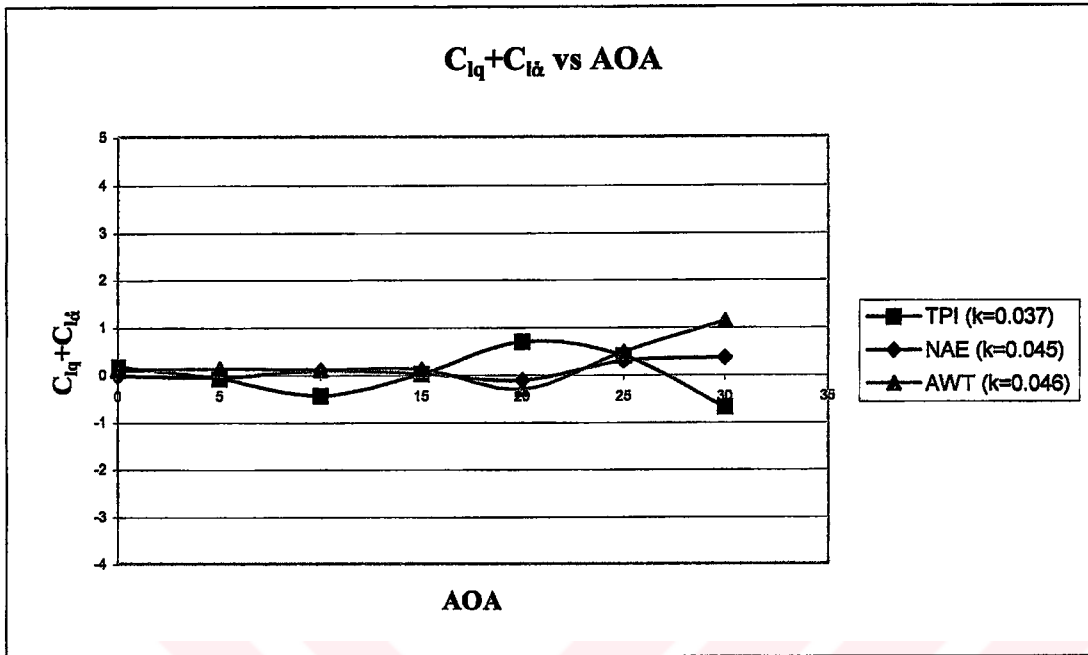


Figure 5.47 Comparisons of $C_{lq} + C_{la}$ coefficient measurements with results obtained in other test facilities

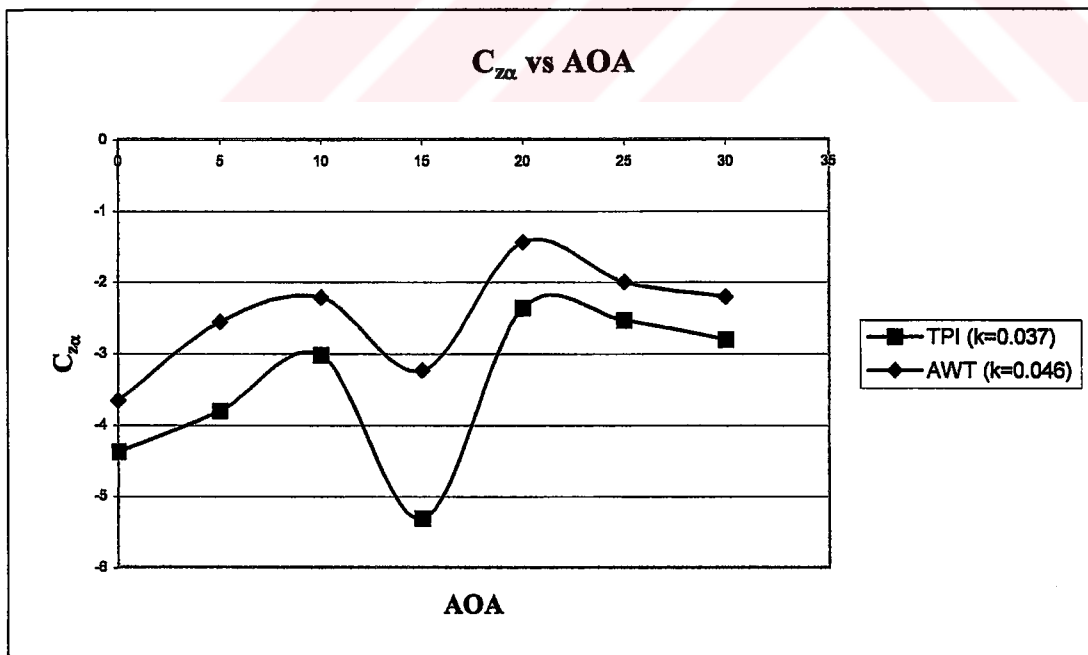


Figure 5.48 Comparisons of $C_{z\alpha}$ coefficient measurements with results obtained in other test facilities

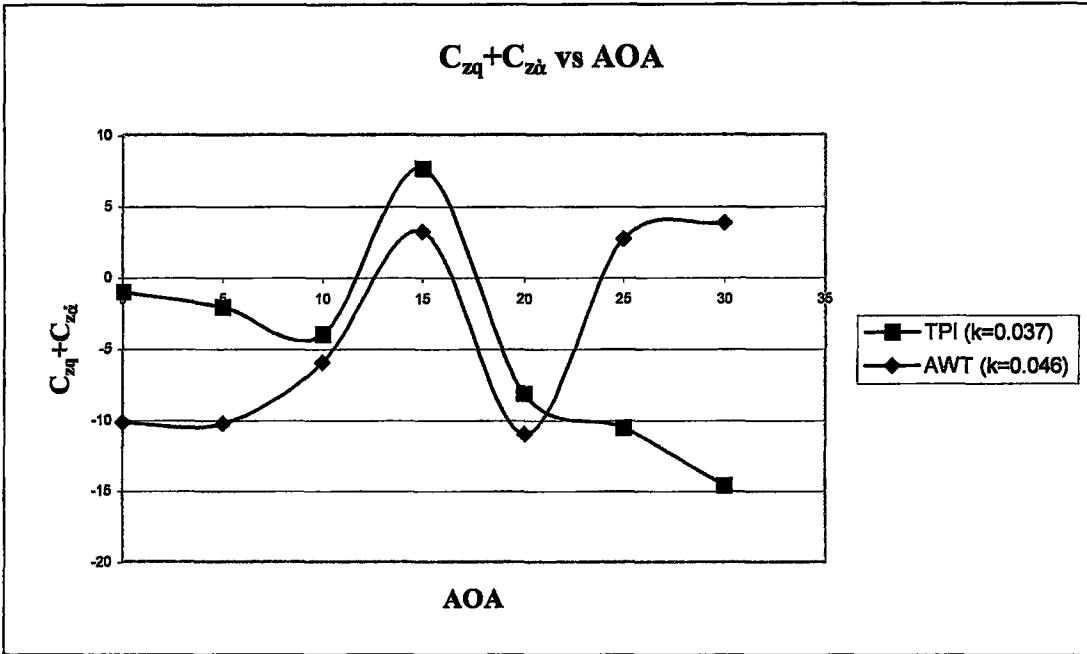


Figure 5.49 Comparisons of $C_{zq} + C_{zd}$ coefficient measurements with results obtained in other test facilities

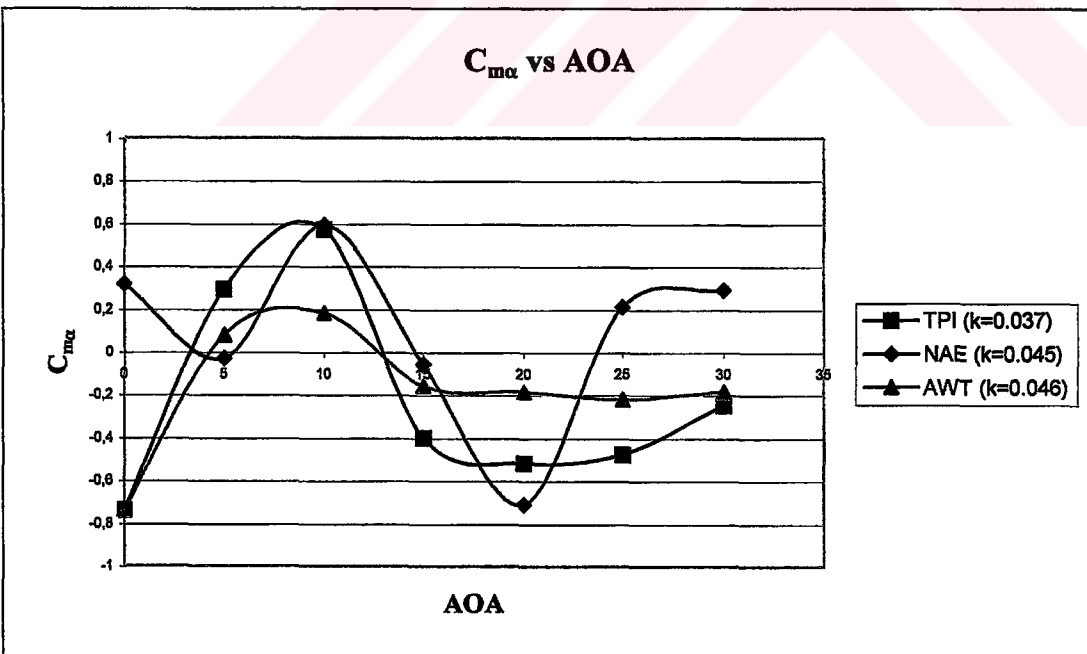


Figure 5.50 Comparisons of $C_{m\alpha}$ coefficient measurements with results obtained in other test facilities

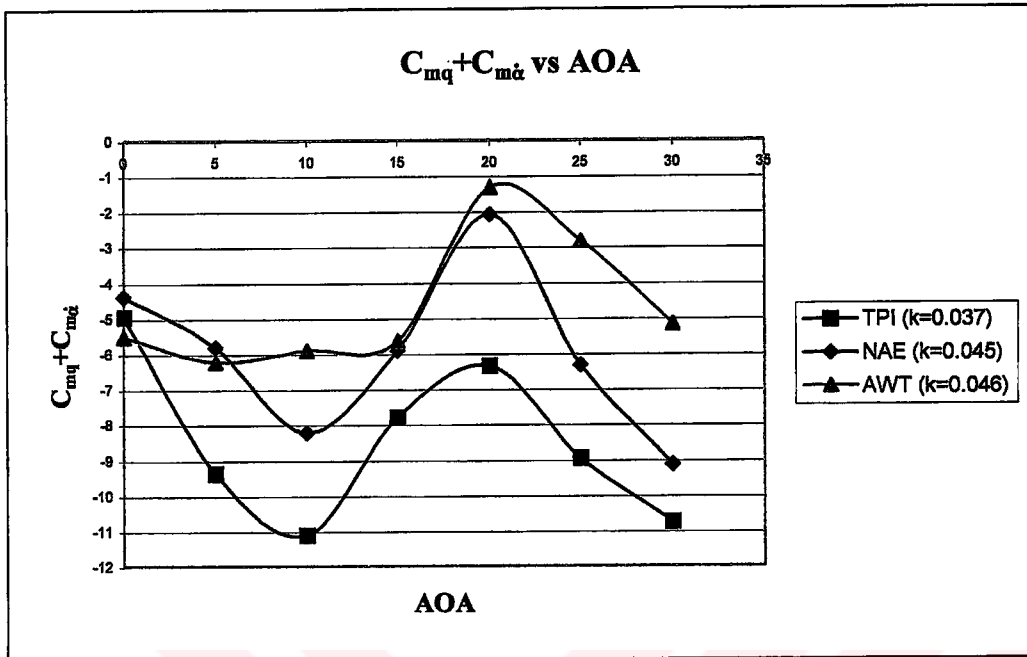


Figure 5.51 Comparisons of $C_{mq} + C_{m\dot{\alpha}}$ coefficient measurements with results obtained in other test facilities

CHAPTER 6

CONCLUSION AND DISCUSSION

Modern military aircraft are often designed to maneuver at relatively high angles of attack and therefore are subjected to flight conditions where the flow becomes highly asymmetric. Most stability derivatives usually display strong non-linearities at high angles of attack. The aerodynamic responses to these maneuvers can be evaluated either from the flow-field computations or from experimental measurements. Most of the current experimental programs are based on wind-tunnel tests where experiments consist of force and moment measurements, surface pressure measurements, surface oil-flow visualization studies, vapor-screen vortex flow visualization, laser velocimeter flow-field measurements, and water-tunnel flow visualization studies. Direct forced oscillation technique, is one of these wind-tunnel experimental techniques, and is used extensively to measure the aerodynamic stability derivatives. The method has been used for many years and has reached a stage of maturity.

High angle of flight is major issue for today's military aircraft and their flight dynamics require the determination of the dynamic stability coefficients. Procedures for estimating the aerodynamic stability derivatives and the mathematical modeling of their flight dynamics are urgently needed. One of the methods to obtain the dynamic stability coefficients is the wind tunnel experiments and the direct forced oscillation technique, which is elaborated in this thesis.

In this respect, the present thesis is an attempt to show the feasibility of experiments using the forced oscillation test technique in the Ankara Wind Tunnel to determine the dynamic stability derivatives. The experimental program carried out at AWT

consisted of forced pitch oscillation tests of a generic combat aircraft model, called the Standard Dynamic Model, to measure the dynamic stability coefficients of this model. The test matrix is given in Table 5.1 and 5.2. Results obtained include a complete set of derivatives due to oscillation in pitch for the basic configuration of the model, BWLVH (B-Body, W-Wing, L-LEX, V-Vertical tail, H-Horizontal tail). Comparison of the present results with the results obtained in other test facilities such as NAE (National Aeronautical Establishment, of Canada) and TPI, (Politecnico di Torino, Italy) are also given.

Static aerodynamic coefficients are obtained for the SDM at angles of attack from -6° to 30° . Effects of wind speed are investigated under conditions of very low wall interference. It was observed that there was no distinct effect of velocity for wind speeds between 20 to 40 m/s. Good repeatability of the measurements are demonstrated for wind speeds in this range.

In Figure 5.14, the position observed for the typical kink in the slope of the normal force coefficient C_z is compared with the results of other facilities and is in good agreement within the proximity of $\alpha=18^{\circ}$ for zero sideslip angle. Differences become noticeable for values of α , larger than 25° for the longitudinal coefficients of C_z and C_m (Figures 5.14 and 5.15). The values obtained for C_l are very small, but consistent with the measurement of the other test facilities. A close examination of the static test results indicate that the results are not influenced by any interference effects such as those of the support geometries or by the shape and the dimensions of the working sections of the wind tunnels.

In dynamic tests, the effects of angle of attack, and the amplitude as well as the frequency of oscillations are investigated over an angle of attack range of 0° to 30° .

Good repeatability of the dynamic test measurements can be seen from Figures 5.16 to 5.33 except for the two cases of the rolling moment damping coefficients, $C_{lq} + C_{l\dot{\alpha}}$. The highly nonlinear nature of aircraft stability

characteristics at high α is once again demonstrated in the dynamic test results shown in Figures 5.16 to 5.33. The direct derivatives due to oscillation in pitch (i.e. pitching derivatives) are highly nonlinear with α at sideslip angle, $\beta=0^0$. Whereas the cross-coupling derivatives are, in general, small at $\beta=0^0$, over the complete range of α investigated from 0^0 to 30^0 .

Effects of the amplitude of the oscillations on the dynamic derivatives are not evident except on the rolling moment derivatives. If the effect of the frequency of oscillations is considered, although the stiffness derivatives are not influenced much, the damping derivatives exhibit large differences with change in frequency of oscillations. This important discrepancy in damping coefficient values with different frequencies can be attributed to the fact that during the experiments the center of gravity of the model and its center of rotation are not made to coincide. The C.G. of the model was located forward of the center of rotation. This inconsistency in the C.G. and rotation center was much more evident and pronounced in the variation of the damping coefficient of the normal force, $C_{zq} + C_{z\dot{\alpha}}$ with different frequencies.

The comparisons of the present results with those obtained in other test facilities are made to put into evidence the influence of various effects such as;

- Different rig support systems,
- Flow characteristics of the wind-tunnels,
- Dimension and geometry of the wind-tunnel working sections,
- Data acquisition and data reduction systems.

It is observed that the flow characteristics of the wind tunnel has little effect on the present measurements conducted in AWT since the level of turbulence is very small, less than 0.05 %.

It is also concluded that the dimensions of the wind tunnel test section of the AWT has very little effect on the measurements. Since the test section of the AWT is

3.05 m in width, 2.44 m in height the blockage effect with the size of the model is negligible for the range of angle of attack studied.

The effect of data acquisition and reduction system is assumed to be negligible since the measurements are performed simultaneously with a sufficiently high sampling rate and the acquired data are observed individually for any discrepancy. The data reduction program is tested for similar data obtained in Politecnico di Torino and exactly the same results are obtained.

Hence the only factor, which no guarantee can be given, is the support interference effect. Since the model is oscillated from its rear while being supported from its fuselage, there is definitely an influence of this support system on the measurements. However, it is quite difficult to assess the order of magnitude of this influence, since there is no data available without any support effect to compare with.

If the present dynamic test results are compared with those of other test facilities, it is observed that the trends of the present curves are similar to those obtained previously with slight differences in numerical values. However, it is observed that the differences become more important for values of α , larger than 25° . Some results are affected by the support systems and flow characteristics of the facilities. In order to alleviate the effect of support system in wind-tunnel experiments, wind-tunnel facilities should be improved to allow interference-free measurements of dynamic stability parameters over a large range of α and β . The present day experimental test rigs are usually massive, which cause large flow obstructions near or above the model. Artificial pressure fields resulting in vortex bursting and erroneous measurements can be observed due to these obstructions. Therefore, the development of support-free magnetic suspension techniques for high- α dynamic testing is of particular interest.

The present tests conducted in AWT can be considered to be as the preliminary tests utilizing the forced oscillation techniques since only a limited number of test cases are studied. These cases can be increased in the near future and the effects of various

number of parameters such as; sideslip angle, leading edge root extension (LEX), forebody strakes, longitudinal transition fixing on forebody, configuration (B, BW, BWHV, etc.) can be investigated.

At present the model can be oscillated in pitch. However, the aircraft is not limited to pitch oscillations only during its flight. Hence in the near future, possibilities of roll and yaw oscillations for the model must be sought and the dynamic stability characteristics of the model must be investigated during these motions.



REFERENCES

- [1] Avcı, S., "Static and Forced Oscillatory Tests on a Generic Combat Aircraft Model in Ankara Wind Tunnel," M Sc. Thesis, Middle East Technical University, Ankara, May 2000.
- [2] Altun, M., "Manufacturing, Assembly and Commissioning of an Oscillating Test Rig to Measure the Dynamic Stability Derivatives in the Ankara Wind Tunnel," M Sc. Thesis, Middle East Technical University, Ankara, Feb 2001.
- [3] "Cooperative Programme on Dynamic Wind Tunnel Experiments for Manoeuvring Aircraft," AGARD-AR-305, 1996.
- [4] Guglieri, G., "Wind Tunnel Experiments Techniques," Lecture Notes, Politecnico di Torino, Italy.
- [5] Orlik-Rückemann, K. J., "Review of Techniques for Determination of Dynamic Stability Parameters in Wind Tunnels," AGARD-LS-114, 1981.
- [6] Guglieri, G., Quagliotti, F. B., "Dynamic Stability Derivatives Evaluation in a Low-Speed Wind Tunnel," Journal of Aircraft, Volume 30, Number 3, May-June 1993, Pages 421-423.
- [7] Orlik-Rückemann, K. J., "Subsonic Aerodynamic Coefficients of the SDM at Angles of Attack up to 90° , Report LTR-UA-93," Forced Oscillation Technique-Reference Documentation, vol.3, Politecnico di Torino, DIASP, Italy.

- [8] Fusco, F., Guglieri, G., "Experimental Investigation on Aircraft Dynamic Stability Parameters," *Meccanica*, vol.28, n.1, 1993, Pages 61-68.
- [9] Guglieri, G., Quagliotti, F. R., "Elements of Data Acquisition-Technical Notes," *Forced Oscillation Technique – Reference Documentation*, vol.1, Politecnico di Torino, DIASP, Italy.
- [10] "SCXI-1121 User Manual," National Instruments, Austin, USA, 1999.
- [11] "Measurement and Automation Catalogue," National Instruments, Austin, USA, 2000.
- [12] Tobak, M., Schiff, L. B., "Aerodynamic Mathematical Modeling-Basic Concepts," AGARD-LS-114, 1981.
- [13] Orlik-Rückemann, K. J., "Sensitivity of Aircraft Motion to Cross-Coupling and Acceleration Derivatives," AGARD-LS-114, 1981.
- [14] Chambers, J.R., Dicarlo, D.J., and Johnson, J.L., "Applications of Dynamic Stability Parameters to Problems in Aircraft Dynamics," AGARD-LS-114, 1981.
- [15] Nelson, R. C., "Flight Stability and Automatic Control," Mc-Graw – Hill, USA, 1989.
- [16] Malcolm, G. N., "Impact of High-Alpha Aerodynamics on Dynamic Stability Parameters of Aircraft and Missiles," AGARD-LS-114, 1981.

- [17] Hanff, E. S., "Direct Forced Oscillation Techniques for the Determination of Stability Derivatives in Wind Tunnels," AGARD-LS-114, 1981.
- [18] Özdemir, E., "Calibration and Instrumentation of Ankara Wind Tunnel," M Sc. Thesis, Middle East Technical University, Ankara, 2000.
- [19] "Labview Tutorial for Windows," National Instrument, Austin, USA, 1998.



APPENDIX A

SEQUENCE OF STATIC TESTS AND LABVIEW PROGRAMMING

In this appendix, the description of how the static tests are performed and the flowchart for the data acquisition program is given. The signals that are collected with the data acquisition program are analyzed to calculate the force and the moment coefficients. The method of calculating these force and moment coefficients will be explained in the light of the flowcharts given. Finally, the details of the Labview programming used for the data acquisition will be detailed.

A.1 Flowchart for Static Tests

The purpose of the static tests is to determine the non-dimensional aerodynamic static coefficients of the aircraft. The model is positioned statically according to a sequence of prescribed aerodynamic angles of attack (α) during wind-on runs. Loads that affect the configuration are measured with the use of the internal balance. While performing these measurements the loads that are measured by the internal balance are collected and stored in the computer with the help of the software prepared using the Labview programming language. The program is called the “data top.vi”. For each angular position of the model, wind-off tare loads are also measured and stored in a file. In order to find the aerodynamic loads, wind-on loads are subtracted from the wind-off tare loads.

The data acquisition program, “data top.vi” consists of 3 subVI’s, which are “AI Start.vi”, “AI Read.vi” and “AI Config.vi” as shown in the flowchart given in Figure A.1. “AI Start.vi” configures the hardware used for data acquisition, “AI Read.vi”

starts the analog input operations, "AI Config.vi" reads the data from a buffered data acquisition. The program, "data top.vi" is a typical data acquisition program written in Labview programming language. The data collected for wind-off and wind-on conditions are first entered in the "balans sinyal.vi" for analysis. The inputs of the "balans sinyal.vi" are the temperature, the velocity and the angle of attack values that are noted for the wind-on test case. For the time being, these information related to the wind tunnel flow parameters are input externally to the program [18]. Then, the data, files corresponding to particular wind-off and wind-on tests are read by the program called, "balans sinyal.vi". These data are stored column wise, each column corresponding to a particular component of the force or moment measured. Then the values corresponding to the rolling moment, normal force and the pitching moment are read according to the column in which they are stored. The average values of each column are then calculated to find the mean values for the corresponding force/moment component.

Then the average values calculated for each component of the force/moment for the wind-off condition are subtracted from the corresponding values of the wind-on condition. The input parameters of the "balanssinyal.vi" program (velocity, atmospheric pressure and temperature) are read by the program "akis parametreleri.vi" where the flow parameters such as density, viscosity and the speed of sound are calculated. The output of "akis parametreleri.vi" program, which are the tunnel velocity, V and the air density, ρ are input to the subprogram "force.vi" where the non-dimensional static aerodynamic coefficients are calculated for the reduced mean values of the aerodynamic force/moment values already calculated in the program "balanssinyal.vi". However since these values are in voltages, they are converted into physical values by multiplying with the coefficients of the calibration matrix.

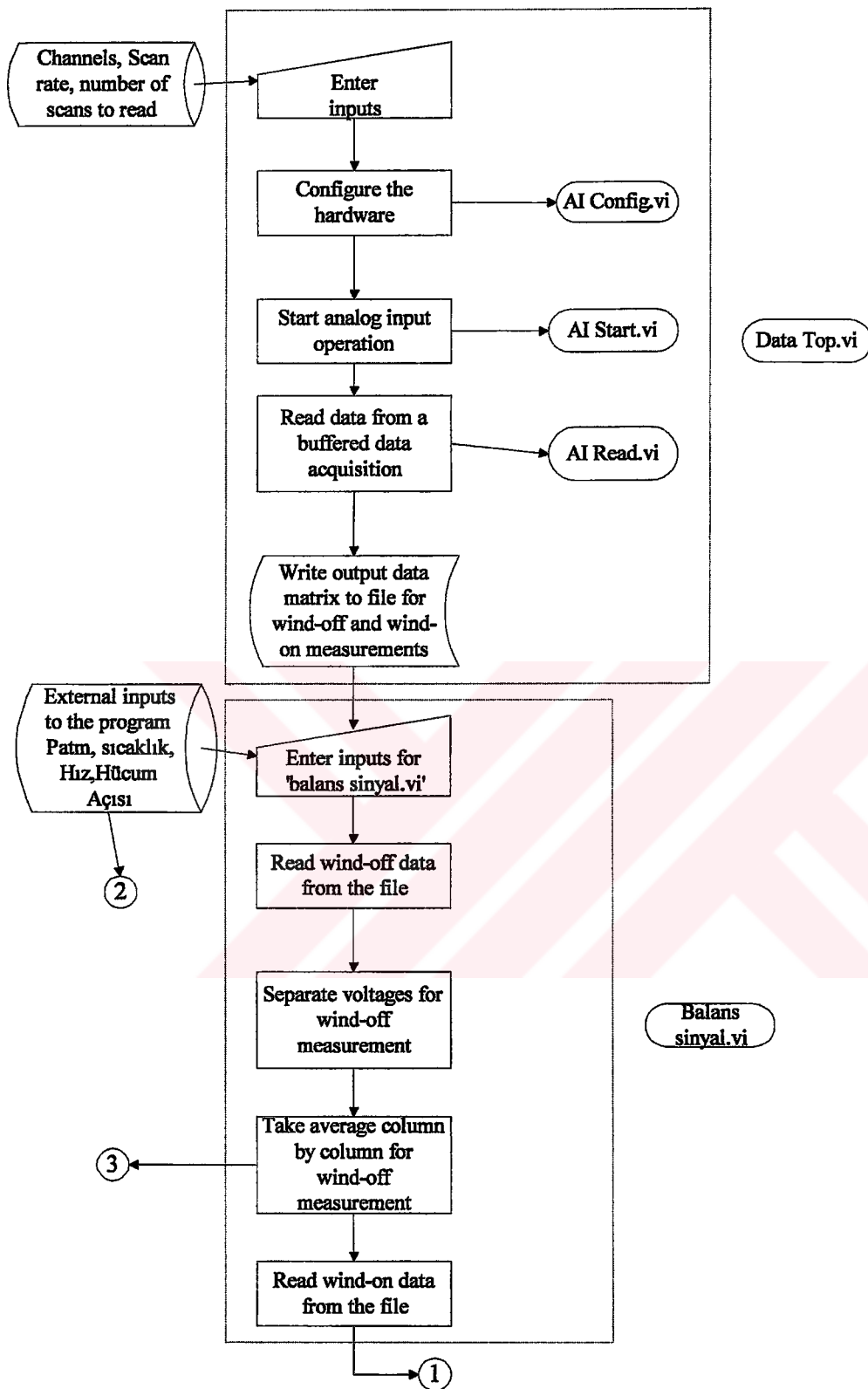


Figure A.1.a Static Test Flowchart (1)

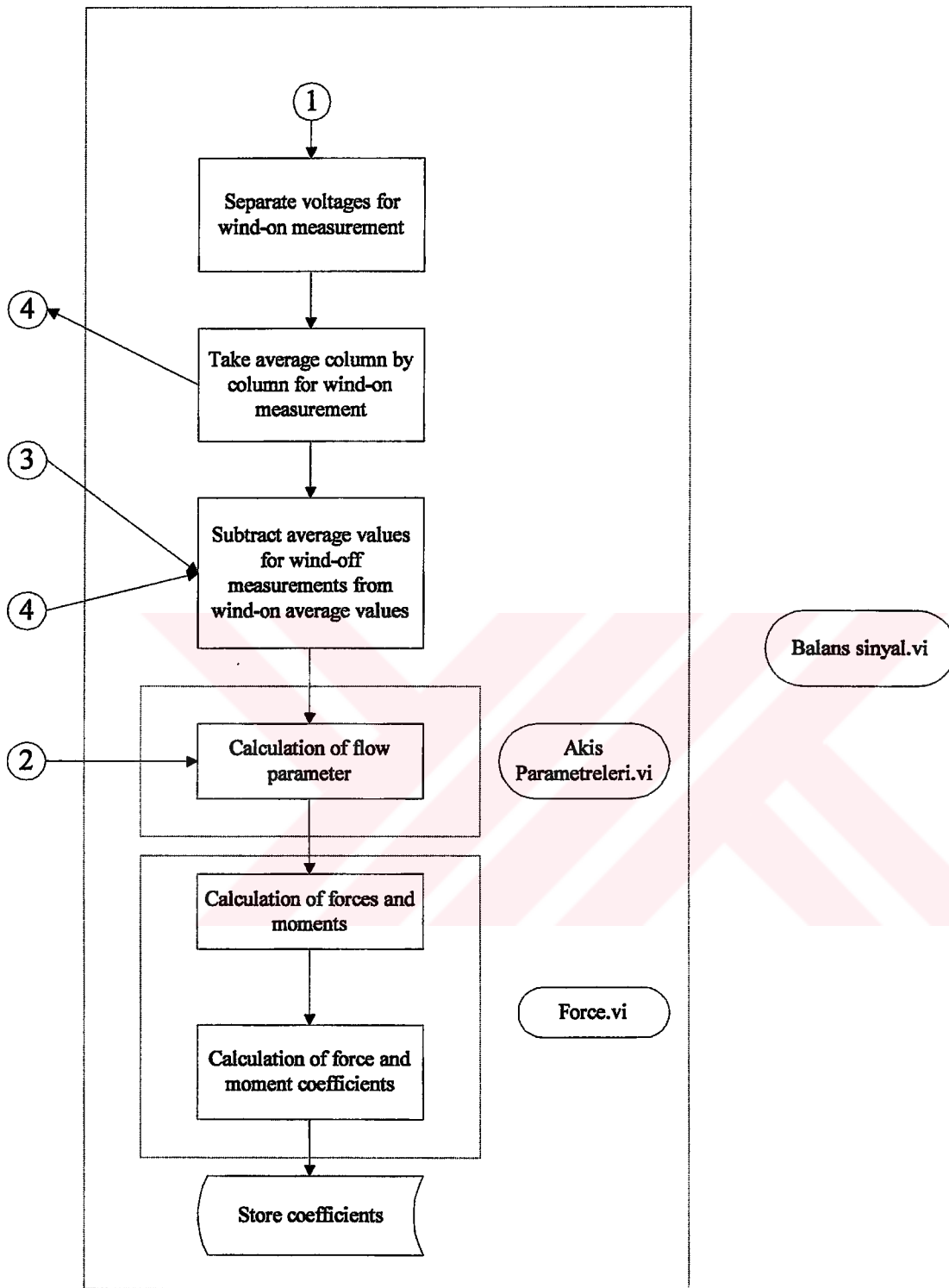


Figure A.1.b Static Test Flowchart (2)

A.2 Program for Static Test

Static and dynamic programs consist of two different parts. First part, typical Data Acquisition program in Labview named “data top.vi” is used not only for static tests but also for dynamic tests. “data top.vi” takes the signals in volts coming from the signal conditioning unit and stores them in files. Second part of the programs performs the signal treatment. Labview programs that are used in static test programs, such as “balanssinyal.vi”, “akis parametreleri.vi”, and “force.vi” are all categorized in this second part.

The “data top.vi” program will be discussed in this part. Furthermore, the other programs that are used during signal treatment as “balanssinyal.vi”, “akis parametreleri.vi”, and “force.vi” will also be examined in detail.

Data top.vi:

This program is initiated after the proper input connections through the panel are done. Figure A.2 gives the labview program for “data top.vi” in diagram format. The inputs of this program are the controls that are used for placing the data such as the list of the analog input channels named “balans girdileri”, “buffer size”, “scan rate” and “okutmak istediđin scan sayısı”. The outputs of this program are the indicators such as scan backlog named “okunamayan veri”, “yapılan scan sayısı”, “gerçek scan rate”, and “data matrixes”. The program, “data top.vi” is composed of sub programs named: “AI Config.vi”, “AI Start.vi”, “AI Read.vi” and “AI Clear.vi” subVI's. Each of these subVI's are explained below;

AI Config.vi:

This subprogram configures an analog input operation for a specified set of channels. This VI configures the hardware and allocates a buffer for a buffered analog input operation for a specified group of channels. The inputs of “data top.vi” are “balans girdileri” and “buffer size”. “Balans girdileri” specifies the set of analog input

channels for a group and task. Buffer size is the number of scans you want each buffer to hold [19].

- **AI Start.vi:**

This subprogram starts a buffered analog input operation. This VI sets the scan rate and the number of scans to acquire. The VI then starts an acquisition. “AI Start.vi” first checks to see if the “input cluster error in” indicates that an error has already occurred. If so, this VI does not start an acquisition, but passes the error information unmodified through “error out”. The input of “AI Start.vi” is the “scan rate” and the output is the “actual scan rate”. Scan rate is the number of scans per second to acquire. This is equivalent to the sampling rate per second. Actual scan rate may differ slightly from the requested scan rate, depending on the hardware capabilities [19].

- **AI Read.vi:**

This subprogram VI reads the data from a buffered data acquisition. The input of “AI Read.vi” is the number of scans to read. The outputs are the scan backlog named “okunamayan veri”, number of scan returned named “yapılan scan sayısı” and “data matrisi”. Number of scans to read is the number of scans the VI is to retrieve from the acquisition buffer. Scan backlog is the amount of data remaining in the buffer after this VI is completed. If the number of scans returned increases steadily, you are not reading data fast enough to keep up with the acquisition, and your newly acquired data may overwrite the unread data and give you an overwrite error. It can be prevented, by decreasing the scan rate, by increasing the number of scans to read, by reading the scans more often, or by increasing the buffer size. The number of scans returned is identical to the number of scans to read unless an error or timeout appears or the VI reaches the end of the data. Scaled data (data matrix) is a 2D array that contains analog input data in scaled data units. This array is scan-ordered which means that each of its rows contains the data of a single scan or value. If you want to index the array in a loop, you get a scan on each iteration. Each column holds the

data of a single channel. The upper array index selects the scan and the lower index selects the channel [19].

- **AI Clear.vi:**

This subprogram VI clears the analog input task associated with taskID in [19].

After forming a matrix out of “AI Read.vi” program outputs, and saving the mentioned matrix in a stated file, “data top.vi” program completes its task and gets ready for data acquisition of a new case.

Balanssinyal.vi:

The VI program, “balanssinyal.vi”, consists of two VI subprograms called, “akis parametreleri.vi” and “force.vi”. The inputs of the “balanssinyal.vi” are the number of scan, velocity, temperature, atmospheric pressure, angle of attack, the file path to read the wind-off measurements and the file path to read the wind-on measurements. The outputs of the program are roll moment, normal force, and pitching moment, and their respective coefficients. The “data top.vi” stores the data coming from the internal balance. These stored data are then read by the VI program “balanssinyal.vi” for both the wind-off and wind-on cases. “balanssinyal.vi” builds two different arrays for the wind-on and wind-off measurements each array containing the roll moment, normal force and the pitching moment signals measured in volts (Figure A.3). Then the mean values for each of these measurements, rolling moment, normal force and the pitching moment are taken separately, column by column. Then the average values calculated for wind-on measurements are subtracted from the respective

- **Akis parametreleri.vi:**

The VI subprogram “akis parametreleri.vi”, is one of the two subVI’s of the program, “balanssinyal.vi”, in which using the “balanssinyal.vi” inputs such as the velocity, atmospheric pressure and the temperature, the density (ρ), as well as the viscosity (μ) and the speed of sound (a) are calculated. Velocity and density, output of “akis parametreleri.vi”, are then sent to the “force.vi” subprogram to obtain the non-dimensional static derivatives (Figure A.4). Temperature, atmospheric pressure and the wind tunnel velocity are taken externally as mentioned previously [18].

- **Force.vi:**

The “force.vi”, is another subVI of the program “balanssinyal.vi”, in which the raw values of the rolling moment, normal force and the pitching moment voltage values are multiplied by the calibration matrix and therefore converted into physical values. Then, using the flow parameters coming from the program “akis parametreleri.vi”, the non-dimensional coefficients for the rolling moment, normal force and the pitching moment are calculated (Figure A.5).

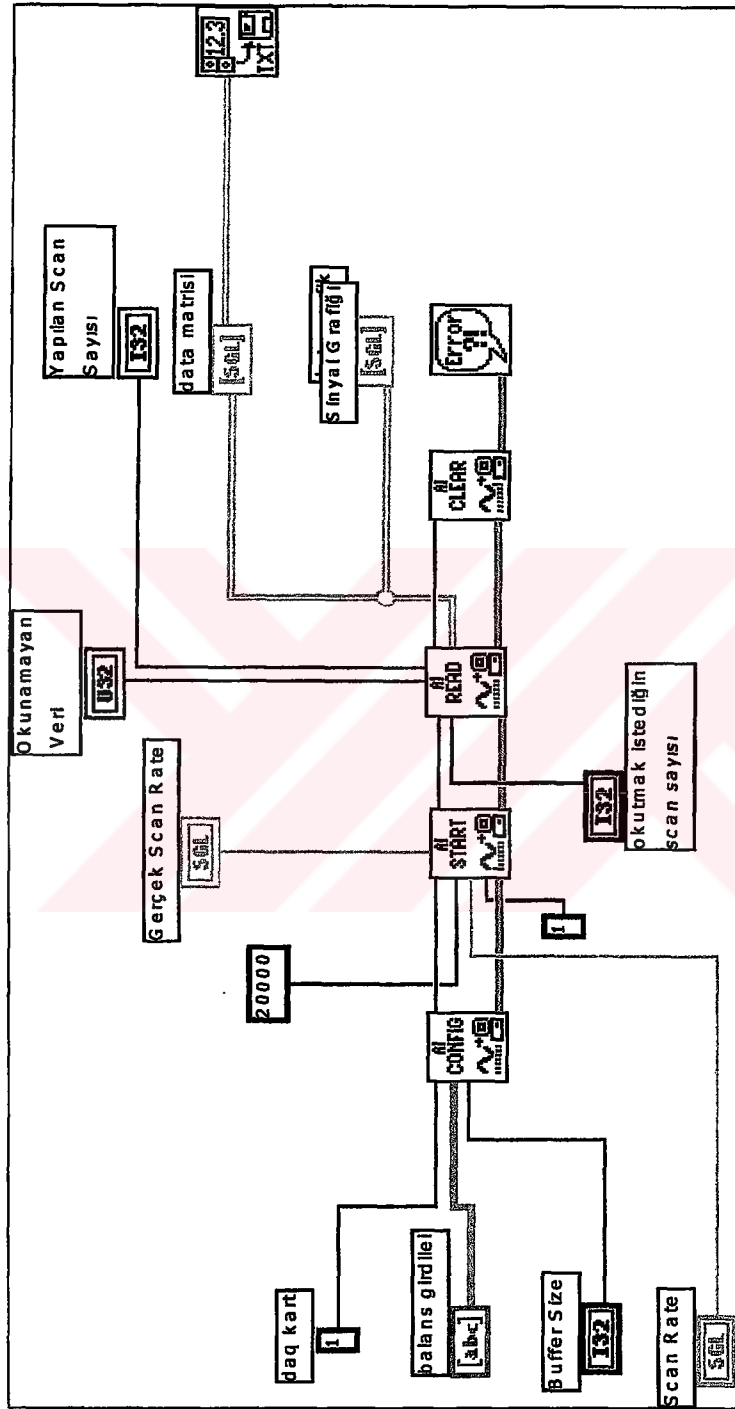


Figure A.2 Diagram of "data top.vi"

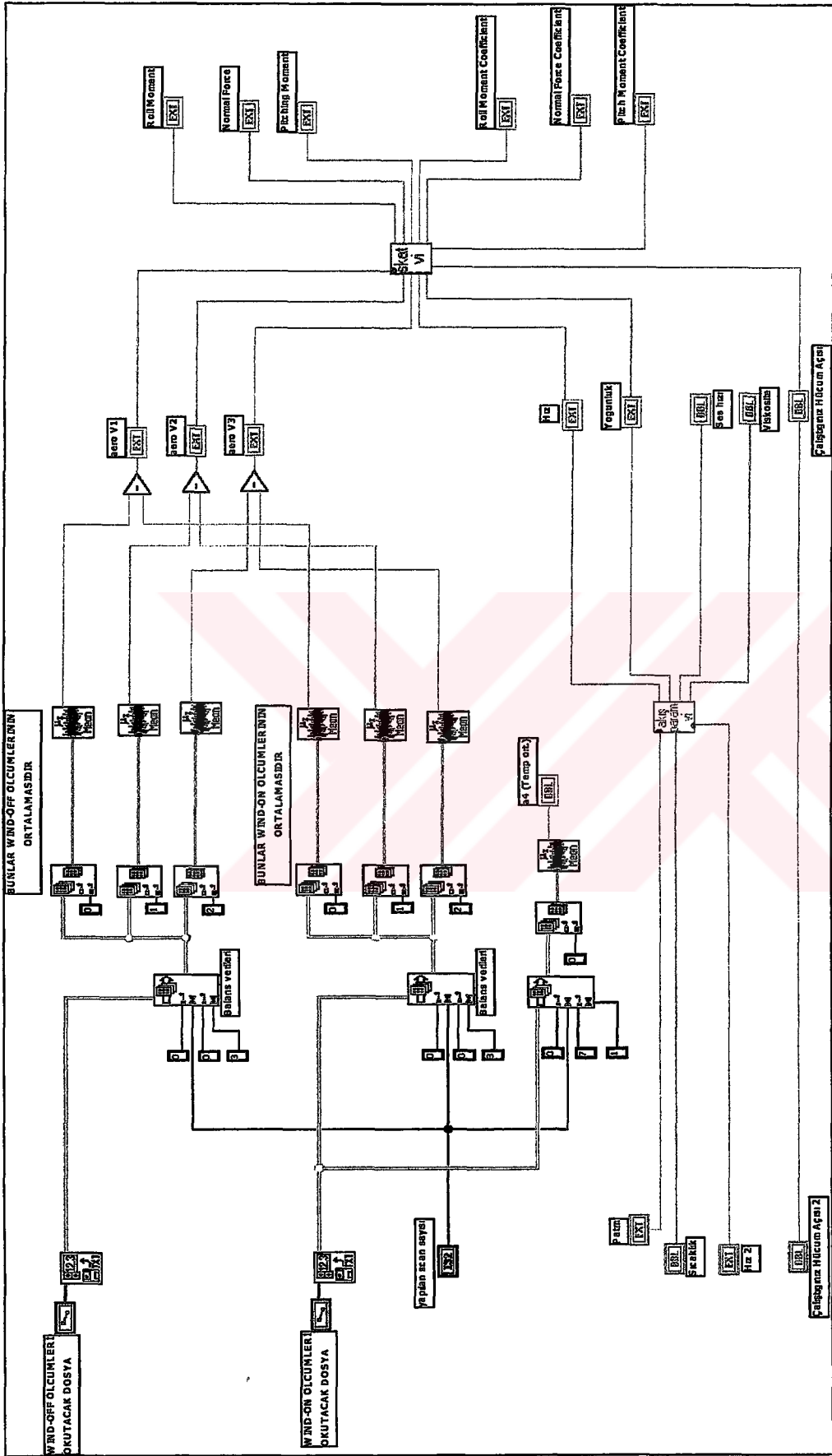


Figure A.3 Diagram of "balanssinyal.vi"

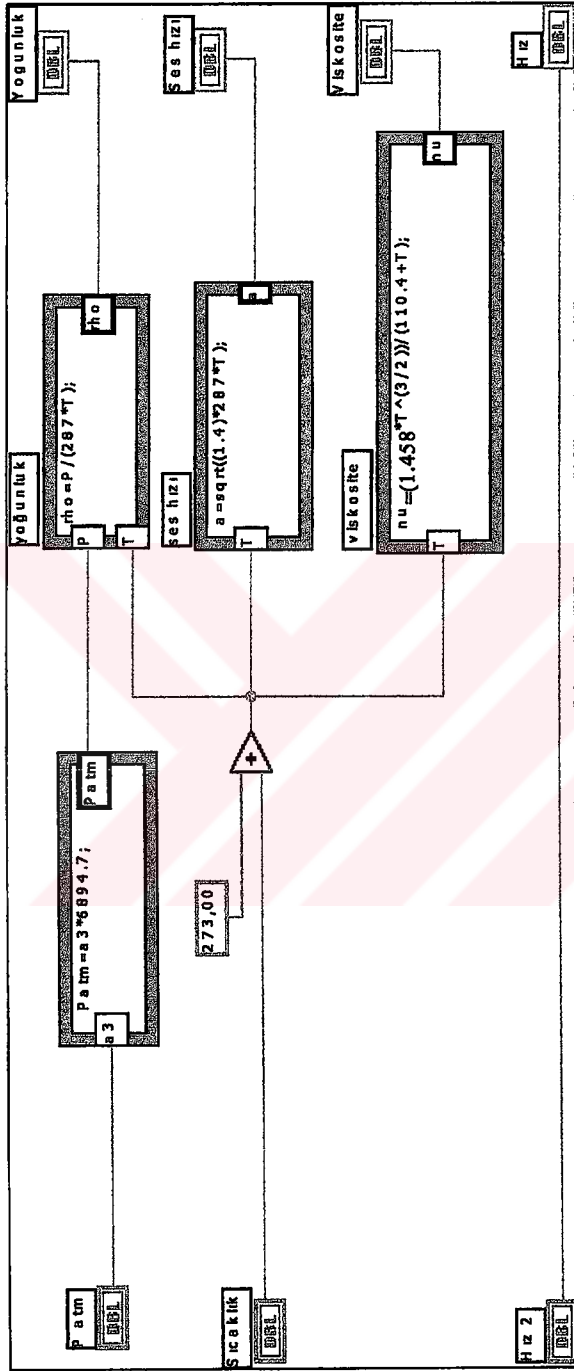


Figure A.4 Diagram of “akış parametreleri.vi”

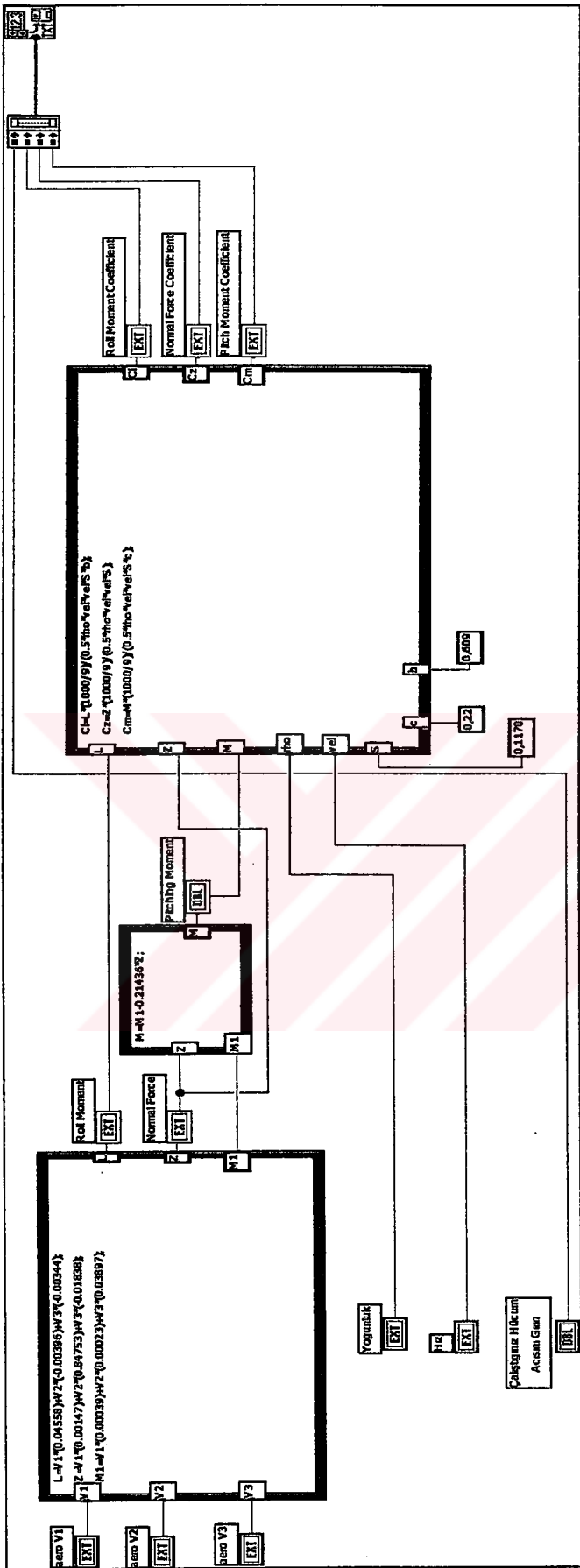


Figure A.5 Diagram of "force.vi"

APPENDIX B

SEQUENCE OF DYNAMIC TESTS AND LABVIEW PROGRAMMING

In this appendix, the description of how the dynamic tests are performed the flowchart for the data acquisition program is given. Using the flowchart given (Figure B.1), the method of calculating the force and the moment coefficients will be explained. Then, the details of the Labview programming used for the data acquisition will be given.

B.1 Flowchart for Dynamic Tests

The test procedure is based on the principle of measuring the external loads acting on the model while it is oscillating with respect to its center of gravity. The model has an internal balance and is forced to oscillate with harmonic forcing function generated by a flywheel mechanism. The method is based on the assumption of small perturbations around a mean value, hence the amplitudes as well the frequencies of oscillations are both small [8].

The forced oscillation experiments are described below:

1. The model is set statically at a mean angle of attack α_m and the amplitude of oscillations is adjusted by setting the offset radius of the flywheel (crank), and the wind tunnel air speed is brought up to the desired velocity.

2. Then, the model is oscillated at a fixed frequency and amplitude while the aerodynamic forces and moments are measured by the data acquisition system for this wind-on condition.
3. The same experiments are repeated without the wind, (the tunnel is turned off and is not running).

Once the data for the wind-on and wind-off conditions are collected, they are then treated by the dynamic program. In the dynamic program, the data which is coming from the “data top.vi” subprogram, are converted into aerodynamic derivatives in the main VI program called the “final.vi” and its main subVI programs “wind-off load.vi”, “wind-on load.vi” and “akis.vi”.

For wind-off calculations, using the subprogram “wind-off load.vi data is averaged column wise in the “tbalans.vi” subprogram. The entries of each one of these columns are reference signal, rolling moment, normal force and the pitching moment voltage readings. The calculated mean values for each column (therefore for each parameter) are then subtracted from each one of the readings of the respective column, thereby reducing the mean values of each column zero. Hence each one of the columns now contains only the fluctuation values. The reduced values of the reference signal in column format are then fed into the subprogram “trefvoltfreq.vi” where the frequency of the signal is calculated. If the calculated frequency of the reference signal is not within the tolerance range of the assigned frequency for the reference signal, these data are discarded, with a program warning, “wrong frequency”. If the calculated frequency is as expected then the reduced values for the balance readings are input into the subprogram called “tphase volt.vi” in which the number of complete oscillation cycles are counted for each entry. There is another subVI program called the “tvolt.vi” in the same program; “tphase volt.vi”. In this subprogram, the in-phase and the out-of-phase voltage components of the rolling moment, normal force and the pitching moment are calculated. Calculated in-phase and out-of-phase voltage components are then input to the “tload.vi” program where these voltage components are converted into in-phase and out-of-phase loads by

using the calibration matrix. Thus, in-phase and out-of-phase load components are obtained for the wind-off tests using “windoff load.vi”. The same procedure is repeated for the wind-on measurements and in-phase and out-of-phase load components are calculated in the program called “windon load.vi”.

In-phase and out-of-phase load components of wind-on tests are subtracted from in-phase and out-of-phase load components of the corresponding wind-off tests, and thus we get the dimensional aerodynamic derivatives.

The velocity, atmospheric pressure and the temperature inputs of the main program are input to the “akis.vi” subprogram where the flow parameters which are used during the calculation of the non-dimensional derivatives are obtained. Finally, dimensional aerodynamic load and moments are converted into non-dimensional forms using the flow parameters calculated in subprogram “akis.vi” and are stored in a file for each case.

B.2 Program for Dynamic Test

As in the static program, the dynamic program also consists of two parts the first part is the data acquisition program named as “data top.vi” same as in the static program. Hence this program is not described here. Second part of the program, which performs the signal treatment, are composed of four main programs named as; “final.vi”, “windoff load.vi”, “windon load.vi” and “akis.vi”. Among these programs, “final.vi” is the main program and the others are subVI’s or subprograms of the “final.vi” program. Although “windoff load.vi” and “windon load.vi” are the subprograms of the “final.vi” program, they also contain several subVI’s. In the following parts, the above mentioned VI programs and their subVI’s will be described in detail.

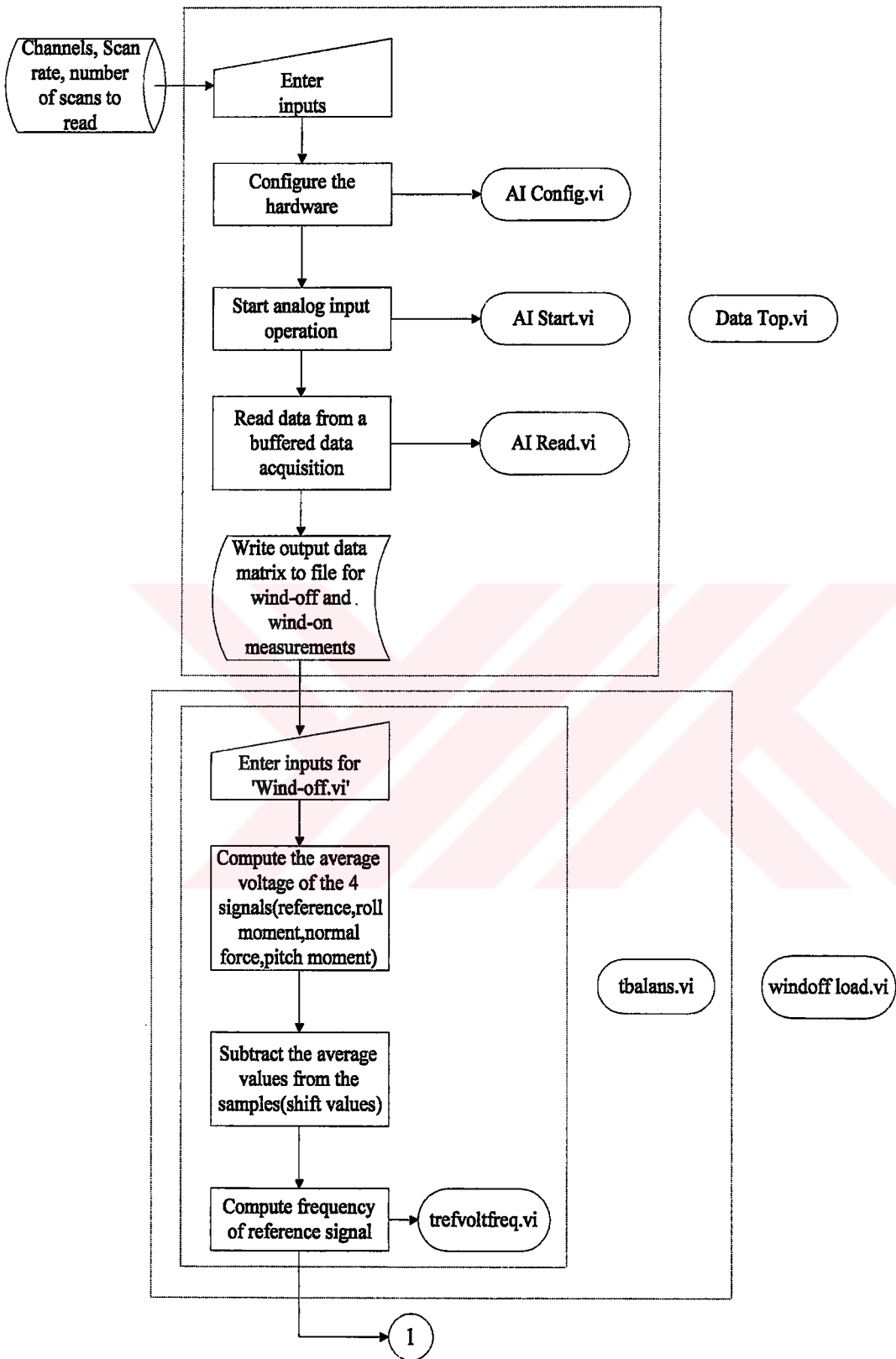
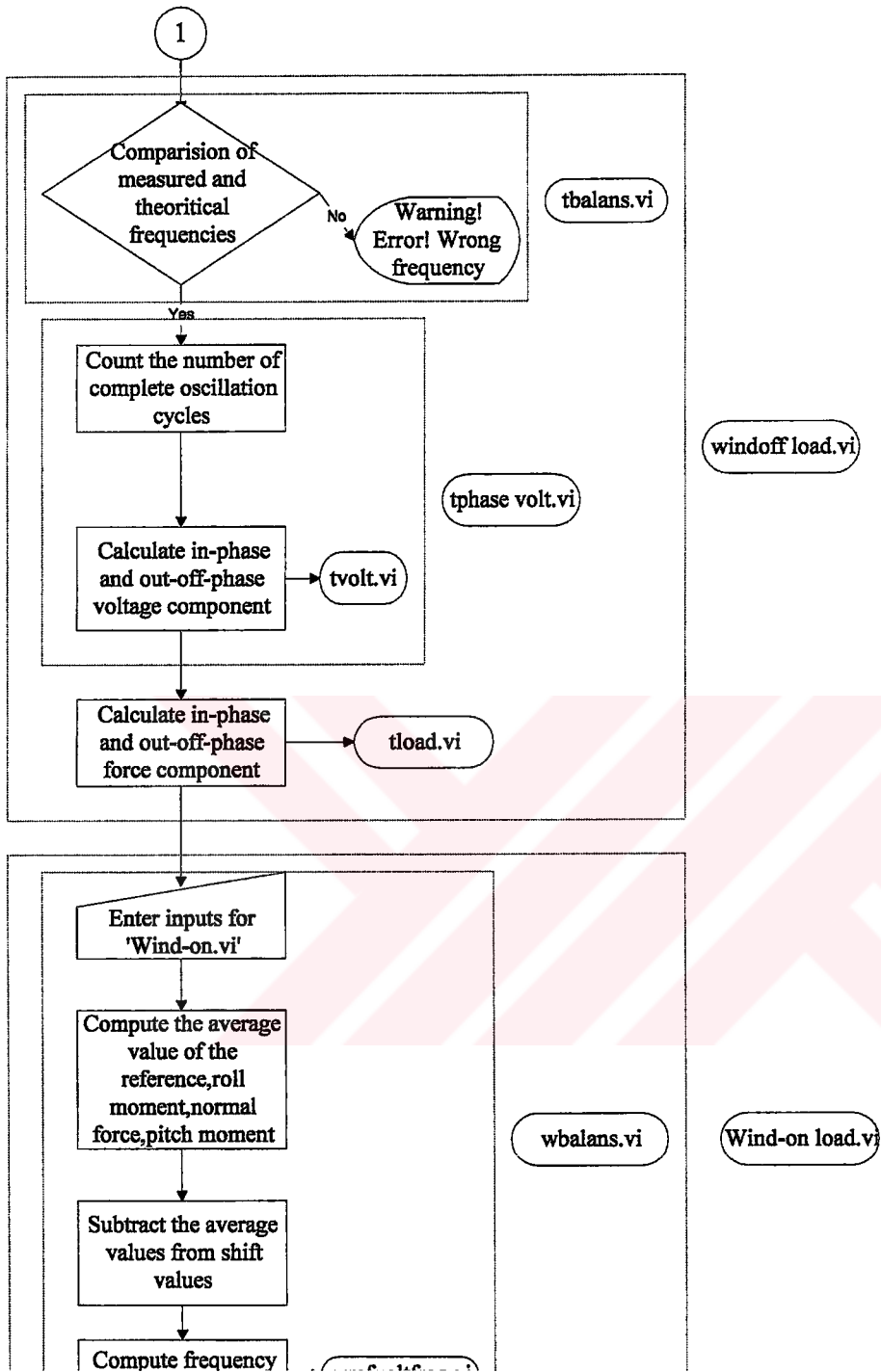


Figure B.1.a Dynamic Test Flowchart (1)



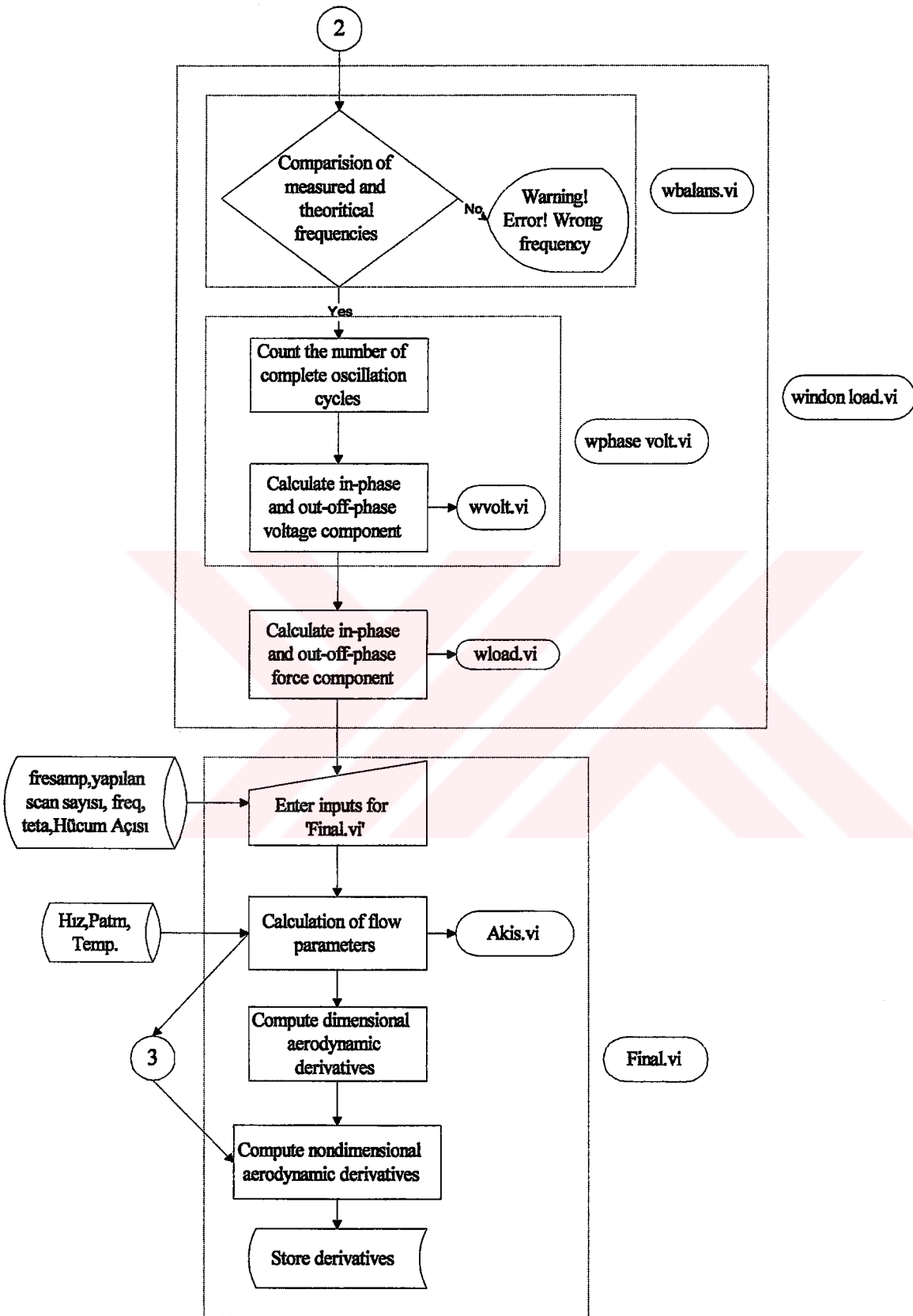


Figure B.1.c Dynamic Test Flowchart (3)

Final.vi:

The VI program, “final.vi”, is the main program for dynamic calculations, in which the aerodynamic derivatives are computed. The inputs of the dynamic programs are entered manually (externally) in the panel of the “final.vi” program and the aerodynamic derivatives as output. The inputs of the program are “fresamp” (scan rate), number of scan, frequency, amplitude, velocity, atmospheric pressure of wind tunnel, temperature, angle of attack, the file path to read wind-off measurements and the file path to read wind-on measurements. Last two files are the results of the “data top.vi” program for wind-off and wind-on tests. The outputs of the program are indicators of stability derivatives, which are $C_{l\alpha}, C_{z\alpha}, C_{m\alpha}, C_{lq} + C_{l\dot{\alpha}}, C_{zq} + C_{z\dot{\alpha}}$ and $C_{mq} + C_{m\dot{\alpha}}$. Diagram format of the program, “final.vi”, can be seen in Figure B.2. The “data top.vi” is run to obtain the voltage signals coming from the internal balance for different cases. These data are stored and read from the same files by the program “final.vi” for wind-off and wind-on tests. These data are input through the “windoff load.vi” and “windon load.vi” for wind-off and wind-on cases respectively. After processing, these signals are converted into the in-phase and the out-of-phase load components of the rolling moment, normal force and the pitching moment by means of the same VI subprogram; “windoff load.vi” and “windon load.vi”. In-phase and out-of-phase load components for the wind-on tests are subtracted from in-phase and out-of-phase load components for the wind-off tests. Subtracted in-phase load components are divided by the “radteta” term, which is the amplitude of the angle in radians. Subtracted out-of-phase load components are divided by ω , which is the angular velocity in radians, in addition to the “radteta” term. Meanwhile, the inputs of the “final.vi” program; the velocity, atmospheric pressure and the temperature are input to the “akis.vi” subprogram where the flow parameters used during calculation of non-dimensional derivatives, are calculated. In-phase and out-of-phase load components and flow parameters input into the formula note of the “final.vi” program (Figure B.2) where the non-dimensional aerodynamic derivatives, $C_{l\alpha}, C_{z\alpha}, C_{m\alpha}, C_{lq} + C_{l\dot{\alpha}}, C_{zq} + C_{z\dot{\alpha}}$ and $C_{mq} + C_{m\dot{\alpha}}$, are computed.

Akis .vi:

The subprogram, “akis.vi”, uses the inputs of “final.vi” program such as; velocity, atmospheric pressure and temperature, and calculates the density, “rhoe” term, as well as the viscosity and the speed of sound to be used in the computations of the aerodynamic coefficients. Velocity and “rhoe”, which are the output of “akis.vi”, are sent to the formula note of “final.vi” to obtain the non-dimensional aerodynamic derivatives (Figure B.3). Temperature, atmospheric pressure and the tunnel speed are input externally to the program as already mentioned in the static program.

Windoff load.vi:

“Windoff load.vi” is a subprogram of “final.vi”. It uses “file path to read win-off test measurement”, frequency, “fresamp” (scan rate) and number of scan as inputs. Its outputs are the in-phase and the out-of-phase components of rolling moment, normal force and the pitching moment. The subVIs of “windoff load.vi” are the “tbalans volt.vi”, “tphase volt.vi” and the “tload components.vi” subprograms (Figure B.4). These VI subprograms also have other subVI programs themselves.

Tbalans volt.vi:

It uses the same inputs as entered to the “windoff load.vi” subprogram. Its output are named as; “V0shift”, “V1shift”, “V2shift” and “V3shift”, which are, the shifted reference voltage values for the rolling moment, normal force and the pitching moment signals respectively. If the mean value of each signal is subtracted from the individual values, shifted signals are obtained. Other outputs of the program are the average voltage value of the power supply for the internal balance which is named “ealim” and the starting point of the effective samples for the complete oscillation periods which is named “izeroV0”. Diagram form of the program “tbalans volt.vi” is given in Figure B.5. As stated previously, “data top.vi” program collects the data from 0th to 7th channels. These channels are used in this order for the rolling moment, normal force, pitching moment, empty, reference signal, power supply, empty and

for temperature signals. The output data of the “data top.vi” subprogram from these eight channels are written in arrays. Program calculates mean values of the power supply and the temperature channels to be used for later. Other data, reference signal, rolling moment, normal force and pitching moment, are named “V0”, “V1”, “V2” and “V3”, respectively. The program calculates the mean values of these signals. These mean values are then subtracted from each sample reading to we get the shifted values for the rolling moment, normal force and the pitching moment samples.

There is another subVI program named “trefvoltfreq.vi” in the “tbalans.vi”. The output of “trefvoltfreq.vi”, is the measured frequency of oscillations named as “freqV0”. This value is compared with the theoretical frequency input of “final.vi” program, named as “fresamp”. If the value of “freqV0” is within ∓ 1 percent of the value of “fresamp” the accuracy of the measured frequency is acceptable. If not, the program outputs “wrong frequency”.

- **Trefvoltfreq.vi:**

“Trefvoltfreq.vi” subprogram uses the shifted “V0” reference signal array elements as input and returns “i20per” and “freqV0” terms as output. “i20per” and “freqV0” terms are the output of the two subprograms of this VI called the “trefvolttest1.vi” and “trefvolttest2.vi” respectively (Figure B.6).

- **Trefvolttest1.vi:**

“Trefvolttest1.vi” program uses the shifted “V0” reference signal array and compares each array element of this array to previous ones in order to find out the first point of the periodic sinusoidal samples called the “izeroV0”. “Trefvolttest1.vi” gives us “izeroV0” as an output (Figure B.7).

- **Trefvolttest2.vi:**

“Trefvolttest2.vi” subprogram uses the shifted values of the “V0” reference signal array starting from the “izeroV0” point and compares each element of the array with the previous ones and finds the point where all the periods are completed. Moreover, it counts the periods in the reference signal (Figure B.8). The number of periods is named as “nper” and the last point of the completed periods is named as “i20per”. These two values are the outputs of the “trefvolttest2.vi” subprogram.

Tphase volt.vi:

The outputs of the “tbalans.vi” subprogram which are the shifted values named as “V0shift”, “V1shift”, “V2shift” and “V3shift” are input to the subprogram “tphase.volt.vi”. “Tphase.volt.vi” has another subVI named as “tvoltaj hesaplamlari.vi”. This subprogram separates the rolling moment, normal force and the pitching moment shifted voltage signals into in-phase and out-of-phase voltage components starting from the “izeroV0” point. In fact, “tphase volt.vi” adds the in-phase and the out-of-phase voltage components coming from the “tvoltaj hesaplamlari.vi” for each period and output the rolling moment, normal force and the pitching moment in-phase and out-of-phase voltage components (Figure B.9).

- **Tvoltaj hesaplamlari.vi:**

The inputs of “tvoltaj hesaplamlari.vi” are “V1shift”, “V2shift”, and “V3shift” voltage arrays. This program computes the rolling moment, normal force and the pitching moment voltage components of each period and sends these components to another part of “tphase volt.vi” in order to sum them up (Figure B.10).

Tload component.vi:

The output of “tphase volt.vi” which are the in-phase and the out-of-phase voltage components of the rolling moment, normal force and the pitching moment are input to the subprogram “tload component.vi”. The average value of the power supply named “ealim” which is computed in the “tbalans.vi” subprogram is also input to this program. This program calculates the load values for the rolling moment, normal force and the pitching moment in-phase and out-of-phase components by multiplying the voltage values used so far with the calibration matrix (Figure B.11).

This completes the total task of the “windoff load.vi” program and all these output are sent to the “final.vi” program.

Wicond load.vi:

While the “windoff load.vi” program computes the in-phase and the out-of-phase load components for the wind-off tests in the “final.vi” program the “wicond load.vi” program computes the in-phase and the out-of-phase voltage components for the wind-on tests. “windoff load.vi” and “wicond load.vi” are therefore the same programs. They have the same subVI’s but names of the subVIs’ are different. While, for “windoff load.vi” programs, the prefix “t” is added to the program names, for the “wicond load.vi” program, the prefix “w” is added to the program names and their contents are kept the same (Figure B.12). Therefore, to avoid repetition the “wicond load.vi” program is not examined here.

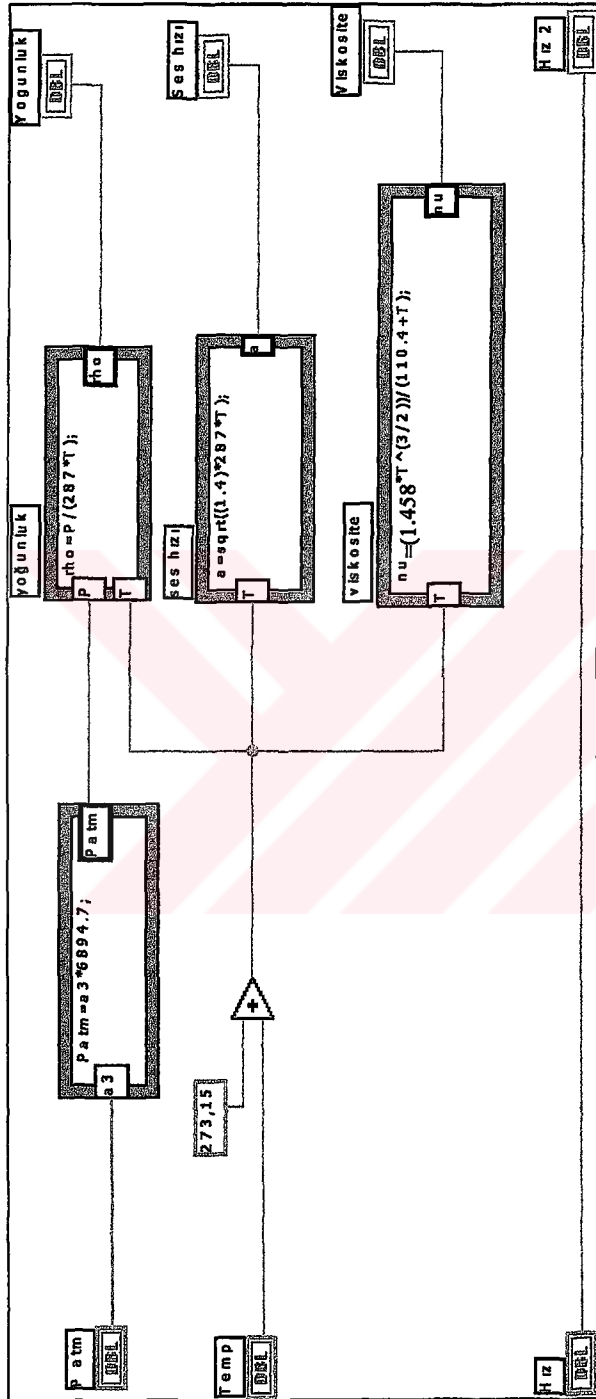


Figure B.3 Diagram of “akış.vi”

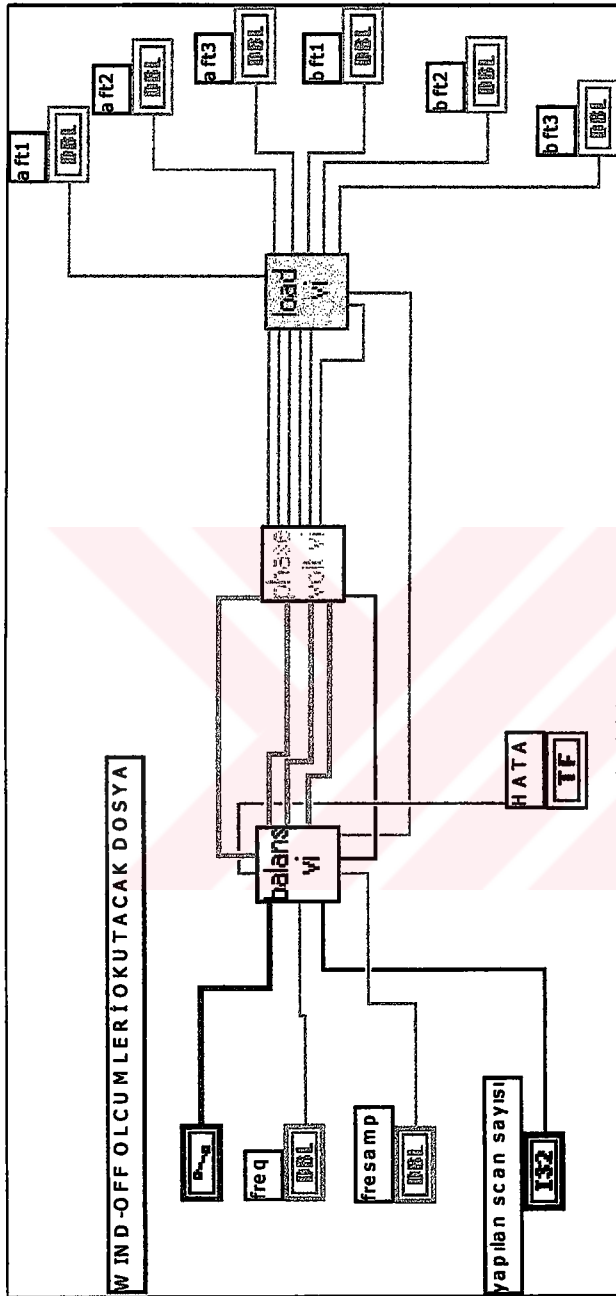


Figure B.4 Diagram of "windoff load.vi"

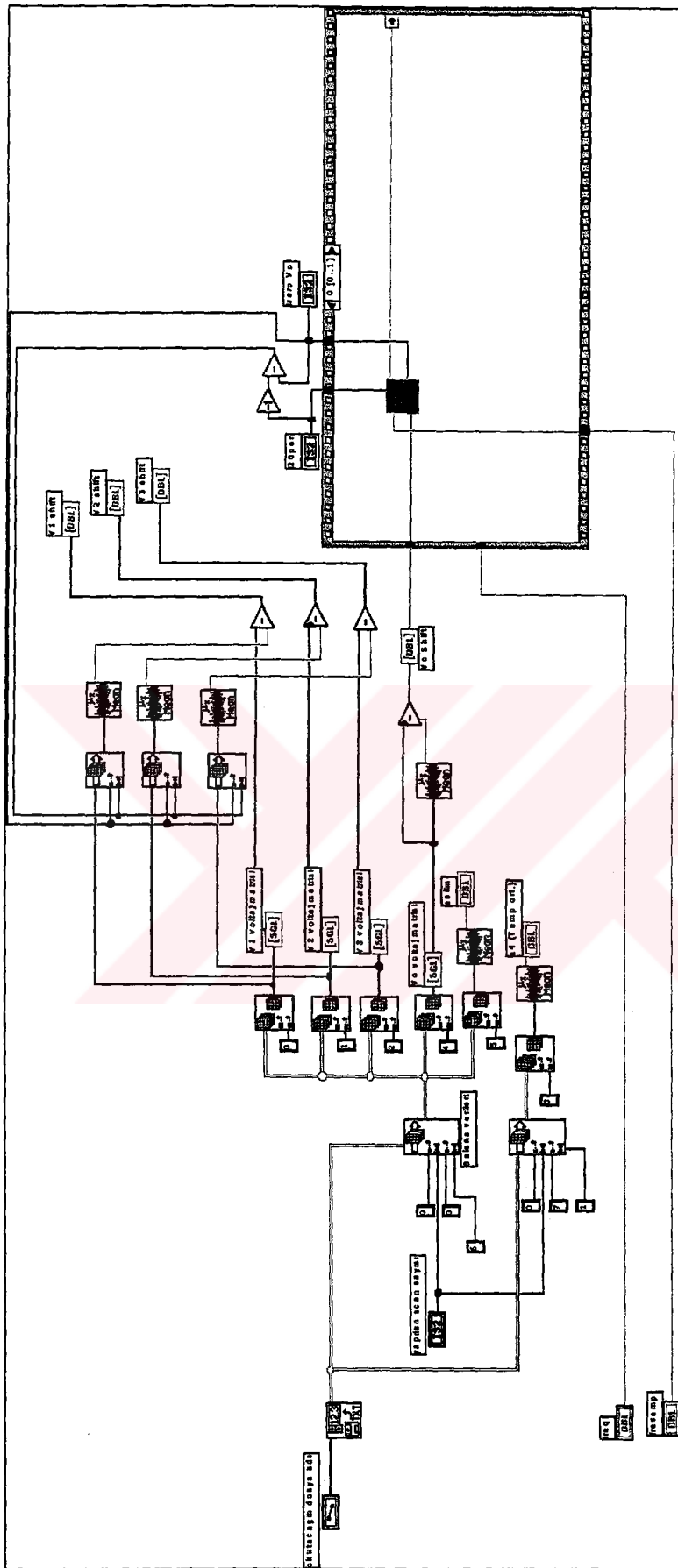


Figure B.5 Diagram of "tbalans volt.vi"

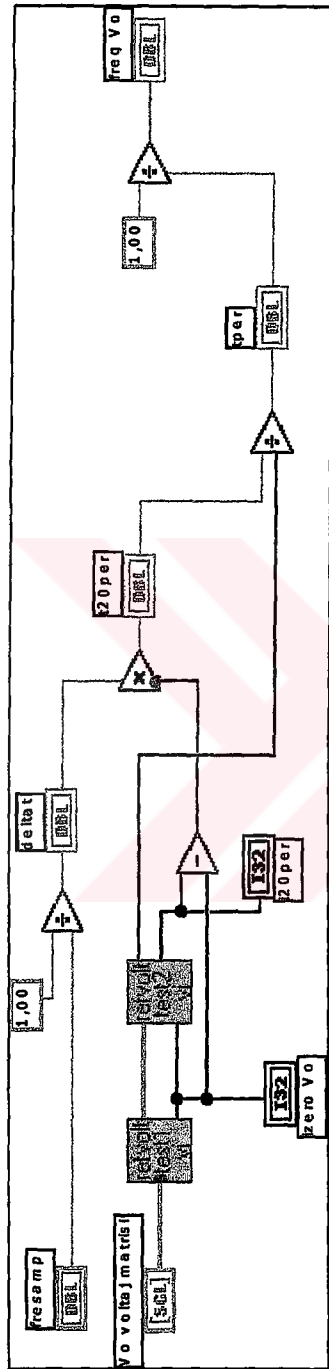


Figure B.6 Diagram of "trefvolfreq.vi"

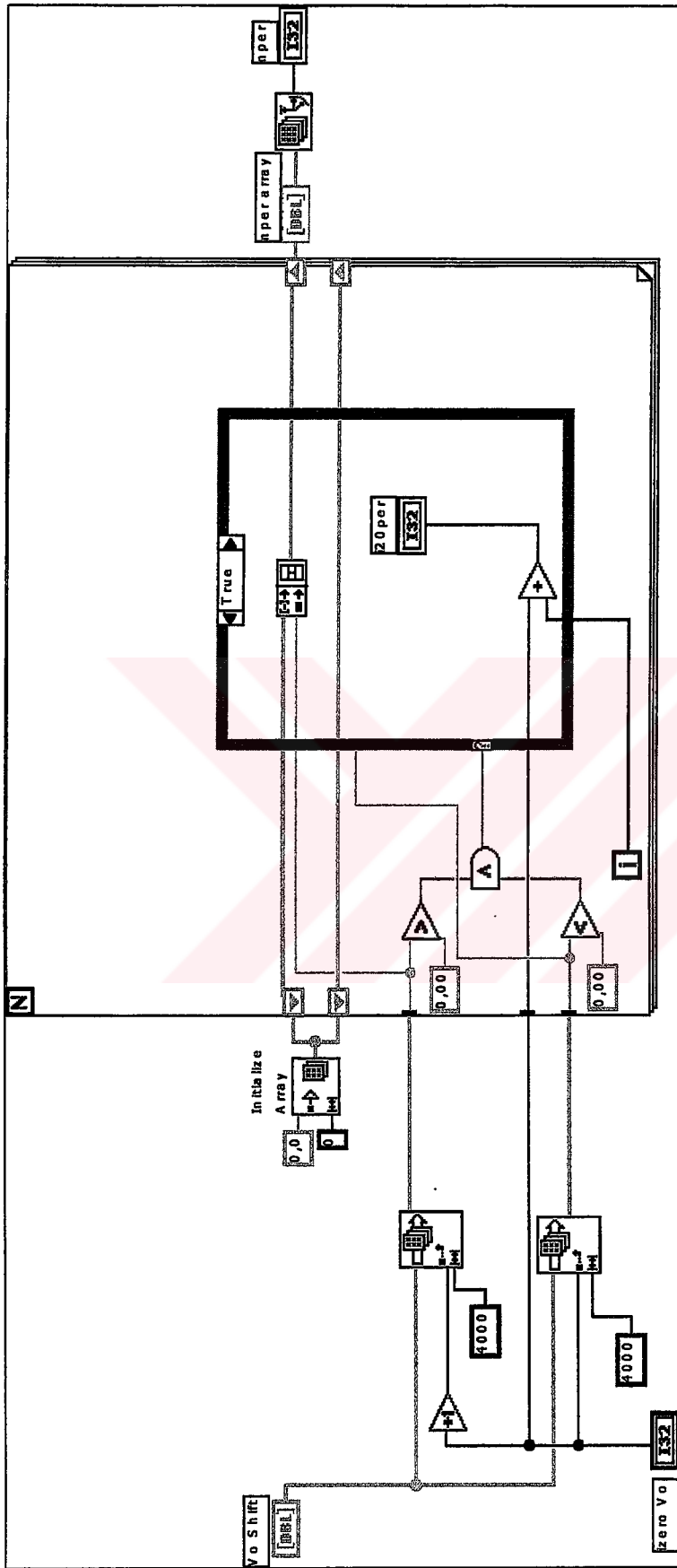


Figure B.8 Diagram of "trefvoltest2.vi"

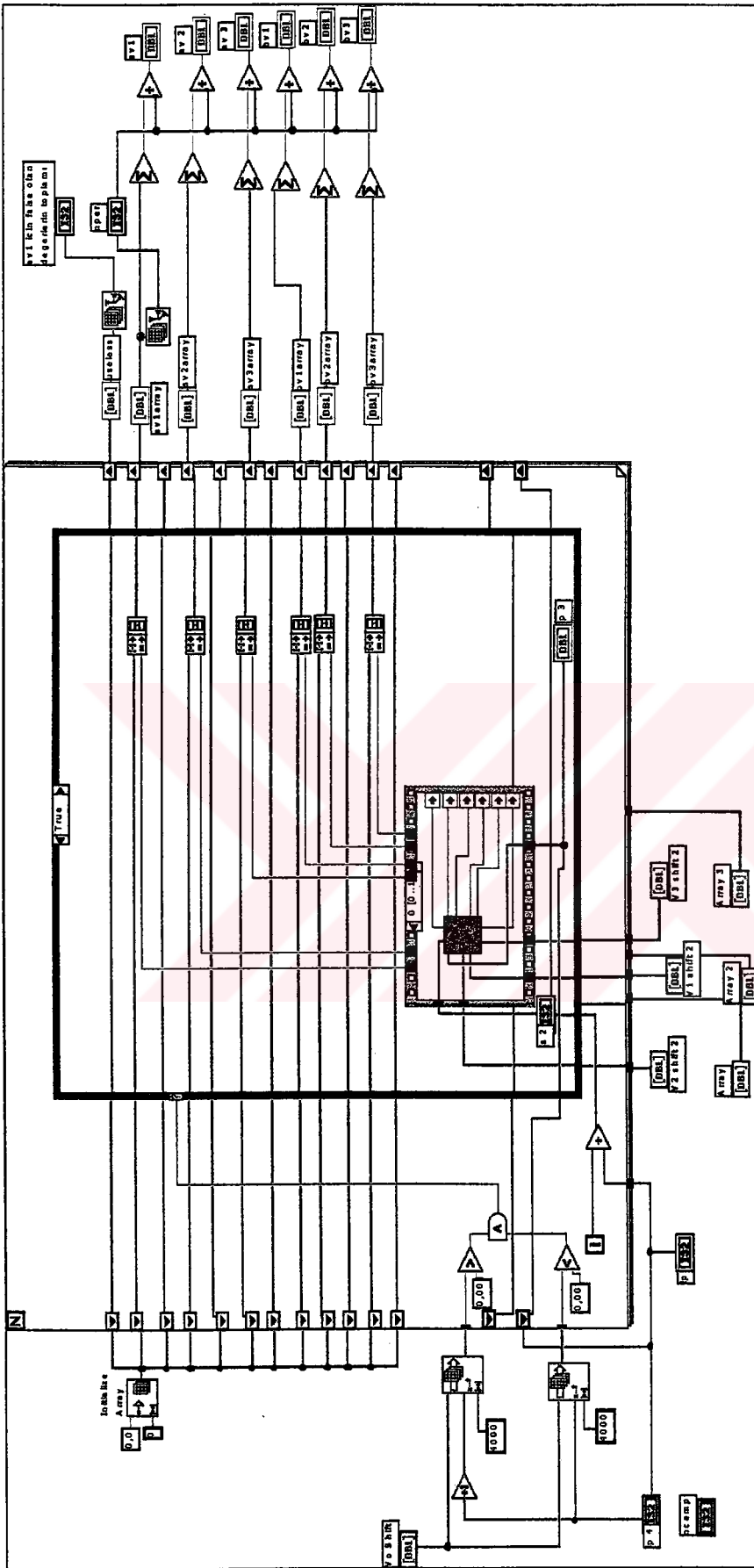


Figure B.9 Diagram of "tphase volt.vi"

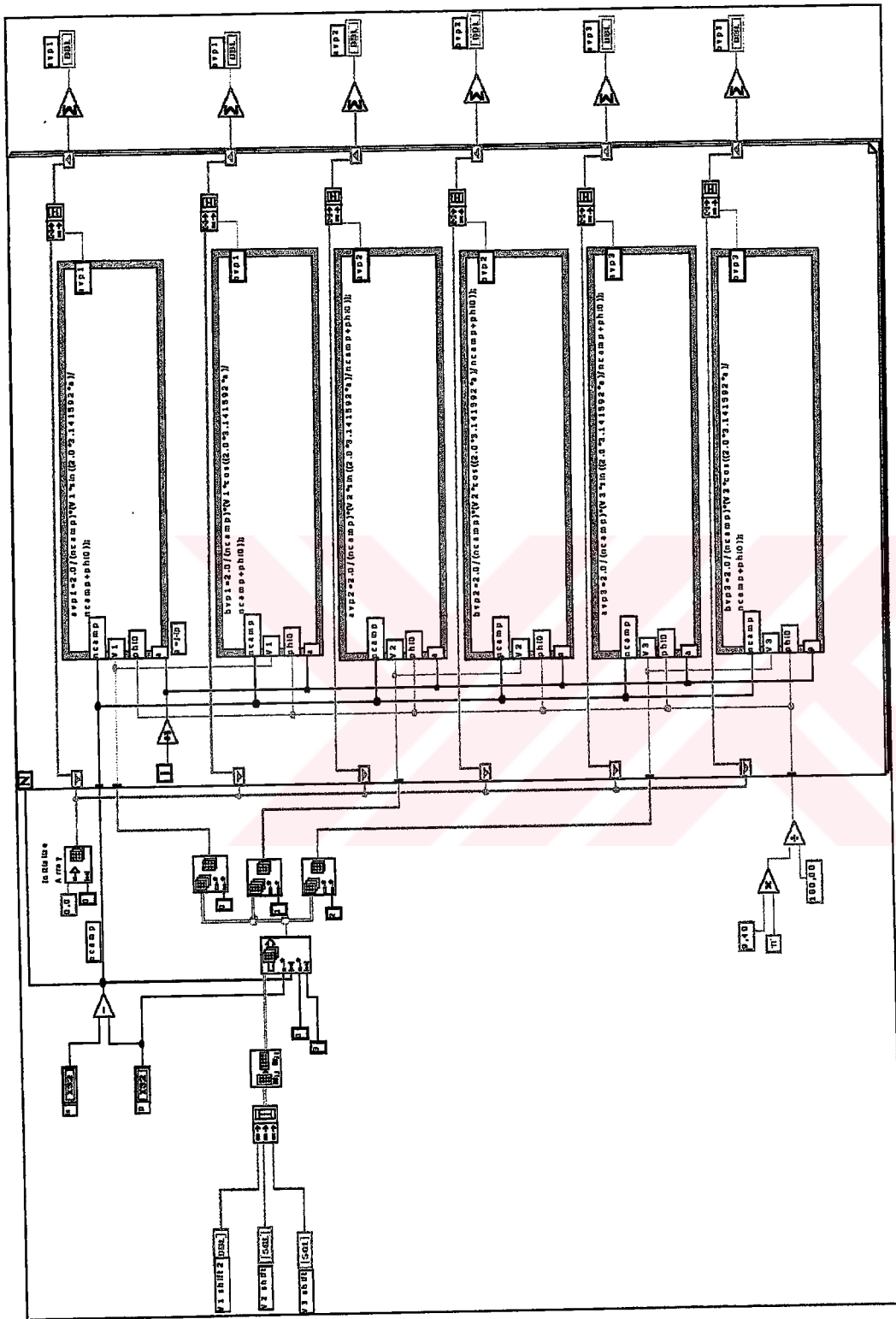


Figure B.10 Diagram of “tvoltaj hesaplamaları.vi”

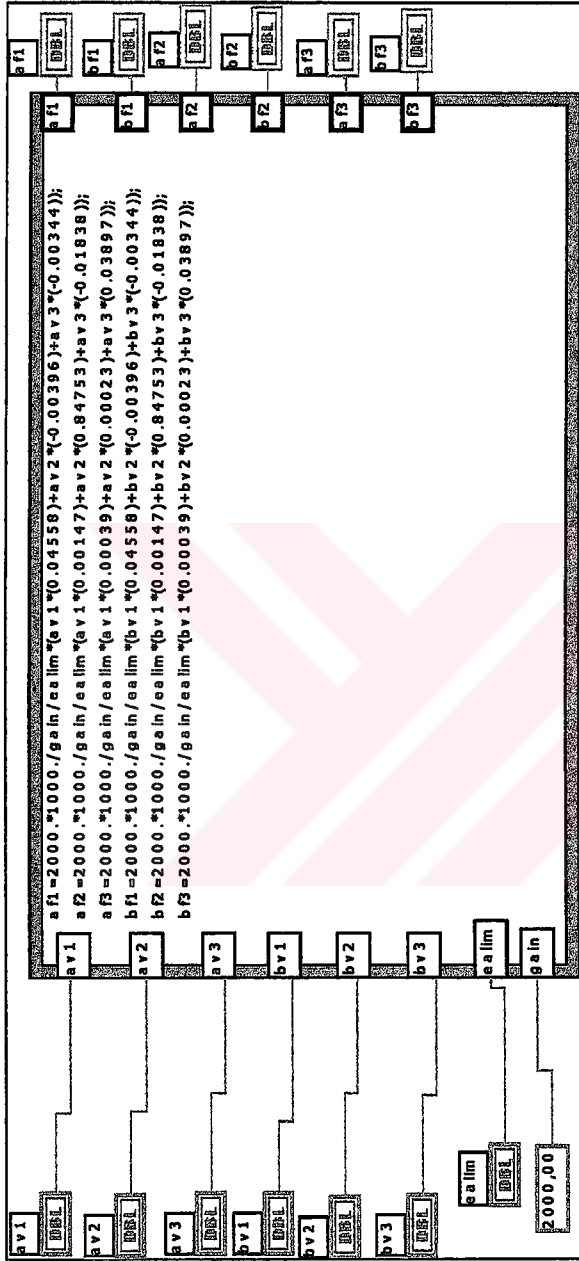


Figure B.11 Diagram of "load component.vi"

